ESPOO 2005 VTT PUBLICATIONS 583

Erja Turunen

Diagnostic tools for HVOF process optimization

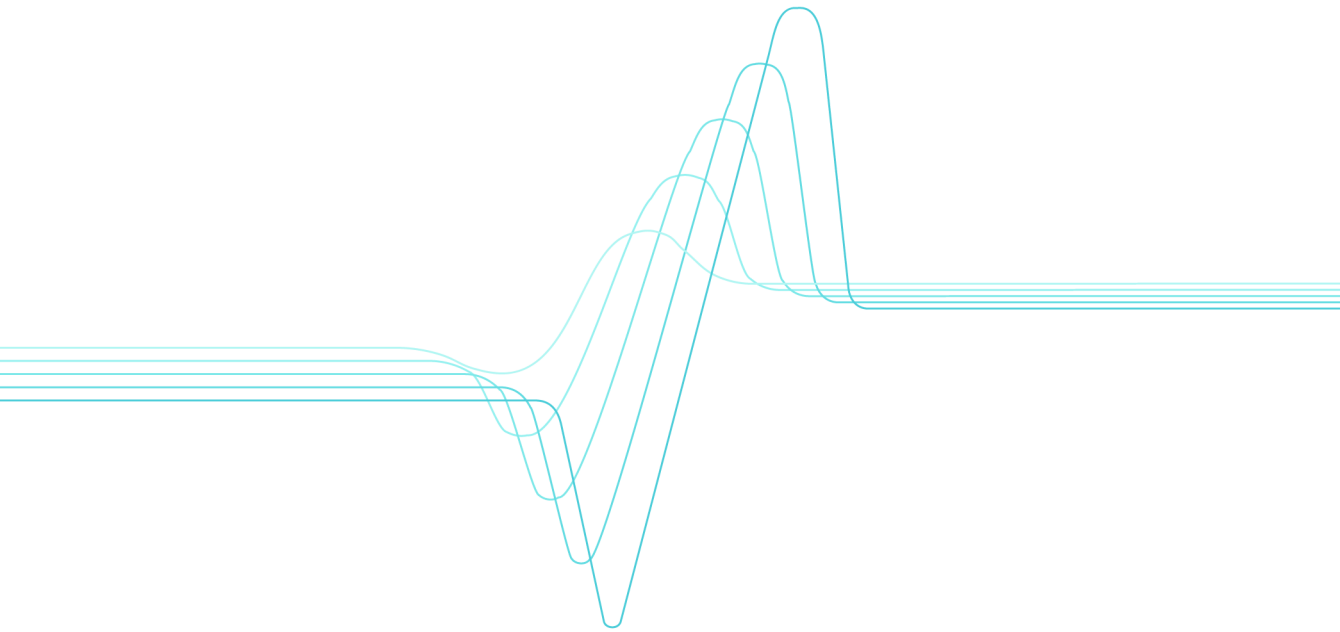

VTT PUBLICATIONS 583

Diagnostic tools for HVOF process optimization

Erja Turunen

VTT Industrial Systems

Dissertation for the degree of Doctor of Science in Technology to be presented with due permission of the Department of Materials Science and Engineering, for public examination and debate in Auditorium 1 (Vuorimiehentie 2 A) at Helsinki University of Technology, Espoo, Finland) on the 16th of December, 2005, at 12 noon.

ISBN 951–38–6677–7 (soft back ed.)
ISSN 1235–0621 (soft back ed.)

ISBN 951–38–6678–5 (URL: http://www.vtt.fi/inf/pdf/)
ISSN 1455–0849 (URL: http://www.vtt.fi/inf/pdf/)

JULKAISIJA – UTGIVARE – PUBLISHER

VTT, Vuorimiehentie 5, PL 2000, 02044 VTT
puh. vaihde 020 722 111, faksi 020 722 4374

VTT, Bergsmansvägen 5, PB 2000, 02044 VTT
tel. växel 020 722 111, fax 020 722 4374

VTT Technical Research Centre of Finland, Vuorimiehentie 5, P.O.Box 2000, FI–02044 VTT, Finland
phone internat. +358 20 722 111, fax +358 20 722 4374

VTT Tuotteet ja tuotanto, Metallimiehenkuja 8, PL 1703, 02044 VTT
puh. vaihde 020 722 111, faksi 020 722 7069

VTT Industriella System, Metallmansgränden 8, PB 1703, 02044 VTT
tel. växel 020 722 111, fax 020 722 7069

VTT Industrial Systems, Metallimiehenkuja 8, P.O.Box 1703, FI–02044 VTT, Finland
phone internat. +358 20 722 111, fax +358 20 722 7069

Otamedia Oy, Espoo 2005

Turunen, Erja. Diagnostic tools for HVOF process optimization. Espoo 2005. VTT Publications 583. 66 p. + app. 92 p.

Keywords thermal spraying, HVOF, high velocity oxi-fuels, process optimizatic diagnostics, single splat studies, surface coatings, alumina, quasicrystals, nanofractions

Abstract

In the thermal spray process the coating is built up from lamellas formed by rapid solidification of the melted or semi-melted droplets attached to the substrate. A typical structure for the coating is a pancake-like lamellar structure, where the flattening stage and adhesion between the lamellas, together with the coating material itself, define the main properties of the coating. Thermal spray coatings are often applied for better corrosion and wear resistance. Therefore, low porosity and good adhesion are desired properties for the coating. High velocity processes – especially HVOF (High velocity oxy-fuel) spraying – are the most potential methods for producing a good adherent coating with low porosity.

From a scientific point of view, particle velocity and particle temperature, together with substrate temperature, are the main parameters affecting the deposit formation. They determine the deposit build-up process and deposit properties. Particle velocity and temperature affect the deposit efficiency as well as the microstructure.

The aim of this work was to show the workability of diagnostic tools in the HVOF process. The focus was on first order process mapping, including on-line diagnostics and single splat studies. Nanocrystalline alumina composites and quasicrystals were selected, two materials that are complex to spray. With both materials the melting state of the particles must be well optimized in order to produce dense, well-adhered coating without unwanted changes in coating phase structure.

The main focus was on the HVOF spraying of alumina. The target was to obtain a systematic understanding of the influence of the process conditions on the

microstructure development in HVOF alumina coatings. Conventional limits of gas ratios and flows were exceeded to obtain a wide velocity-temperature range. The study aimed to produce information for a first order process map, and was carried out at a much deeper level than previously reported. Propylene and hydrogen as fuel gases were compared, and other variables, such as total gas flow rate, fuel gas/oxygen ratio, and standoff distance were also varied. The obtained data was applied for nanostructured alumina composite coatings, and the effect of the process conditions was compared on the obtained coating microstructure and properties.

On-line diagnostic measurements, in which particle temperatures and velocities in the flame can be measured, were performed. The main work was carried out for alumina by using a DPV-2000 system. Two clear regions of different temperature and velocity arise from the use of different fuel gases. Single splat studies correlated well with the obtained coating properties, and a first order process map for alumina was created showing the window for the spray parameters producing best coating quality plotted against coating hardness and abrasive wear resistance.

It was shown that diagnostic results can be correlated with the coating microstructure and coating properties in HVOF spraying. It was also demonstrated that the coating properties and coating quality can be improved by optimizing and carefully selecting the spray parameters.

Preface

The research work for this thesis was carried out in the Surface Engineering group at VTT, the Technical Research Center of Finland, from 2000 to 2005. The work related to Publication IV was partly carried out during the 6 weeks research period I spent at Stony Brook University, USA, in the summer of 2002. The work was then continued in Finland, as well as finalizing the publication. The thesis was supervised by Professor Simo-Pekka Hannula, to whom I would like to express my sincere gratitude for his guidance, support and fruitful discussions around the issues related to this thesis.

My sincere thanks also go to my co-workers at VTT. My closest co-workers, Tommi Varis, Kimmo Ruusuvuori and Maria Oksa, have all been very supportive and understanding during my most hectic period when I was preparing this work. Markku Lindberg, Alpo Viitanen and Seija Kivi get special thanks for their technical support in making coatings and samples. Jari Keskinen, Pertti Lintunen, Teppo Fält and Tom E. Gustafsson have also all an unique role in this co-operation. I also want to thank my group leader, Jari Koskinen, for all his support and late evening discussions, which increased my motivation even more. I want to give special thanks to all the other members of my group for creating such a good and motivating atmosphere to work in.

Acknowledgement is also due to Professor Sanjay Sampath and his group at Stony Brook University, USA, for their co-operation and the resources made available to me. Special greetings go to Jonathan Gutleber and Anirudha Vaidya for those long hours in the spray booth together.

The financial support provided by VTT, the National Technology Agency (Tekes), and Finnish industry is gratefully acknowledged.

I also want to thank my family and friends for all their support, encouragement and care over these years. And, last but not least, I thank Elina for her positive attitude and patience towards my work.

Espoo, November 2005

Erja Turunen

Contents

Appendix I of this publication is not included in the PDF version.
Please order the printed version to get the complete publication
(http://www.vtt.fi/inf/pdf/)

List of included publications

This thesis consists of a summary of the main results and six appended publications I–VI.

I Turunen, E., Varis, T., Vierimaa, K. & Hannula, S.-P. Spray parameter optimisation and tribilogical properties of thermally sprayed quasicrystalline and partially quasicrystalline coatings. Proc. Estonian Acad. Sci. Eng., 9, 4 (2003), pp. 293–303.

II Huttunen-Saarivirta, E., Turunen, E. & Kallio, M. Microstructural Characterisation of Thermally Sprayed Quasicrystalline Al-Co-Fe-Cr Coatings. Journal of Alloys and Compounds, 354, 1–2 (2003), pp. 269–280.

III Huttunen-Saarivirta, E., Turunen, E. & Kallio, M. Influence of Cr Alloying on the Microstructure of Thermally Sprayed Quasicrystalline Al-Cu-Fe Coatings. Intermetallics 11 (2003), pp. 879–891.

IV Turunen, E., Varis, T., Hannula, S.-P., Vaidya, A., Kulkarni, A., Gutleber, J., Sampath, S. & Herman, H. On the role of particle state and deposition procedure on mechanical, tribological and dielectric response of high velocity oxy-fuel sprayed alumina coatings. Materials Science and Engineering. Accepted for publication, in print (2005).

V Turunen, E., Varis, T., Gustafsson, T.E., Keskinen, J., Fält, T. & Hannula, S.-P. Parameter optimization of HVOF sprayed nanostructured alumina and alumina-nickel composite coatings. Surface and Coatings Technology. Accepted for publication, in print (2005).

VI Turunen, E., Varis, T. Gustafsson, T. E., Keskinen, J., Lintunen, P., Fält, T. & Hannula, S.-P. Process optimization and performance of nanoreinforced HVOF-sprayed ceramic coatings. Proceedings of 16th International Plansee Seminar, May 30–June 3, 2005, Reutte, Austria. Pp. 422–433.

Author's contribution

I was the main author of the Publications I, IV–VI. I prepared the test matrixes and schedules, participated in the spray and diagnostic tests, studied the diagnostic data and compared them with the splat results and coating performance data. Co-authors were essential in the following tasks: T. Varis was in charge of the thermal spray studies at VTT, and J. Gutleber and A. Vaidya at Stony Brook University, USA; T. E. Gustafsson made the SEM studies and T. Fält the nanoindentation studies; J. Keskinen produced special nanostructured ceramic powders; and Professor Hannula supervised this work.

E. Saarivirta-Huttunen made separated, wide microscopy studies for quasicrystalline coatings and was the main author of Publications II and III. For those publications, E.T was in charge of thermal spray coating manufacturing, process optimization and coating properties characterization, including microstructure and Pin-on-Disc testing. The button test was carried out by K. Vierimaa of Metso Corp.

List of symbols

HVOF	High velocity oxy-fuel
APS	Atmospheric plasma spray
CTE	Coefficient of thermal expansion
XRD	X-ray diffraction
SW	SprayWatch on-line diagnostic equipment
CCD	Charge-coupled device
IR	infrared
α, γ	Symbols for different alumina phases
SEM	Scanning electron microscope
TEM	Transmission electron microscope
C_3H_6	Propylene
O_2	Oxygen
H_2	Hydrogen
CoF	Coefficient of friction
PoD	Pin-on-disc
QC	Quasicrystal
m/s	meters per second
kW	kilowatts
°C	Celsius degree
kg/h	kilograms per hour
µm	micrometer
nm	nanometer
l/min	litres per minute
∅	diameter

1. Introduction

1.1 Thermal spraying

Thermal spraying is a general term to describe all methods in which the coating is formed from melted or semi-melted droplets. In thermal spraying the material is in the form of powder, wire or rod and is fed into the flame produced by a spray gun, where it melts and the formed droplets are accelerated towards the substrate to be coated. The thermal and kinetic energy of the flame can be produced either with burning mixtures of fuel gas and oxygen, or by using an electrical power source. Based on the energy source, thermal spray methods can be divided into a few main groups: plasma spray methods, flame spray methods, high velocity oxy-fuel methods, electrical arc methods, and, as the latest technology, cold gas methods.[1, 2, 3]

In thermal spraying the coating is built up from the lamellas formed by rapid solidification of the melted or semi-melted droplets attached to the substrate. A typical structure for the coating is a pancake-like lamellar structure, where the flattening degree and adhesion between the lamellas, together with the coating material itself, define the main properties of the coating. The adhesion and porosity of the coating is mainly defined by the particle melting behavior and the velocity when attaching to the surface. In addition, due to the fast cooling rate of the particles, some special features, such as residual stresses and the metastable phases can be observed in the thermally sprayed coatings.[1, 2, 3]

Thermal spray coatings are often applied for better corrosion and wear resistance. Therefore, low porosity and good adhesion are desired properties for the coating. High velocity processes – especially HVOF (High velocity oxy-fuel) spraying – are the most potential methods for producing a good adherent coating with low porosity. In HVOF spraying heat is produced by burning mixtures of oxygen and fuel gas, mainly hydrogen, kerosene, propane, propylene, natural gas or acetylene. Due to the special nozzle design, a jet with supersonic speed is produced. Another commonly used method is APS (Atmospheric plasma spray), where the energy is based on the plasma produced by ionizing an inert gas, typically a mixture of argon and hydrogen or helium, between the anode and the cathode in the spray gun. Due to the high energetic ionized plasma, the temperature of the plasma flame is very high.

The main difference between HVOF and APS is the relationship between the kinetic and thermal energy of the process described by the particle velocity and the flame temperature. Typical ranges of these parameters for each of the process are given in Table 1.

Table 1. Characteristic features of HVOF and APS processes.[3]

Spraying method	**Particle velocity (m/s)**	**Flame temperature (°C)**
HVOF	500–700	~ 3 000
APS	150–400	~8000–12000

The ability to produce dense coatings with low amount of phase transformations and oxidation is the main feature of the HVOF process. This is due to the short dwell time of the particles in a relatively cold flame. It is widely used to produce cermet and metal coatings. The HVOF process has also demonstrated an ability to deposit dense ceramic coatings, such as alumina.[4, 5, 6, 7]

Due to the high process temperature, APS which enables good melting of the ceramic particles is often used to produce a ceramic coating.

The use of thermal spray coatings has traditionally been based on extending the life of the component. However, thermal spray coatings have increasingly been considered "prime reliant" and such coatings are already being included in the design of the systems.[8] This requires considerable enhancement of the reliability and reproducibility of the coatings. Thermal spraying is a very complex process and includes number of variables. A better understanding of the relationship of these variables and their effect on the coating properties must be obtained in order to apply thermal spray coating to "prime reliant" applications.

1.1.1 HVOF Spraying

In the HVOF process the combustion fuel and oxygen are led to the combustion chamber together with the spray powder. The combustion of the gases produces

a high temperature and high pressure in the chamber, which causes the supersonic flow of the gases through the nozzle. The powder particles melt because of the flame temperature in the combustion chamber and during the flight through the nozzle. The flame temperature varies in the range of 2500 °C–3200 °C, depending on the fuel, the fuel gas/oxygen ratio and the gas pressure. In the HVOF process the particles melt completely or only partially, depending on the flame temperature and material's melting point. The degree of melting depends on the flame temperature and the dwell time in which the particles occupy the flame. These are adjustable process parameters and they affect the properties of the coating.[1]

The interest in the HVOF process to produce coatings with a wider range of materials has been growing continuously. For those materials that are sensitive to phase transformations due to evaporation or oxidation, HVOF spray is a very potential coating method due to the process condition, which combines a relatively low flame temperature with a low exposure time in the flame.

A few different HVOF spray systems exist with partly different gun designs and capacities. Each one has differences in design, but all are based on the same fundamental principles. The combination of high pressure (over 4 bar) and gas flow rates of several hundred liters per minute generate hypersonic gas velocities.[7] These systems can be roughly divided into the first, second and third generation. In all first and second generation guns the pressurized burning of gaseous fuel with oxygen is used to produce an exhaust jet traveling at a speed of about 1800 to 2000 m/s. Spray systems belonging to this category are Jet Kote, Diamond Jet (DJ), HV-2000 and CDS. Under standard spray conditions the systems are operated at a power level of about 80 kW and are capable of spraying about 2–3 kg/h of WC-Co. The third generation systems are for power levels ranging from 100 to 200 kW, being capable of spray rates up to about 10 kg/h. The difference between the third generation systems (JP-5000 and DJ Hybrid) and the previous ones is the operation at higher gas/fuel flows and higher chamber pressures (8 to 12 bar versus to 3 to 5 bar). [7, 9, 10]

A comparison of different spray systems has shown that only one model from the second generation can transfer enough heat to the particle to be able to melt a ceramic particle. This system is called Top Gun or HV-2000.[9]

Despite the fact that the first HVOF method was introduced in 1982, there has only been limited effort towards understanding the effect of process parameters on the structure and properties of the coating compared to the work carried out in the field of plasma spraying. The main reason for this is the common use of the method to produce coatings from a few standard materials, such as cermets, where the process parameters are optimized and specified by the powder and equipment manufacturers. In these applications, coating quality optimization is widely carried out form the powder development point of view. Recently, more interest in understanding the HVOF process and the effect of process variables on the coating quality has arisen due to the growing interest in the development of closed loop process control.[10]

1.1.2 Microstructure of thermal spray coatings

The microstructure of a thermal spray coating is a complex mixture of lamellas formed from melted or semi-melted particles as well as many irregularities. Metallic coatings typically contain oxide films due to the oxidation of the particles in the hot flame. Ceramic coatings often contain cracks due to the relaxation of stresses.[11] Three typical groups of porosity can be identified: interlamellar pores, globular pores, and intrasplat cracks.[4] The differences between the pore structures are mainly due to the melting stage and the impact velocity of the particles.[5] Interlamellar pores are parallel to the coated substrate and are typically formed by a reduced cohesion between two splats. Globular pores are formed by the incomplete melting or fast re-solidification of the particles. Intrasplat cracks are perpendicular to the splat interface and are formed by the stress relaxation during cooling of the coating-substrate system with a difference in CTE (coefficient of thermal expansion).[11]

A large number of studies are being carried out to try to understand relationship between the plasma spray process and the coating properties.[12] Only recently have more detailed studies been carried out to try to understand the effect of the HVOF process variables on the coating microstructure and performance more deeply (more details in Chapter 1.2.3).

1.2 Tools for process optimization

From a scientific point of view, particle velocity and particle temperature together with substrate temperature are the main parameters affecting the deposit formation. They determine the deposit build-up process and deposit properties. Particle velocity and temperature affect the deposit efficiency as well as the microstructure.

Different tools are being developed in order to better understand the deposit formation and relationship to the coating properties. These tools are currently being collected under a concept of "Process Map". This can be considered to have two different meanings, aiming at either a) optimization and mapping of the different in-flight process conditions of the particles, producing a different melting range of the particles, or b) finding the influence of different splat structures and substrates on the final structure and properties of the deposited coating. These two maps have lately been named "First order map" and "Second order map" by Prof. Sampath.[8] Figure 1 illustrated the philosophy of such a map.

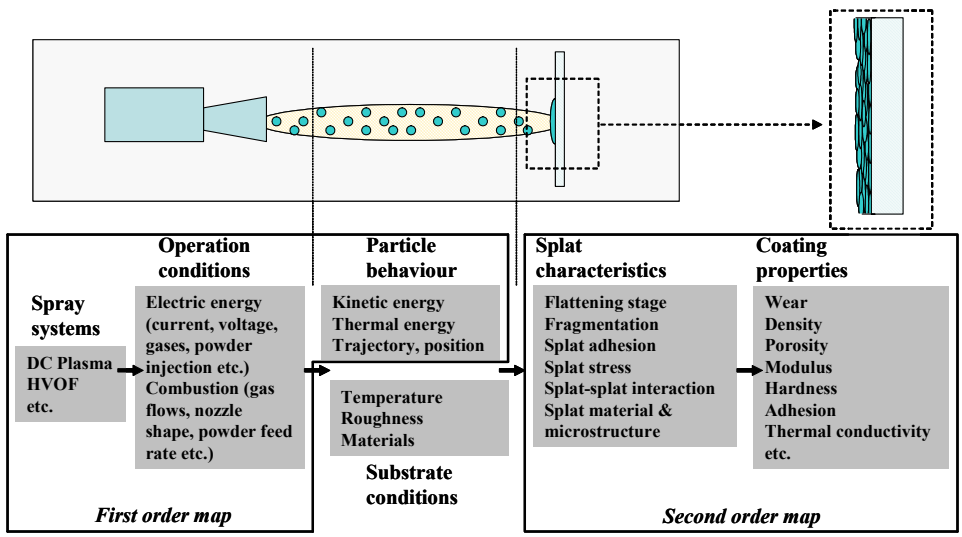

Figure 1. Schematic overview of process maps (modified from reference 8).

Single tools mainly used in process mapping are i) in-flight diagnostics, where particle velocity and temperature are measured during their flight in the flame, ii) splat studies, where the particle melting stage and droplet spreading/solidification is

studied from the behavior of single particles, and iii) droplet/surface or previously deposited layer interaction, where the substrate temperature has been found to have significant influence on the particle morphology, deposit microstructure and properties.[8]

Process maps can also mean equipment and material-specific studies to define the interaction of a certain velocity-temperature range with the final properties of the coating. In this case both diagnostic measurements and mathematical modeling are used to create "a process window" to ensure the desired coating microstructure within certain approved limits of parameter fluctuations.[13]

On-line diagnostic and single splat diagnostic tools are presented in more detail in Chapters 1.2.1 and 1.2.2. The effect of HVOF process variables on the coating microstructure and properties is discussed in more detail in chapter 1.2.3.

1.2.1 On-line diagnostic methods

Different on-line diagnostic tools have been developed to be able to measure direct thermal spray jet properties such as enthalpy, particle temperature, particle velocity, particle size and total particle flux. These are the main parameters that influence the characteristics of the deposited coating. On-line diagnostic tools can be used either for process optimization of thermal spray coating with certain material and spray processes or for process control during deposition.

The most sophisticated systems are too complex for process control. Therefore, a large number of simple, fast, and cost effective systems for the measurement of the jet shape and direction, ignoring information on single particles, have been developed, such as Particle Flux Imaging-PFI, DifRex M, PlumeSpector and SDC.[14]

The enthalpy available in the jet can be measured by using enthalpy probes specially developed for the measurement of enthalpy, temperature and velocity of gaseous effluents. This technology gives overall information on the jet properties, but, depending on the spray material, no detailed information on the particle conditions or other spray conditions, such as gas pressure.[15]

More sophisticated tools are needed when more detailed information on a single particle is wanted, as is the case in process optimization work. The most advanced on-line diagnostic tools are based on the measurement of the thermal emission of the particles. In these systems the temperature is determined using a two-color pyrometer and velocity determined from images captured with fast CCD camera systems.[16] Single particle techniques require that the number of particles is limited in some methods due to the ability to observe the light emitted by a single particle without overwhelming interference from surrounding particles. Depending on the technology, the amount of powder varies from a few tens of grams to the normal powder feed rate up to 5–10 kg/h. This limits the usability of some technologies in quality control applications in real production work.

Only a few commercial equipment applications are suitable when detailed information on particles is wanted for different spray conditions in order to optimize spray parameters. This is especially the case in HVOF spraying, where particle velocities are high and particle temperatures are low compared with the plasma spray.

Temperature measurement is based on the optical system and on the well-known fact that objects emit electromagnetic radiation, in which the intensity and wavelength depend on the temperature of the object; the radiation is shifted towards shorter wavelengths during heating. Measurement is based on the two-color pyrometer measuring the radiance of hot, incandescent particles. Two-color pyrometer is a method for optical temperature measurement that is based on the measurements of the light emitted by the object in two separate wavelength ranges. The method eliminates the effect of particle size, emissivity and non-ideal focusing, and is, therefore, usable with all materials without material specified calibration[17]. For lack of better information, the particles are generally assumed to behave as gray body emitters[18]. This will cause some inaccuracy in the measurements, especially in the case of metal particles where the error can be up to 100 °C[17].

The measurement of particle velocity is generally performed by laser Doppler velocimetry or by transit timing techniques.[18]

DPV-2000 (Tecnal Ltd) is based on two-color pyrometry at two different spectral ranges in the near IR wavelength region around 790 nm and 990 nm,

respectively. The particle velocity is determined by the on-flight technique during the passage of particles in front of a two-slit mask.[19] The mean and standard deviation of the particle temperature distribution can be obtained from observations of sufficient numbers of individual particles.[20] The measurement spot is small and the positioning must be performed carefully. The measurement is also relatively insensitive to spatial movement of the spray pattern. If information through the whole flame is required, the measurement must be performed by scanning the probe, which increases the measurement time for several minutes per condition. The benefit of the system is in its ability to measure dimensional information on single particles.

SprayWatch (Oseir Oy) is based on the CCD camera. The particles are imaged onto a CCD camera sensor with the aid of spectrally resolving optics. Particle velocity is measured using the time-of-flight method. The length of the particle traces on the CCD detector is measured by the image processing algorithm, and is then converted to velocity by dividing it by the known camera shutter time[17, 21]. The temperature of the particles is measured with two-color pyrometry. The benefit of this technique is the possibility to obtain information through the whole jet. A disadvantage is that the information is always an average, and, therefore, the temperature values are lower than the values obtained by DPV-2000 when measured from the centre of the jet.

It is shown that particle velocity and temperature varies widely at different positions in the jet, and monitoring of particle properties at one single position in the jet is not sufficient for describing the complete particle jet.[22]

1.2.2 Splat studies

Splat forming research studies have been carried out to better understand the relationship between the particle in-flight conditions and the coating microstructure. The bulk of the work has been done in the field of plasma spraying and some important results have been produced. The research work has been carried out by both theoretical simulations and experimental observations.

The splat morphology is described with various terms, including mushroom-like, pancake-like, flower-like, and fingered-like splats[23, 24]. Splat morphology has

important implications for the coating microstructure development, porosity and, finally, coating properties. It can be concluded that the main factors affecting the splat morphology are particle velocity, particle temperature, substrate temperature and the Reynolds number of the particle[24, 25]. Many other parameters, such as impact angle, particle surface chemistry, and many substrate parameters, including contamination by condensates and absorbates, oxidation stage, roughness and thermal properties, also have an effect[25].

Fukanuma et al.[26] have classified the formation of splat into four different groups: 1) the molten viscous particle impinges and spreads as a thin disc, 2) the molten viscous particle impinges and splashes with some part of the particle remaining on the substrate, 3) the plastic particle impinges and is deformed plastically, 4) the elastic particle impinges and bounces off the substrate. The first two are the main mechanisms for thermal spray coating formation, including particle melting. Fukanuma's classification does not consider the cases when particles are only partly melted or when the spray material does not deform plastically.

More detailed studies are being carried out on the complete molten droplets. It has been found that no significant solidification of the splat occurs before the spreading is complete. The spreading of the liquid stops when the kinetic energy of the droplet is dissipated[23]. Temperature has been recognized to have an important role both in the splat morphology and the splat dimension forming. An increase in the substrate temperature will produce a more uniform splat with a lower amount of fragmentation. The phenomenon has been shown to occur at relatively low substrate temperatures for most materials (100–400 °C).[27] An increase in the Reynolds number has shown a trend for an increased cooling rate in the lamella.[28] An increase in particle temperature has also been shown to have an effect on the splat morphology: an increased particle temperature lowered the droplet viscosity, and the fragmentation of the alumina particle was increased[24].

All the studied particle conditions have particle velocities of less than 50 m/s, and thus the findings in these studies cannot be directly used in the case of high velocity spraying where particle velocities are hundreds of meters/second.

Splat formation for high velocity spray methods has not been studied in such detail. The previous work has mainly concentrated on a demonstration of

different molten stages of the particles in different spray conditions and on the effect of that for the coating microstructure and properties[4, 29, 30, 31, 32]. Sobolev et al. have developed a uniform model to estimate the flattening of the composite powder that is also suitable for HVOF spraying[33, 34]. Work within high velocity spraying is mainly being carried out for metal and hardmetal coatings. Only Kulkarni[4] and Sundararajan[29] have published some splat studies for high velocity spraying of alumina.

1.2.3 HVOF process optimization

So far, only a small amount of work has been carried out in order to understand the different phenomena behind HVOF spraying.

The creation of a first order process map in the case of HVOF would include interaction studies between spray parameters, such as fuel gas/oxygen ratio, total gas flow and standoff distance on the velocity-temperature behavior of the particle and the splat structure. A second order map would include a coating properties evaluation, such as residual stresses, porosity, adhesion, hardness, mechanical properties, and wear/corrosion resistance compared with the different splat structures.

Some comparison between different spray processes – mainly APS and HVOF – has been carried out. The differences in particle velocity and temperature between these two processes, and their effect on the properties of metallic coating, have been clearly demonstrated by Sampath et al.[35]

A more detailed study on the effect of different fuel gases in HVOF spraying has been carried out by Lugscheider et al.[36] They investigated MCrAlY powders and noticed that higher flame temperatures are obtained by using propane compared with hydrogen as a fuel gas. An increase in standoff increased particle temperatures. Particle velocities were higher when spraying with hydrogen. The findings were screened towards the oxygen content and oxidation resistance of the MCrAlY coatings. Similar results were obtained by Lugscheider et al.[31] and Hanson et al.[37] for AISI316L stainless steel.

Planche et al.[38] have studied the influence of the HVOF spray parameters on the in-flight characteristics of Inconel 718 particles and their correlation with the electrochemical behavior of the coating. In their studies the total gas flow was not constant between different spray conditions, so it is not possible to directly compare their results with the other published results. However, in their measurements particle velocity increased with an increasing total gas flow rate and the temperature was highest at fuel-rich conditions.

The relationship between different HVOF spray parameters for NiWCrBSi coatings and the corrosion performance of the coatings was studied by Gil et al.[39]. They varied a number of parameters and found that only standoff distance, fuel gas/oxygen and powder feed rate formed a clear correlation for porosity and corrosion resistance.

Li et al.[10, 40, 41] have recently carried out extensive research aiming to understand the relationship between gas parameters and particle temperature and velocity in the flame. Their main target is the development of model-based estimations of particle velocity and temperature aiming at the design of closed loop process control for the HVOF spray system[10, 40]. The first part of the modeling work concentrated on modeling the gas phase and particle behavior[41]. The latter part of the large modeling work has been the creation of a rule-based modeling of the coating microstructure. In that model the velocity, temperature and degree of melting of the particles hitting the substrate are determined by a mathematical model.[42] So far, the simulations and modeling are mainly being carried out for nickel with different particle sizes.

Calculations and simulations are also being carried out by other researchers aiming at a better understanding of the HVOF process.[54, 43] Optical flow visualization techniques are being used to examine the rapid turbulent mixing of the supersonic jet with the surrounding atmosphere.[44] However, despite the deep understanding of the gas dynamics, a gap exists in the understanding of the melting behavior of the particle in the jet. Some other studies are also being performed to optimize the process conditions in HVOF spray, but these are mainly focused on the metal or cermet materials and only a few different spray conditions are being measured.[45, 46, 47, 48]

Some results for the optimization of HVOF spraying of ceramics have been published with a limited amount of diagnostic results[49, 50]. Furthermore, investigations have been published for detonation spraying of alumina. The main findings of the studies were that the spray parameters have a strong effect on the coating quality, such as hardness and porosity. The best coating was obtained with a fuel gas/oxygen ratio of 0.28 and with a spray distance of 145 mm[51]. Some work is also being carried out to understand the correlations between spray conditions and microstructure for alumina coatings produced by HVOF and plasma spray. [4, 5, 6, 7, 52, 53] In these studies the coatings are produced using different spray methods, and such coating properties as microstructure, elastic behavior and wear resistance have been compared among the coatings. Other work published for HVOF spraying of alumina mainly focuses on the optimization of deposition parameters via determination of deposition efficiency and coating properties[6, 7]. In some studies the melting capability of different fuel gases has been compared and it has been found that despite the higher flame temperature of the acetylene-oxygen flame, the best coating structure is obtained when using hydrogen[6, 7]. Previous work carried out for a deeper understanding of the HVOF process for ceramics mainly focused on mathematical calculations[5, 54]. It has been shown that sufficient melting of the ceramic particles in the supersonic flame is critical due to the heat energy distribution during the HVOF process; the particles spend most of their time in the supersonic part of the flame, where the temperature is lower compared with the combustion chamber.[54]

Only a few studies concerning thermal spraying of quasicrystalline materials have been published. The studies have mainly focused on APS spraying of quasicrystals, the coating structure thus produced and the behavior of produced coatings in different wear and corrosion tests[55, 56, 57, 58, 59]. Some comparison between APS and HVOF sprayed coatings is presented[60, 61, 62]. These studies have focused on differences in the coating structure and behavior when produced with different thermal spray systems. No process optimization work is presented.

1.3 Coating materials and properties

The crystal structure depends upon the conditions under which the liquid droplets solidify. Due to the rapid cooling of the droplets in the thermal spray process, metastable phases can be produced.

In this study two different coating materials are introduced based on their different requirements for optimal spray conditions.

- Alumina was selected as a representative material that has a high melting point. The target was to spray nanostructured alumina by combining sufficient melting to ensure good lamella adhesion with the capability to retain a nanostructured composite structure.
- Quasicrystal materials were selected due to their sensitivity to composition changes in the flame. The spray parameters for these materials should be optimized in order to produce dense coatings without phase transformations.

1.3.1 Alumina

Ceramic coatings offer an interesting alternative protective layer over a steel structure due to their excellent chemical, corrosion and thermal resistance.[4, 5, 7, 63, 64]. Thermal-sprayed alumina coatings also show interesting electrical properties and can offer an economical solution as dielectric coatings in a variety of thick film and insulated metal substrate-based electronics applications[64, 65]. The melting point of alumina is 2049 °C[66], which is only slightly below the flame temperature produced in the HVOF process. Therefore, from the point of view of HVOF process, it is a challenging material to spray. The HVOF process is of special interest when aiming at dense ceramic layers for environmental protection applications.

A stable phase for alumina at room temperature is hexagonal α-Al_2O_3. Alumina also has a large number of metastable crystalline phases.[67] Due to the rapid cooling during the thermal spray process, these metastable phases are commonly recognized to form in the coating. Process variables in the thermal spray process give a wide spectrum of phase structures. Alumina coatings are reported to mainly consist of α-, γ- and δ-phases[68], of which cubic γ-alumina is the most reported metastable phase.[6, 69] The gamma phase has also been reported to be the dominant phase in the coatings.

The mechanical properties of alpha alumina are better than those of gamma-alumina and this phase is basically more desirable. The physical and electrical

properties are also different[5]. However, the final properties of the coating depend on the coating microstructure, especially on the bonding between the splats.

Plasma spraying of alumina has been studied much more widely than HVOF spraying. Studies have been carried out on the phase structure of the thermal sprayed coatings by using different spray methods, but the results reported are not all in line. Some studies show that the α phase content is lower in the HVOF sprayed coatings compared with the plasma sprayed coatings, suggesting that more complete melting occurs in HVOF spraying due to the differences in powder trajectories and heat transformation[5]. However, most of the studies have shown that the resulting alpha content is somewhat higher when using HVOF spray than the plasma spray.[4, 6, 7]

1.3.2 Nanostructured alumina

Nanocrystalline materials have been recognized as having special mechanical properties. Typically, the strength of crystalline materials increases with decreasing grain size and materials with a small grain size often exhibit superplastic behavior at elevated temperatures. Furthermore, the hardness and wear properties of the coatings are usually improved. There are several recent reviews on the mechanical properties of nanocrystalline materials[70, 71, 72]. Nanocrystallinity has been shown to have a positive influence on the toughness of ceramic materials when alloyed with nanophased metals[73, 74]. The ceramic coating research is mainly focused on development of APS alumina-titania coatings (grain size below 70 nm).[75, 76, 77, 78]

HVOF offers an interesting opportunity to combine dense coatings with a minimum amount of grain growth because of the higher particle velocities when compared to the plasma spray.

1.3.3 Quasicrystals

Quasicrystals are materials in which a repeating periodicity in an atom arrangement exists together with a rotational symmetry forbidden to crystalline materials; fivefold, eightfold, tenfold and even twelvefold symmetries have been encountered in quasicrystals.[79] A large number of properties that are not

common in material based on metal elements have been reported, including high hardness, low coefficient of friction, good oxidation and corrosion resistance, low thermal conductivity and low electrical conductivity.[80]

The majority of studies on thermally sprayed quasicrystalline coatings have concentrated on the different modifications of the ternary base alloys Al-Cu-Fe and Al-Ni-Co[55, 56, 57, 58, 60, 61, 62] by plasma spray.

Sprayed material is sensitive to phase transformations due to the changes in composition during the in-flight phase, such as evaporation of some elements or oxidation. The quasicrystal phase is rather sensitive to the correct elemental composition and can, therefore, be easily transformed from the original quasicrystal structure to the other inter-metallic phases due to the evaporation of some single elements such as alumina or copper during the in-flight phase of the particle in the thermal spray flame. Material stability depends on the spray parameters and the stability of the starting material.[59]

1.4 Aim of the research

In order to produce a coating with the desired properties it is not enough to just control the material structure inside one lamella. The interaction between lamellas, the stress states of the final coating, the adhesion to the substrate and cracking must also be controlled. The different phenomena affecting the final quality of the coating are described schematically in Figure 2.

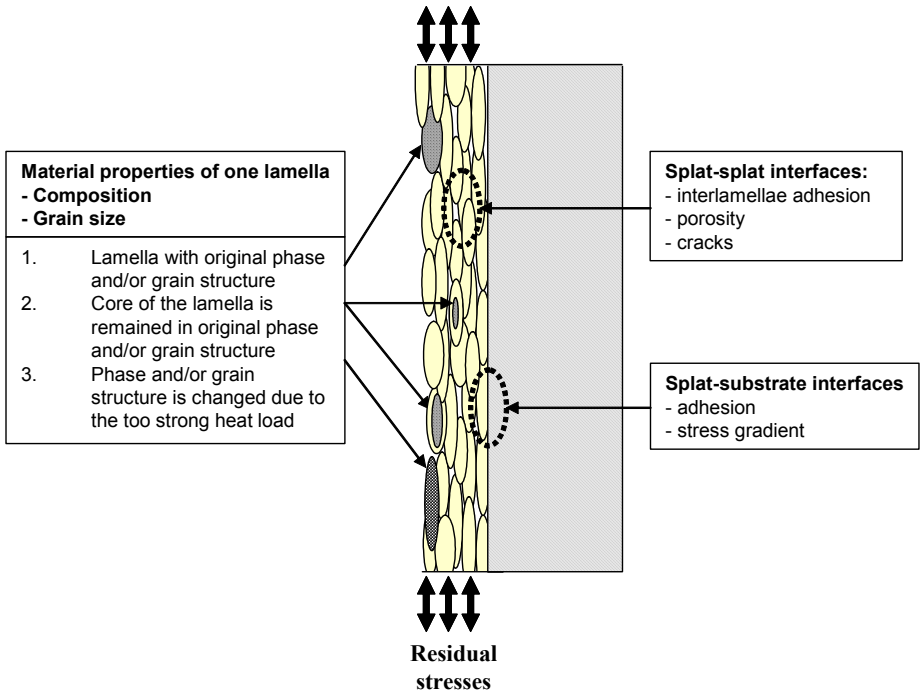

Figure 2. Factors influencing the quality of thermally sprayed coating.

The usability of diagnostic tools, on-line diagnostics and single splat studies is widely demonstrated for plasma spraying. Process mapping as a wider technique is also partly demonstrated for plasma spraying.

The aim of this work was to show the workability of diagnostic tools in the HVOF process. The focus was on first order process mapping, including on-line diagnostics and single splat studies. Nanocrystalline alumina composites and quasicrystal were selected, two materials that are complex to spray. With both

materials the melting state of the particles must be well optimized in order to a produce dense, well-adhered coating without unwanted changes in coating phase structure.

The main focus was on the HVOF spraying of alumina. The target was to obtain a systematic understanding of the influence of the process conditions on the coating microstructure development in HVOF spraying of alumina coatings. Conventional limits of gas ratios and flows were exceeded to obtain a wide velocity-temperature range. The study focused on producing information for a first order process map, and was carried out at a much deeper level than previously reported. Propylene and hydrogen as fuel gases were compared, and other variables, such as total gas flow rate, fuel gas/oxygen ratio, and standoff distance were also varied. The obtained data was applied to the manufacturing of nanostructured alumina composite coatings, and the effect of the process conditions was compared with the obtained coating microstructure and properties.

In the case of quasicrystals, the effect of spray conditions on the formed phase structure of the coating was studied. The main focus was to study whether the evaporation of some critical elements, such as aluminum, can be controlled by varying the spray conditions.

The main focus was placed on the online diagnostic measurements and single splat studies i.e., on the information for a first order process map. Despite the fact that this information was plotted against some coating properties, the creation of full information for a second order process map is not included in this work.

The hyphothesis of this work was that by using diagnostic tools, mainly on-line diagnostics and single splat studies, the formation of the HVOF coating structure can be predicted and the diagnostic tools can be used for process optimization when aiming at a coating with a certain structure and properties.

2. Experimental methods

2.1 Materials

Commercial alumina powder Al-1110HP from Praxair Inc. (39 Old Ridgebury Road, Danbury, CT 06810 USA) was used for the process optimization and as reference powder in the material development work due to the easy availability of the powder. Agglomerated nanofraction alumina powder produced by VTT was used as another reference powder in the process optimization. Synthesis of n-Al_2O_3 powder with and without alloyed nanoparticles was carried out using boehmite (AlO(OH)) as a starting media (trade name Disperal from Sasol Germany GmbH, Anckelmannsplatz 1, 20537 Hamburg, Germany). Nanofraction and nanocomposite powders were manufactured in various ways by using chemical and mechanical routes. The powder preparation has been discussed in Publications V and VI. Table 2 summarizes the sprayed powders.

Table 2. Sprayed alumina powders.

Powder	Material code	Manufacturer and method	Agglomerate size [µm[	Crystal size
Al-1110	ref-Al_2O_3	Praxair, fused and crushed	5–22	conventional
Boehmite	n-Al_2O_3	VTT, agglomerated and sintered	2–25	< 200nm*
Boehmite	n-Al_2O_3 -2% Ni	VTT, agglomerated and sintered	4–23	< 200nm*
Boehmite	n-Al_2O_3 -5% Ni	VTT, agglomerated and sintered	2–26	< 200nm*
Boehmite	n-Al_2O_3 -5% NiO	VTT, agglomerated and sintered	2–21	< 200nm*
Boehmite	n-Al_2O_3 -5% ZrO_2	VTT, agglomerated and sintered	2–29	< 200nm*
Boehmite	n-Al_2O_3 -5% SiC	VTT, agglomerated and sintered	2–29	< 200nm*

*given by the manufacturer

The quasicrystal powders used in this work were manufactured by Saint-Gobain Advanced Ceramics SNMI, France. Details of the used powders are presented in Table 3.

Table 3. Sprayed quasicrystal powders.

Powder	Material	Nominal composition*	Particle size [µm] *	Particle size (measured) [µm]
Christome F1	Al-Cu-Fe	40.8 wt.% Al 41.2 wt.% Cu 17.0 wt.% Fe 0.8 wt.% B	20–53	30–59
Christome A1/S	Al-Cu-Fe-Cr	54.1 wt.% Al 17.8 wt.% Cu 13.0 wt.% Fe 14.9 wt.% Cr	20–53	30–59
Christome BTI	Al-Co-Fe-Cr	52.8 wt.% Al 20.4 wt.% Co 15.3 wt.% Fe 11.2 wt.% Cr.	20–53	23–50

*given by the manufacturer

2.2 Thermal spray test setup

The coatings were deposited using a Praxair HV-2000 spray gun and combustion chambers having lengths of 12mm, 19mm and 22mm. Nitrogen was selected as the carrier gas. The fuel gases were hydrogen and propylene.

2.3 On-line diagnostics

Online diagnostic measurements were carried out using two different types of equipment: Tecnar DVP-2000 and Oseir Spraywatch 2i. The main work was carried out for alumina by using the DPV-2000 diagnostic system. A large number of different spray conditions were measured by varying the total gas flow from 243 l/min to 361 l/min for propylene, and from 893 l/min to 1,050 l/min for hydrogen. Within a certain total gas flow the fuel gas/oxygen ratio was varied from 0.15 to 0.36 for propylene, and from 1.92 to 3.29 for

hydrogen. The stoichiometric ratios are 0.25 for propylene and 2.00 for hydrogen. Other variable parameters were standoff distance, from 150,mm to 200 mm, and length of the combustion chamber, 19 mm and 22 mm. Typically used spray conditions were exceeded in purpose to produce as wide a velocity-temperature range as possible.

For quasicrystals, two spray conditions were measured by changing the standoff distance from 150 mm to 375 mm. The total gas flow in both conditions was 900 l/min and the fuel gas/oxygen ratio was changed, being 2.83 and 2.21.

2.4 Single splat studies

Single splats were collected on polished steel substrates in order to study the melting level of the particles under different spray conditions. The splats were produced by spraying a low powder feed rate using the same standoff distance as was used in the coating deposition.

Splats collected were studied by optical microscopy to determine the extent of melting of the particles. While the temperature data from diagnostic tests, based on the emissivity of a particle in-flight, provide the surface temperature of the particle, single splats enhance our understanding on the particle state.

Despite the fact that splat collection over a polished surface does not give exact information of the splat spreading over a rough surface, it will give important information of the melting state of the particles in different spray conditions. Studying effect of surface roughness of the splat behavior is included for the process map 2, and is therefore excluded from this study. Table 4 summarizes the spray parameters used for splat studies.

Table 4. Spray parameters in splat studies.

alumina					
Ratio C_3H_6/O_2	**Total flow [l/min]**	**Standoff [mm]**	**Ratio H_2/O_2**	**Total flow [l/min]**	**Standoff [mm]**
0.28	361	150	2.00	1.050	150
0.28	361	200	2.48	1.050	150
0.22	361	150	2.85	1.050	150
0.28	283	150	2.85	1.050	200
			2.17	890	150
			2.85	890	150
quasicrystals					
			2.21	900	150
			2.21	900	225
			2.21	900	300
			2.21	900	375
			2.83	900	150
			2.83	900	225
			2.83	900	300
			2.83	900	375

2.5 Coating deposition

The coatings were sprayed onto grit-blasted carbon steel plates. Table 5 summarizes the spray parameters used in the coating experiments.

Table 5. Spray parameters for coatings.

alumina					
Ratio C_3H_6/O_2	**Total flow [l/min]**	**Standoff [mm]**	**Ratio H_2/O_2**	**Total flow [l/min]**	**Standoff [mm]**
0.28	361	150	2.00	1.050	150
0.28	361	200	2.48	1.050	150
0.22	361	150	2.85	1.050	150
0.28	283	150	2.85	1.050	200
			2.17	890	150
quasicrystals					
			2.21	900	300
			2.83	900	300

2.6 Characterization

The crystal structures of the powders and coatings were characterized by X-ray diffraction (XRD) using Cu-K_α and Mo-K_α radiation. Powder particle size was determined using a Lecotrac – LT100 particle size analyzer.

The scanning electron microscopes used in this work were a JEOL JSM-6400 (SEM) combined with a PGT PRISM 2000 X-ray analyzer, a LEO982 Gemini (FEG-SEM), a Philips CM 200 (FEG-STEM) combined with a Noran Voyager X-ray analyzer, a LEO 1550 model with a Schottky Field Emission gun and a Siemens XL30 equipped with an energy dispersive spectrometer model DX-4 by EDAX. The details of the microscopy used in each study are given in publications related to this work.

Free-standing deposits were evaluated for the porosity content using a Helium pycnometry technique. The skeletal density of the coating in this measurement was measured by the volume of gas (Helium) displaced by the known mass of the substance.[81]

The hardness of the coatings was determined by the Vickers microhardness method using a mass of 300 grams. Instrumented nanoindentation tests with Nanotest 550 and Nanotest 600 instruments, both from Micro Materials Limited UK, equipped with a 0.79 mm ball indenter, were used to characterize the elasto-plastic properties of the coating. Calculation of the elastic modulus was made using the method developed by Field and Swain[82].

The wear resistance of the alumina coatings was evaluated by a rubber wheel abrasion test according to the ASTM G 65-91 standard. The coefficient of friction of the quasicrystal coatings was determined using the Pin-on-Disc test method at room temperature and at 500 °C. The test was carried out according to the ASTM 99 standard. A button test was carried out to study the influence of contact pressure and temperature on friction and wear with higher loads. The test is explained in detail in Publication I.

The thermal conductivity measurements were carried out on a 12.5 mm (0.5”) diameter disk, coated with carbon on both surfaces, using a Holometrix laser flash thermal diffusivity instrument. In this test, the sample is irradiated

uniformly on one side using a single laser beam pulse (1.06 μm wavelength). The temperature rise on the other side is recorded as a function of time using an HgCdTe infrared detector (2–5.5 μm wavelengths). The recorded temperature-rise data, with allowance for the measured sample thickness, are used to calculate the thermal diffusivity directly. Knowledge of the bulk density, together with the thermal diffusivity and specific heat, allows determination of the thermal conductivity.[83]

The dielectric properties were measured using an HP 4294A Impedance Analyzer according to ASTM D150. Using parallel plate principles, the dielectric behavior was observed from 40 Hz to 100 MHz; the values at 10 kHz and 1 MHz are reported here.

The electrical strength of the coatings was tested according to IEC 60243-1 C1.9.1 by increasing the voltage up to the breakdown point. A brass electrode, ∅25 mm, was used over the coating, and a larger brass electrode, ∅75 mm, was placed under the specimen. The voltage was increased linearly from zero up to breakdown with a rate of rise 0.03–0.05 kV/s.

3. Results

3.1 Powder characterization

3.1.1 Alumina

Figure 3 shows the typical morphology of the agglomerated composite powder.

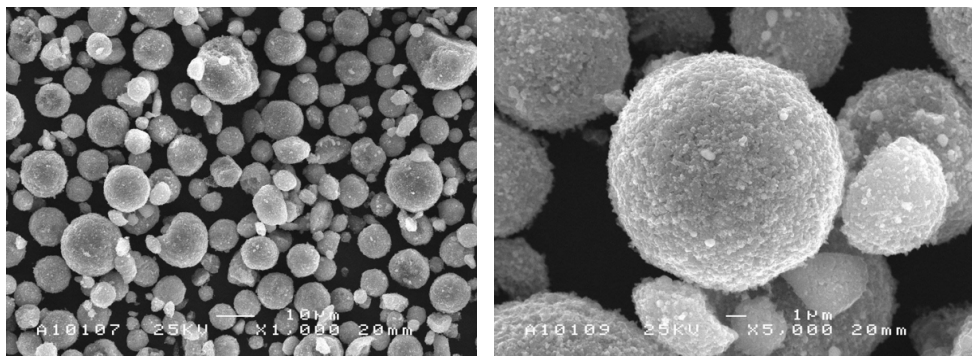

Figure 3. SEM micrographs of the spray-dried Al_2O_3 – 5%Ni particles at a magnification of 500× and 2500×.

3.1.2 Quasicrystals

The quasicrystal powders were analyzed by SEM and Figure 4 shows the morphologies of the quasicrystal powders.

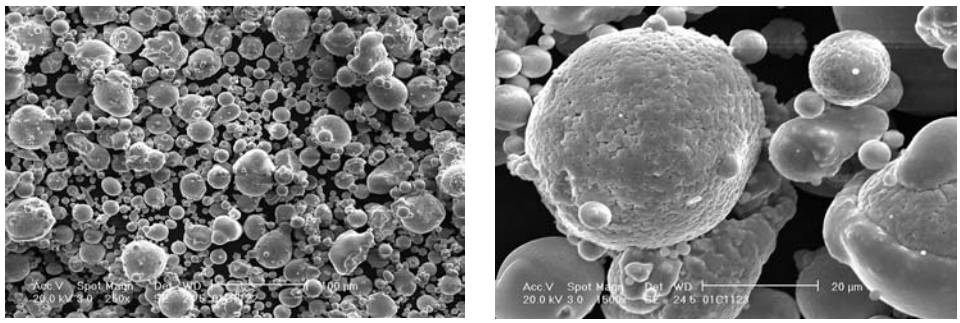

a)

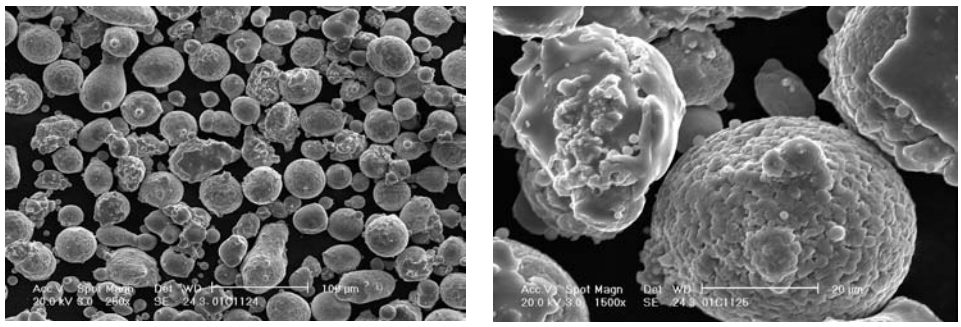

b)

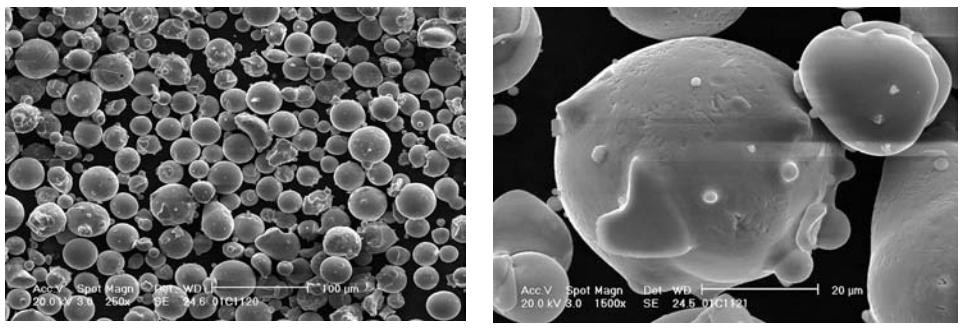

c)

Figure 4. SEM micrographs of the quasicrystal spray particles at a magnification of 125× and 750×. a) F1 powder, b) A1/S powder, c) BTI powder.

3.2 Process optimization

3.2.1 On-line diagnostics

Two different types of on-line diagnostics equipment, DPV-2000 and SprayWatch, were used to determine the effects of variations in the fuel gas, the gas ratios and the total gas flow on the particle velocity and temperature range.

The main work was carried out for alumina by using a DPV-2000 system. Two clear regions of different temperature and velocity arise from the use of different fuel gases as presented in the Figure 5. The operating range of the gas flows and fuel to oxygen ratios was quite different for the two mixtures. The hydrogen-oxygen mixtures typically resulted in a greater velocity of the particles than the propylene-oxygen mixtures. On the other hand, a higher variation between the minimum and maximum values in temperature and velocity was obtained with propylene than with hydrogen. The highest temperatures for propylene were obtained using a fuel gas/oxygen ratio of 0.30. In the case of hydrogen as a fuel gas, the highest temperature was obtained by using a ratio of 2.48.

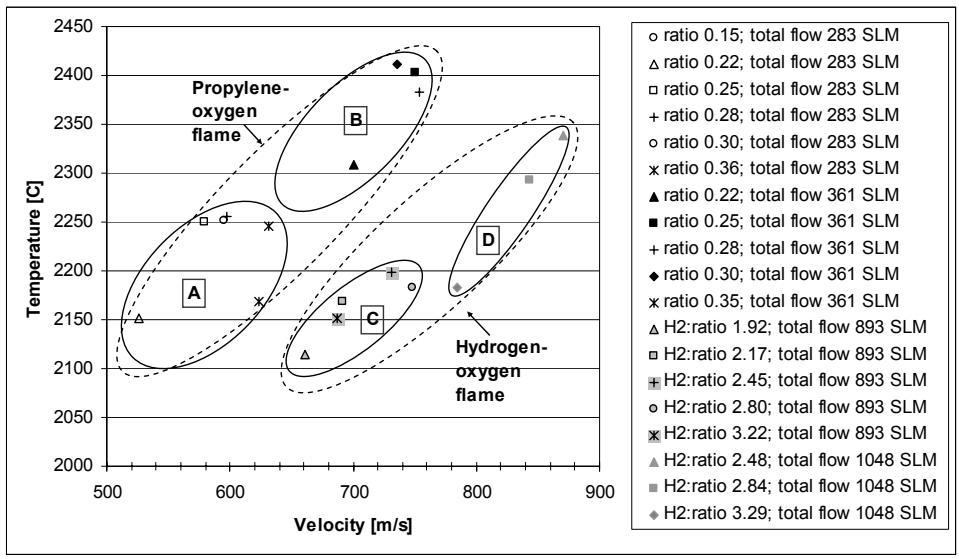

Figure 5. A first order process map for HVOF alumina depicting the range of particle temperatures and velocities for two fuel gas/oxygen mixtures.

Figure 5 also summarizes the findings of the diagnostic study from altering the total gas flow and oxygen/fuel gas ratio. In the Figure, (A) and (B) refer to the zones of velocity and temperature achieved by using a gas mixture of propylene and oxygen while maintaining a total gas flow of 283 l/min and 361 l/min respectively. In general, there was a strong correlation between the velocity and temperature since the two total flow rate zones were separated quite clearly. A similar effect was observed for the zones (C) and (D), which are the values for hydrogen – oxygen gas mixtures with total flow rates of 893 l/min and 1,048 l/min. Within each group of conditions, there is a systematic variation of particle condition depending on the operating parameters.

The total gas throughput flow through the gun had a strong influence on the gas velocity and temperature. Because of this, an almost linear increase in both particle velocity and temperature for a certain fuel gas/oxygen ratio was measured as shown in Figure 6.

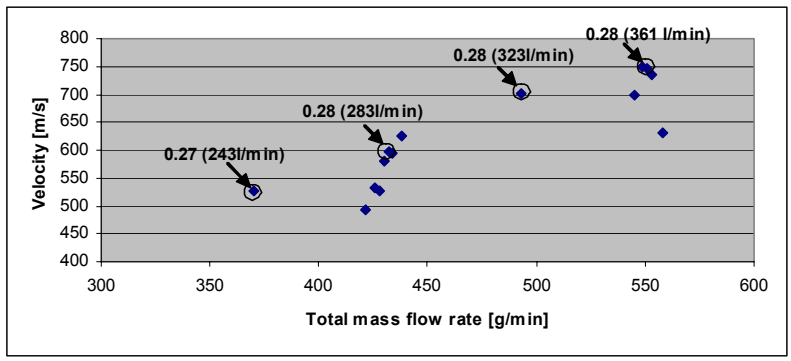

a)

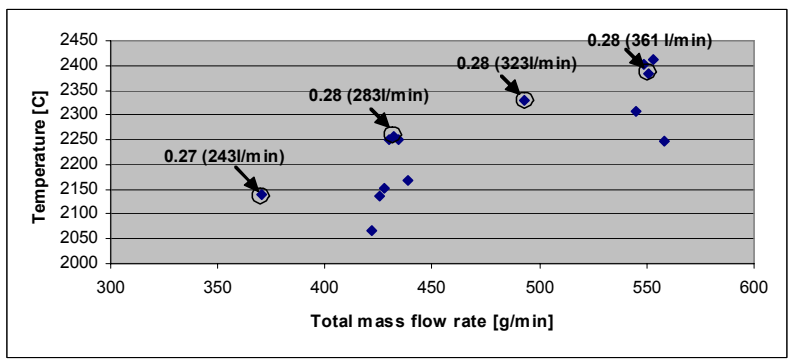

b)

Figure 6. Effect of total gas throughput flow on a) velocity, and b) temperature.

Within a certain total gas flow between different fuel gas/oxygen ratios it was recognized that maximum particle velocities are nearly always obtained at the same time as maximum temperatures. The temperature-velocity maximum was obtained with fuel-rich conditions. Figure 7 shows this trend for the propylene with a total gas flow of 361 l/min, and for hydrogen with a total flow of 893 l/min.

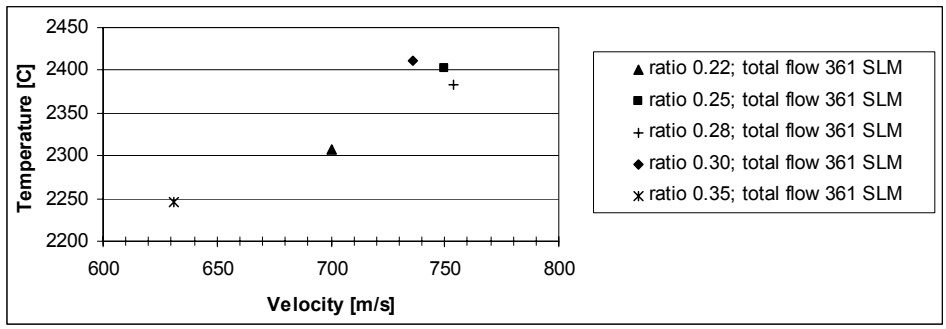

a)

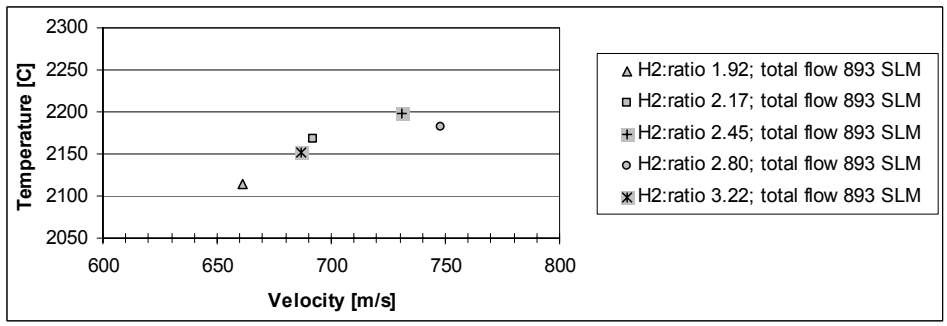

b)

Figure 7. Process diagnostic data for different spray parameter combinations: Effect of gas flow ratio.

The effect of combustion chamber length (22 mm and 19 mm) and the effect of changing the spray distance on the particles temperature-velocity spectrum are shown in Figure 8. Comparing the performance of combustion chambers, it is clear that the length has a significant effect on the particle temperature, but not on the velocity. Longer nozzle length seemed to allow for better combustion of gases and heat transfer to the particles, thereby raising the temperature, but velocity is influenced more by the throughput of gases.

The effect of standoff distance on particle conditions was examined for three different spray distances. As seen in Figure 8, the highest velocity and temperature point was that measured at the shortest spray distance (150 mm), the one with medium values at 175 mm, and the lowest velocity and temperature point at 200 mm.

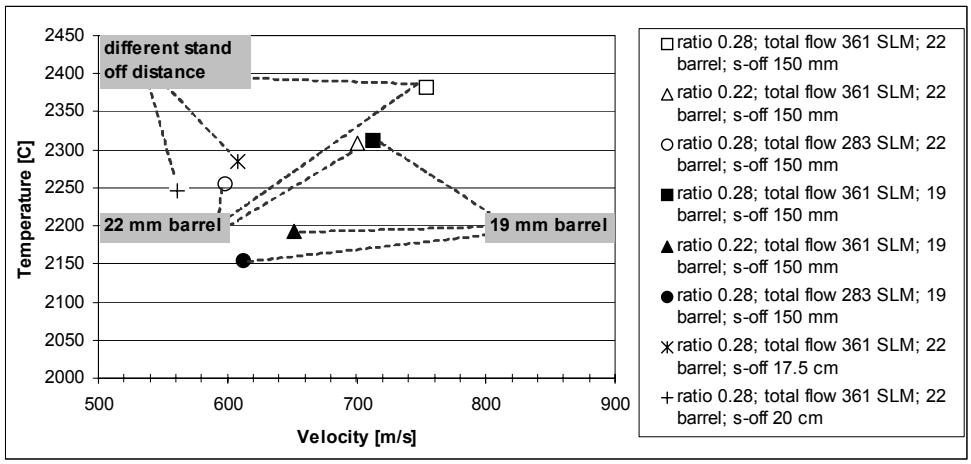

Figure 8. Process diagnostic data for different spray parameter combinations: Effect of barrel length and standoff distance.

3.2.2 Single splat studies

3.2.2.1 Alumina

Single splat studies were carried out for certain selected spray conditions. Large variations in the melting states were obtained under different conditions. Some of the main trends are presented in Figure 9.

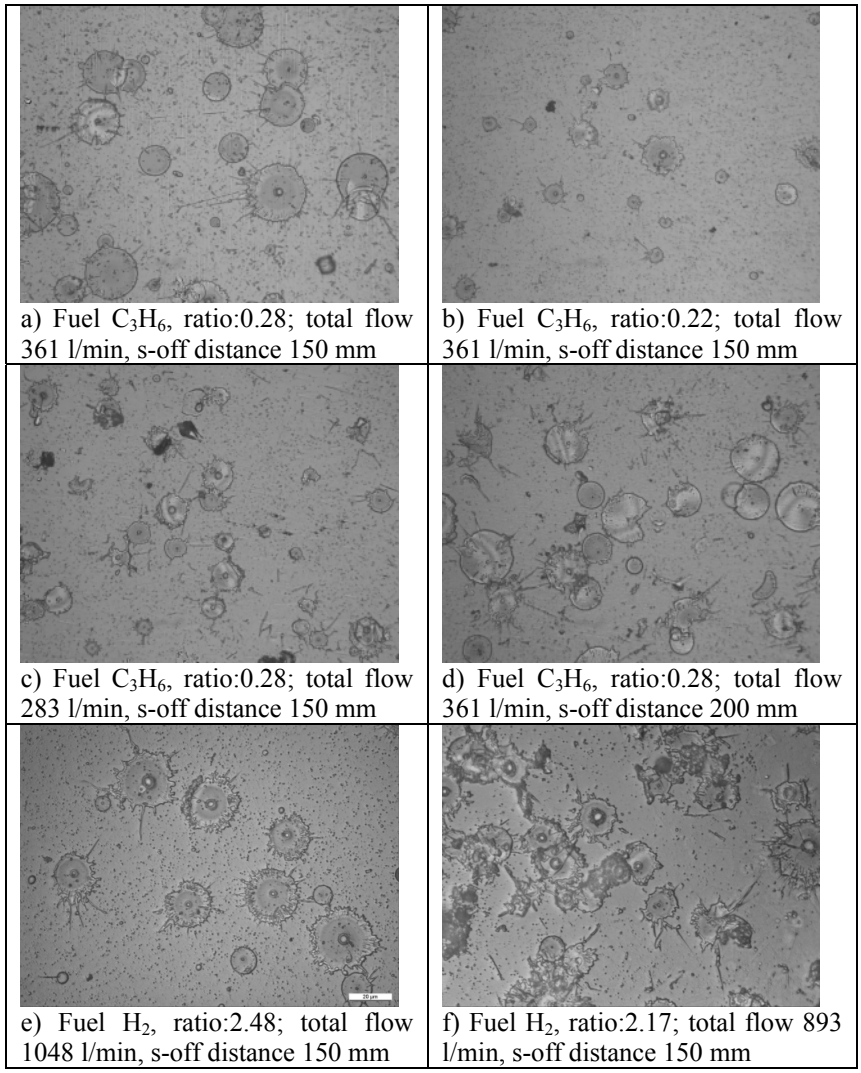

a) Fuel C_3H_6, ratio:0.28; total flow 361 l/min, s-off distance 150 mm

b) Fuel C_3H_6, ratio:0.22; total flow 361 l/min, s-off distance 150 mm

c) Fuel C_3H_6, ratio:0.28; total flow 283 l/min, s-off distance 150 mm

d) Fuel C_3H_6, ratio:0.28; total flow 361 l/min, s-off distance 200 mm

e) Fuel H_2, ratio:2.48; total flow 1048 l/min, s-off distance 150 mm

f) Fuel H_2, ratio:2.17; total flow 893 l/min, s-off distance 150 mm

Figure 9. Micrographs depicting the morphology of the alumina splats collected at different spray parameters. The parameters are explained in detail in Table 4.

Different temperature-velocity points were selected to investigate the effect of the particle surface temperature on the melting behavior of the particle. Particle wetting and flattening is dependent on the particle conditions in the flame. The highest melting stage was obtained for the parameters detailed in Figure 9 (a), thus producing the highest temperature and velocity. A decrease in particle temperatures and velocities due to the changes in fuel gas/oxygen ratio decreased the extent of the melting of the particles (Figure 9 (b)).

The effect of particle flight time on the melting stage in the flame is demonstrated in Figures 9 (c) and (d). With these two parameters, the data obtained from diagnostic measurements were identical but at different stand off distances. Extended dwell time due to the higher standoff distance caused a better melting stage for the particles.

Figures 9 (e) and (f) present splats sprayed by using hydrogen as a fuel gas with two different total gas flows and ratios. Diagnostic studies showed that hydrogen gives slightly lower maximum particle temperatures, but higher velocities compared to propylene (Figure 9 (a)). Hydrogen fuel gas with a lower total gas flow rate (Figure 9 (f)) was selected for comparison of lower and higher particle temperature and velocity to the melting stage of the particle. Melting is good with both hydrogen parameters. In general, the use of hydrogen as a fuel gas resulted in a larger degree of fragmentation compared to the use of propylene as a fuel gas (compare Figures 9 (a) and (d)). This is attributed to increased particle velocities.

Splat thicknesses were analysed in more detail with three hydrogen conditions: those being A) 2.85–1,050 l/min-150 mm, B) 2.85–1,050 l/min-200 mm and C) 2.00–1,050 l/min-15 0mm. The average thickness was found to be 0.55 µm for condition A, 0.76 µm for condition B, and 0.48 µm for condition C. The results confirm the visual observations and diagnostic data, showing the lowest flattening at condition B due to the lowest particle temperature and velocity. Flattening of the particles increased (thickness decreased) with increasing particle velocity and temperature. The medians of the splat diameters were 19.25 µm for condition A, 18.8 µm for condition B, and 19.8 µm for condition C. As expected, the trend as, opposite to that of the diameters. Diameter was smallest with condition B, where splat thickness was highest. In all cases, the largest particles have not attached to the substrate. Partly, this is assumed to result from the polished surface, and partly from the semi-molten state of the larger particles.

3.2.2.2 Quasicrystals

Two fuel gas/oxygen ratios with a total flow of 900 l/min were selected for the splat studies. It was found that the powder melting state varies with the spray distance. Figure 10 is clear proof of this.

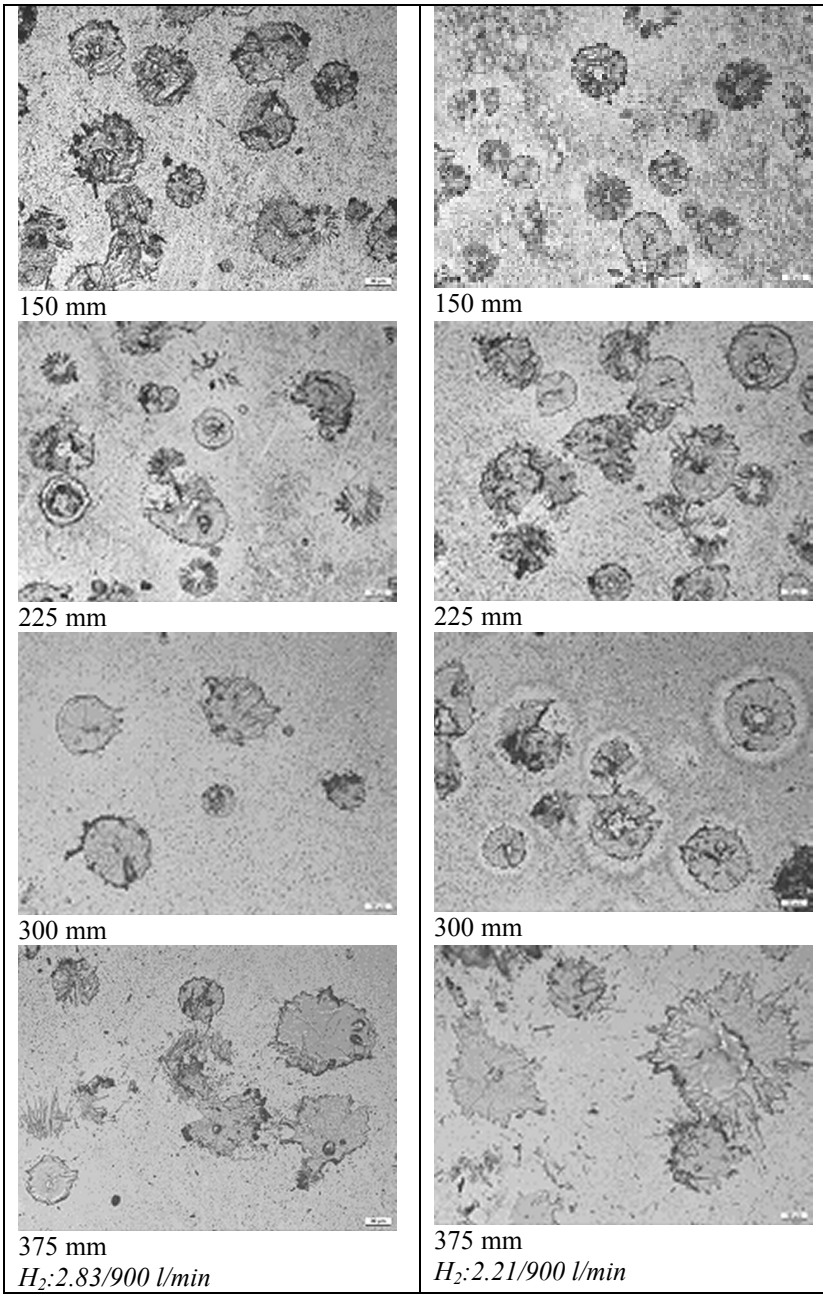

Figure 10. Illustration of the sprayed quasicrystal splats.

The melting stage of the particles when using a standoff distance of 300 mm is much higher than that produced with standoff distances of 150 mm and 225 mm. The shorter spray distances do not give enough time for the particles to melt. The melting was even more extensive with a spray distance of 375 mm, but this condition showed reduced particle flux, as well as low particle velocity, and cannot, therefore, result in good coating quality with a good deposition rate.

3.2.3 Coating characterization and properties

Alumina. Alumina coatings were produced from the powders presented in Chapter 2.1.

The coatings produced from commercial alumina powder with a conventional grain size have a clear correlation between their microstructure and the data obtained from the diagnostic tools. The best quality coatings were produced in conditions manifested by the highest particle temperature and velocity: a fuel gas /oxygen ratio of 0.28 with a total flow of 361 l/min for propylene, and a fuel gas /oxygen ratio of 2.48 with a total flow of 1050 l/min for hydrogen.

When working with agglomerated powder having a pure or composite nanofraction structure, the optimum spray conditions were slightly shifted from the ratio of 2.48. A stoichiometric fuel gas ratio (ratio 2.00) and ratio of 2.85 produced coatings with a highest density. Both conditions representing slightly lower particle temperatures compared with the ratio of 2.48. While working with nanostructured powders, the optimal spray condition should include sufficient melting without overheating combined with high particle velocity. Based on the splat studies, melting was sufficient with the gas ratios of 2.00 and 2.85. This can be assumed to result from the agglomerated powder structure. Condition 2.48, which was found to be best for the fused and crushed reference powder, caused a large amount of fragmentation, which can in turn be assumed to decrease coating uniformity. In the case of the agglomerated structure, a fuel-rich condition with a ratio of 2.85 was found to result in the best quality coatings ranked on the microstructure and wear behavior.

Increasing the spray distance was found to degrade the quality of the coating microstructure, resulting in a coating with higher porosity and poor flattening of

the particles. The differences in the microstructures are presented in Figure 11. These are micrographs from polished cross sections obtained by SEM in BEI mode in order to ensure a good contrast for illustrating the flattening stage and coating microstructure.

In all cases the amount of alpha phase was very low because of the high melting level of the particles. For n-Al_2O_3 powder the α/γ ratio was 9%/91% for a coating of 2.85–1050 l/min-150mm, 8%/82% for a coating of 2.85–1050 l/min-200mm, and 3%/97% for a coating of 2.00–1050 l/min-150mm.

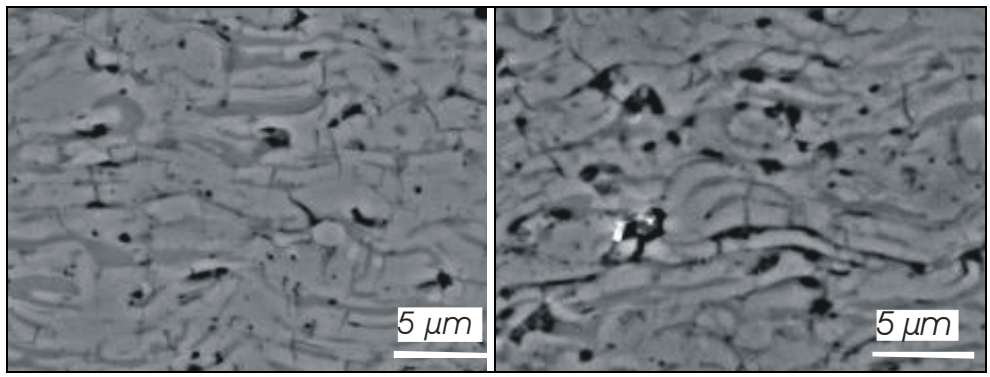

Figure 11. Effect of the standoff distance on the coating microstructure a) 150 mm, b) 200 mm.

A coating microstructure inside one lamella was studied by high resolution SEM. A high resolution SEM image of the fracture surface of an n-Al_2O_3 coating (2.00–1,050 l/min-150 mm) is shown in Figure 12. Alumina grains with dimensions in a range of hundreds of nanometers are observed. It should be noted that the fine structure seems to have been retained in spite of extensive melting of the powder in the HVOF process and only a small amount of α-Al_2O_3 in the structure.

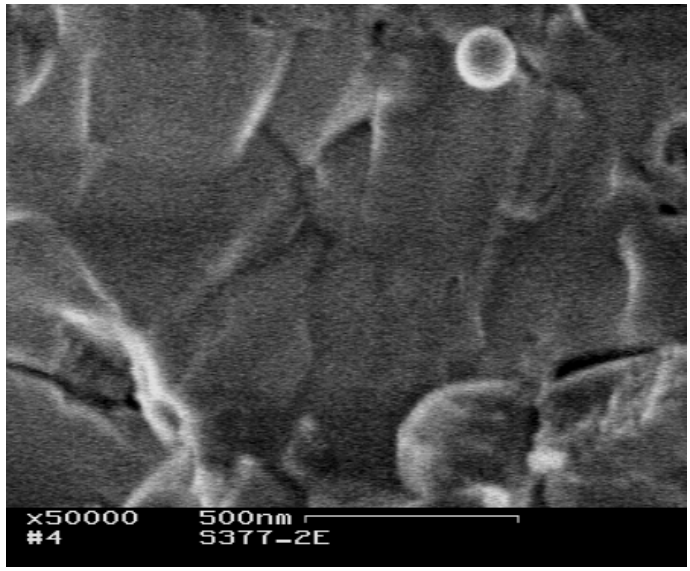

Figure 12. An FEG-SEM micrograph of a fracture surface of an n- Al_2O_3 - HVOF coating.

Some differences in the coating microstructure were observed for the Ni-alloyed nanostructured composite coatings between spray conditions with a ratio of 2.00 and a ratio of 2.85. The distribution of nickel in the polished cross sections of the samples as revealed by the back-scattered electron imaging is shown in Figures 13 (a) and (b). These micrographs indicate that nickel is partly deposited into the splat boundaries, i.e. interlamellarily. A coating sprayed with a ratio of 2.00 has a lower amount of nickel transferred to the lamella boundaries.

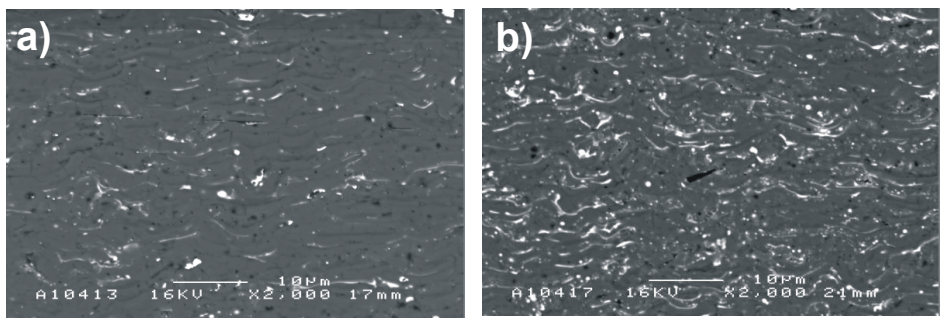

Figure 13. SEM-BEI micrograph of the polished cross sections for the coatings sprayed with different spray parameters a) n-Al_2O_3-5%Ni (ratio 2.00), b) n-Al_2O_3-5%Ni (ratio 2.85).

Different mechanical properties were determined for alumina coatings, including hardness, abrasive wear resistance and elastic modulus. Some electrical properties were also studied, including dielectric constant and breakdown strength. Figure 14 summarizes some results.

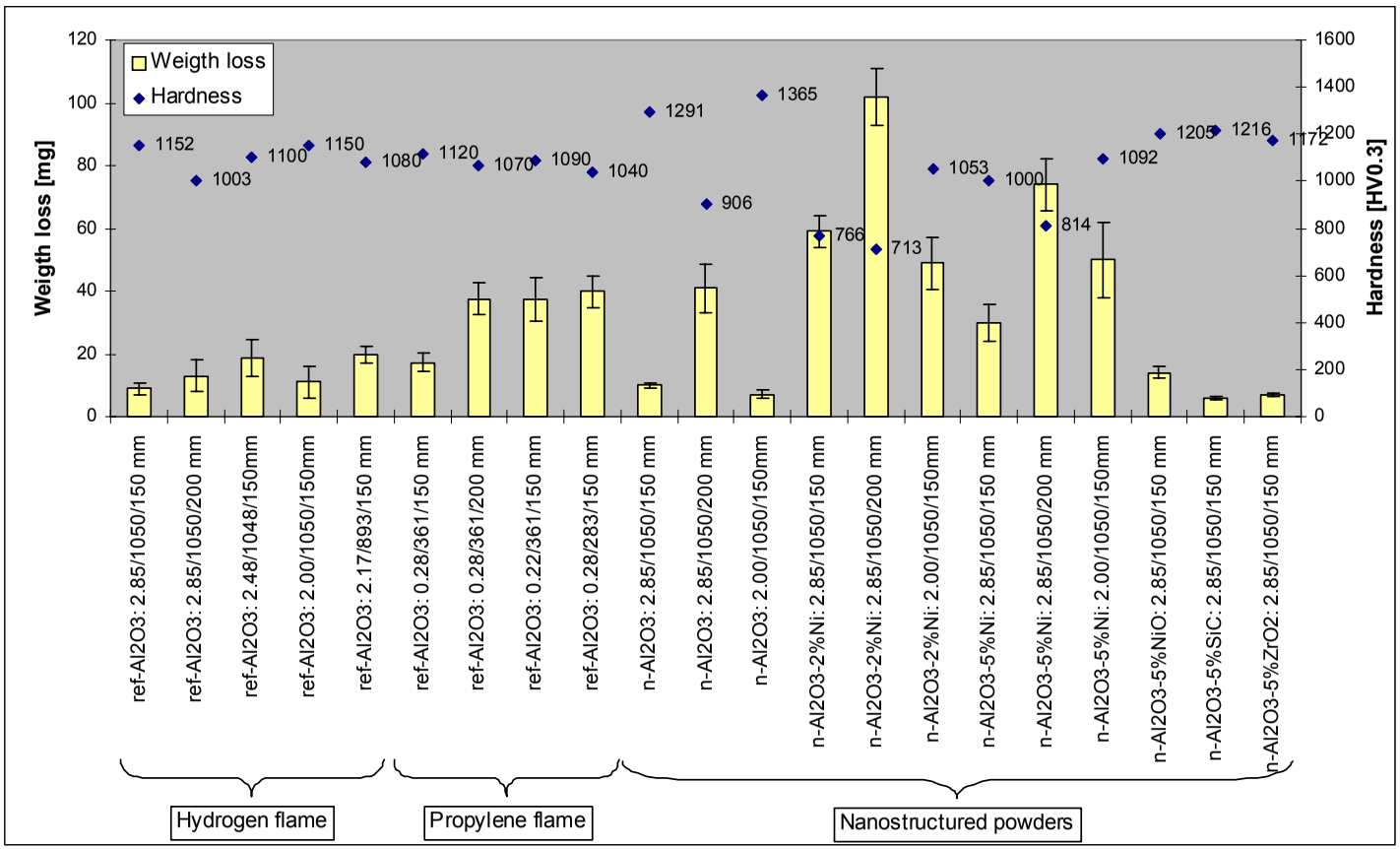

Figure 14. Hardness and weight loss in the abrasive rubber wheel wear test measurements for different alumina coatings.

Quasicrystals. The microstructure and the phase structure were studied for the coatings sprayed with the parameters detailed in the Table 5. It was found that dense and well-bonded coatings with partially or almost 100% quasicrystalline microstructures could be obtained, depending on the coating material. The main differences in the coatings made using spray parameters A and B were in the amount of porosity and oxidation of the particles.

It was concluded from the differences in the phase transformation and coating structure optimization between the different powders that the *Al-Cu-Fe* coating (F1) could only be deposited with a partially quasicrystalline coating consisting of quasicrystalline icosahedral i-$Al_{65}Cu_{20}Fe_{15}$ and crystalline cubic β-AlFe phases. The main difference between the two conditions was the formation of a thicker oxide layer with parameter A. An *Al-Cu-Fe-Cr* coating (A1/S) also formed a two-phase structure, but in this case both phases were quasicrystalline: $Al_{80}Cr_{13,5}Fe_{6,5}$ and $Al_{13}Cr_3Cu_4$. The *Al-Co-Fe-Cr* coating (BT1) was most interesting and consisted of the very rarely reported dodecagonal phase $Al_{70.6}Co_{12.5}Fe_{9.4}Cr_{7.5}$.

It was found that the Al-Cu-Fe alloy (F1) was the most sensitive to phase transformations, Al-Cu-Fe-Cr (A1/S) formed two different phases, but was mainly quasicrystalline, and Al-Co-Fe-Cr (BT1) was the most stable and fully quasicrystalline with a wide range of process parameters.

Relatively high values of the coefficient of friction (CoF) were obtained in the PoD test. These tests yielded friction values typically varying between 0.4–0.6, independent of the counter material. While the coefficient of friction was unexpectedly high at low temperatures, it seemed that increasing the temperature up to 500 °C did not increase the CoF. This is an encouraging result regarding the possible high-temperature use of these coatings. Based on the results, it can be concluded that the material is very stable up to relatively high temperatures, and no change in tribological behavior was recorded.

Interesting results were obtained in torsional testing of the coatings with various counter materials. In general, friction appeared to depend on the contact pressure induced, but not in a straightforward manner as depicted in Figure 15. During the tests, the contact pressure was varied between 5 and 15 MPa. The coefficient of friction increased first with the increased surface pressure being highest (0.35)

at the pressure of 10 MPa. A further increase in surface pressure decreased CoF close to the starting value (approx. 0.25). When the surface pressure was adjusted back to 10 MPa, the measured CoF was much lower (0.18–0.23) compared to the previously measured values. The history-dependence of the friction seems to indicate that pressure-dependent changes occur in the tribofilm. In certain circumstances this seems to be very beneficial when friction decreases with increasing pressure.

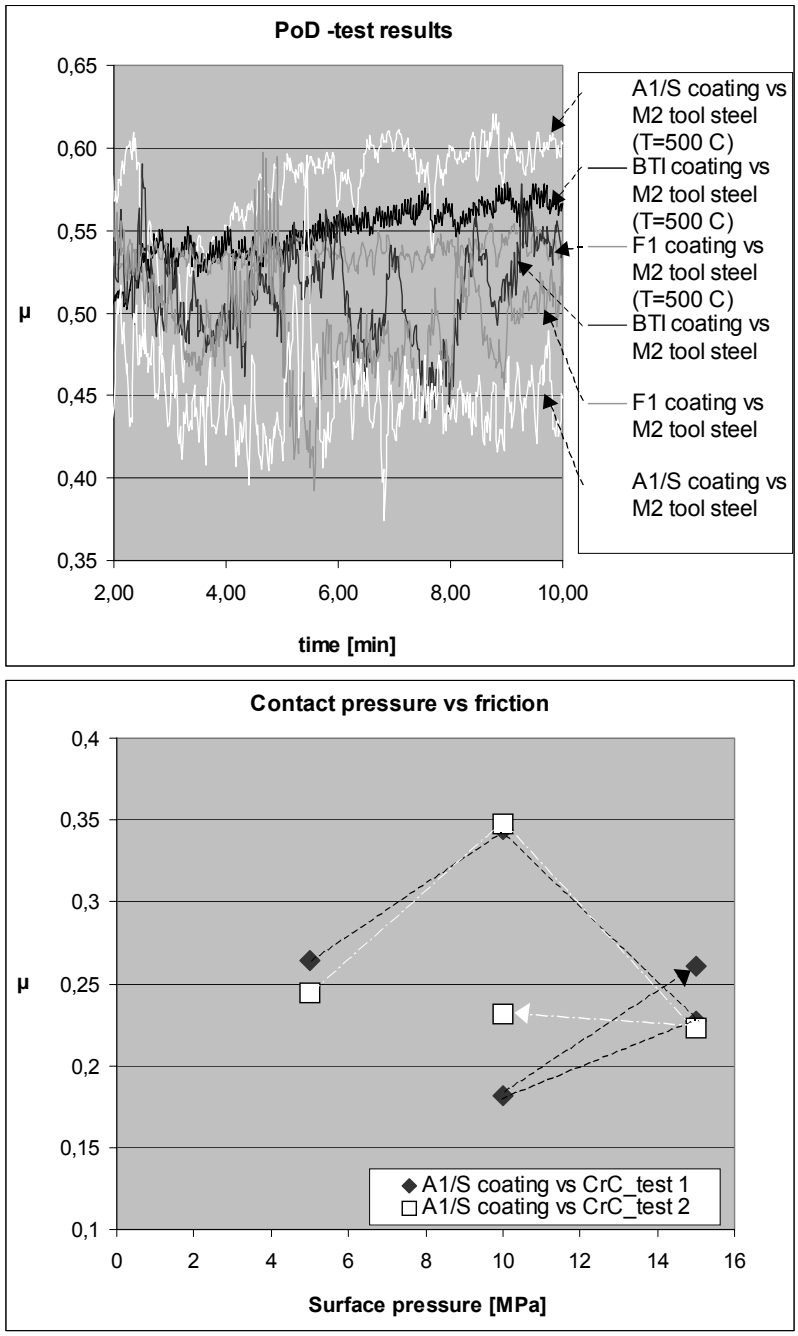

Figure 15. a) PoD test of the QC coatings against M2 steel, b) average friction v. contact pressure in A1/S-Cr_3C_2-NiCr contact.

4. Discussion

Detailed on-line diagnostic studies were carried out on HVOF-sprayed alumina coatings for the first time. These were based on investigation of the fuel gas/oxygen ratio and total gas flow effect on the coating structure.

Diagnostic studies confirmed the findings of Lugscheider[31, 36] and Hanson[37] who proposed that hydrogen produces particles with higher velocity and lower temperatures. Therefore, hydrogen can be considered a more optimal fuel gas when spraying materials that are sensitive to overheating. On the other hand, use of propylene offers a wider process window in terms of particle temperature and velocity, and allows more variation in the process conditions. Normally this can be considered to increase the risks in process reliability, but in some special cases this can be also considered to offer more possibilities to affect the coating structure.

Total gas throughput has a straightforward effect on the gas velocity. An increase in total gas flow increases both particle velocity and temperature at a certain fuel gas/oxygen ratio. This correlates well with the findings of Planche[38].

Maximum temperature was obtained with fuel-rich conditions – 0.25–0.30 for propylene-oxygen ratios and 2.45–2.85 for hydrogen-oxygen ratios – in the case of alumina. It was also recognized that maximum particle velocities inside one total gas flow were nearly always obtained at the same time as maximum temperatures.

Particle velocity is clearly dependent on the spray distance, this being highest with a short spray distance. In the case of alumina the decrease in velocity was 25% when the standoff distance increased from 150 mm to 200 mm. In the case of quasicrystals the decrease was 10–20% when the standoff distance increased from 150mm to 225 mm. The difference is correlated to the weight of the particles. Due to the higher weight of the quasicrystal particles, the decrease in velocity is not as high as that of the alumina particles. The effect of the standoff distance on the particle temperature was different for alumina and QCs. In the case of alumina the measured temperatures decreased by 5% due to the growth in the spray distance. In the case of quasicrystals the temperature rose 1–2% with standoff distances of 150 mm to 225 mm and were highest at the longest

spray distance of 375 mm. The behavior of the QCs correlates well with the findings of Lugscheider for MCrAlY materials[36]. The reduction in temperatures with alumina powder can be assumed to result from the poorer flight properties of the smallest alumina particles. Thus larger particles with a lower surface temperature were measured at greater distances.

Splat formation correlated well with the diagnostic studies. The melting stage was typically most advanced at the highest temperatures. However, the dwell time had an effect on the melting stage, which cannot be directly observed from the diagnostic studies. An increased standoff distance with "hotter" flame parameters resulted in a higher melting stage for the particles compared with a lower standoff distance and "colder" flame parameters. Still, these two conditions gave equal particle velocity-temperature data in the diagnostic studies. This is a clear example of the fact that information obtained from the on-line diagnostics gives only the v/T data for the particle in a certain position and does not take into account the v/T -history concerning what the particle has gone through previously.

The microstructure of the alumina coating was related to the particle velocities and the melting stage of the particles. In the case of pure alumina with a conventional grain size, the maximum melting of the particle was expected to produce a dense coating. Figure 16 summarizes the findings. Measured particle velocity and temperature data is plotted against coating abrasive wear resistance and hardness. A weight loss of 20 mg and hardness of HV 1,100 were taken for the limits. The formed first order process map shows the clear correlation between particle melting behavior and the abrasive wear resistance and the hardness. The process map shows that by using hydrogen as a fuel gas, higher variations in spray conditions are tolerated in order to produce a coating with good wear resistance. The change in hardness was slightly more sensitive for hydrogen gas flows. A decrease in particle velocity is assumed to have an effect on the lamella adhesion.

A wider melting spectrum was obtained for propylene. Due to this, the number of process conditions producing the high temperature suitable for sufficient alumina melting is lower than that for hydrogen. This results in a much narrower window for optimal spray parameters when working with propylene as a fuel gas.

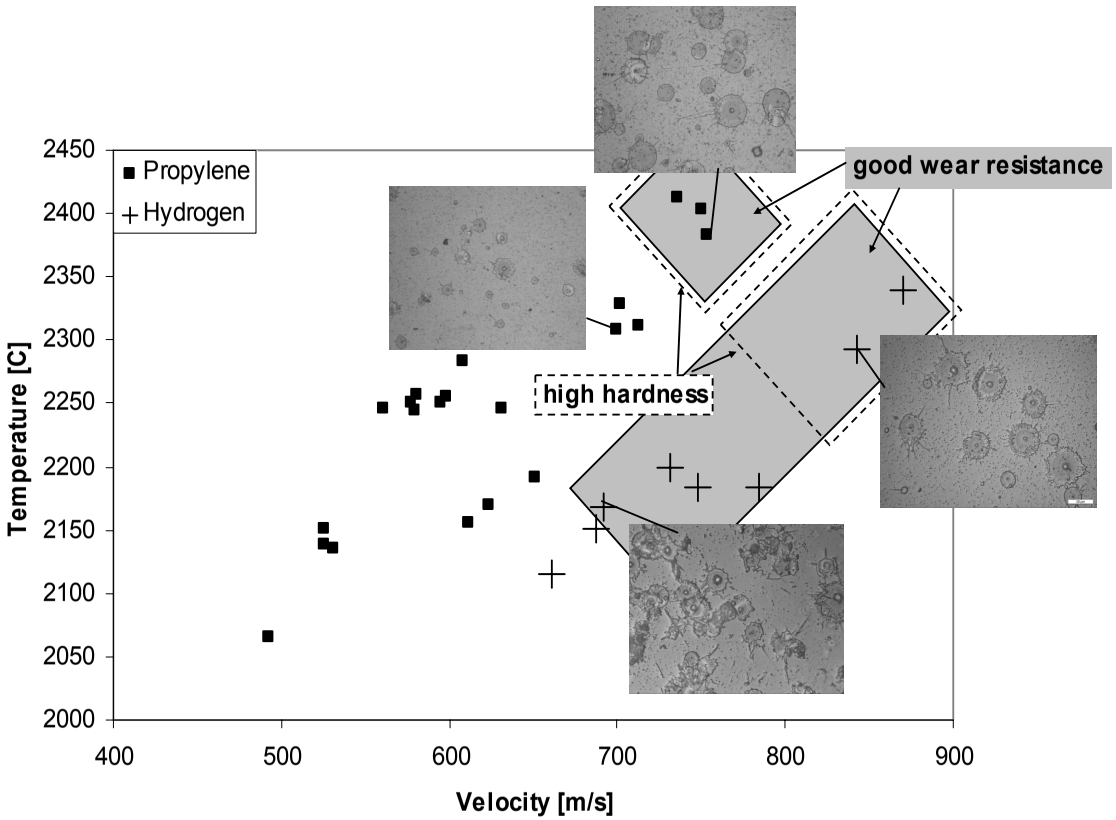

Figure 16. The first order process map for alumina plotted against wear resistance and hardness of the produced coatings.

With nanostructured alumina the coating microstructure and mechanical properties also correlated strongly with the particle melting stage. It was recognized that it is not possible to improve the mechanical properties of the entire coating without sufficient interlamellar adhesion, despite the desired microstructure and crystal size of one lamella. Therefore, the interlamellar adhesion is dominant for the mechanical properties of the coating and must be prioritized in the parameter selection. The obtained results correlated with the results published for APS sprayed nanostructure alumina-titania coatings, where obtained hardness values are reported to be in the range of 1,100 $HV_{0.3}$.[75]

The studies showed that the coating microstructure can be estimated from the diagnostic data and splat studies. Due to the coarser particle size of the quasicrystalline materials, and their higher density, the standoff distance for optimal coating formation was much higher than that for alumina; 300 mm was found to be optimal. The two selected conditions did not markedly change the coating structure. The main difference between the two parameters was the thickness of the oxidation layer for composition *Al-Cu-Fe* being higher for condition A, which is a more oxygen-rich condition than that of condition B. A similar trend was observed with the composition *Al-Co-Fe-Cr*, where the oxygen-rich condition produced a higher amount of oxidation. Introducing chromium into the structure (composition *Al-Cu-Fe-Cr*) increased the amount of quasicrystalline phases and was concurrently reflected in the negligible oxidation. It must be noted that the particle temperature and velocities were not actually varied much compared with the dwell time of the particle in the flame due to the long standoff distance. Therefore, no large differences in particle melting behavior between the two conditions can be expected. The formed coating structure was in agreement with the earlier studies made by APS spraying for the same type of composition, although HVOF spraying produced a coating with less porosity.

5. Summary and conclusions

Diagnostic tools, including on-line diagnostic and single splat studies, were shown to be an effective tool for the process optimization of the HVOF spray process. The usability of diagnostic tools was demonstrated when working with materials having a narrow processing window with regard to melting and degradation temperatures.

It was shown that diagnostic results can be correlated with the coating microstructure and coating properties in HVOF spraying. It was also demonstrated that the coating properties and coating quality can be improved by optimizing and carefully selecting the spray parameters.

This work concentrated on the optimization of the micro and phase structure of the coating. It must be pointed out that control of the internal stresses of the coating is also essential in order to develop high-performance coatings.

It was clearly pointed out during the work that the coating density, including splat flattening and interlamellar adhesion, is important in order to produce high-performance coatings and that it must be prioritized in the coating parameter optimization.

References

[1] Davis, J.R. (Ed.). Handbook of Thermal Spray Technology. Thermal Spray Society, ASM International, Materials Park, OH, USA (2004), p. 338.

[2] Heinrich, P. Thermal spraying – Facts and state of the art. Sonderdruck, E10/92 (1992), p. 28.

[3] Pawlowski, L. The science and engineering of thermal spray coatings. John Wiley & Sons, New York, NY, USA (1995), p. 432.

[4] Kulkarni, A., Gutleber, J., Sampath, S., Goland, A., Lindquist, W.B., Herman, H., Allen, A.J. & Dowd, B. Studies of the microstructure and properties of dense ceramic coatings produced by high-velocity oxygen-fuel combustion spraying. Materials Science and Engineering A369(2004), pp. 124–137.

[5] Ramm, D.A.J., Clyne, T.W., Sturgeon, A.J. & Dunkerton, S. Correlations between spraying conditions and microstructure for alumina coatings produced by HVOF and VPS. Proceedings of the 7th National Thermal Spray Conference, 20–24 June, 1994, Boston, Massachusetts, USA (1994, pp. 239–244.

[6] Sturgeon, A.J., Harvey, M.F.D. & Blunt, F.J. The influence of fuel gas on the microstructure and wear performance of alumina coatings produced by the High Velocity Oxyfuel (HVOF) thermal spray process. British Ceramic Proceedings, Vol. 54(1997), pp. 57–64.

[7] Sturgeon, A.J. Recent advantages and applications of thermal sprayed ceramic coatings, British Ceramic proceedings, Vol. 55(1996), pp. 3–12.

[8] Sampath, S., Jiang, X., Kulkarni, A., Matejicek, J., Gilmore, D.L. & Neiser, R.A. Development of process maps for plasma spray: case study for molybdenum. Materials Science and Engineering A348(2003), pp. 54–66.

[9] Kreye, H., Schwetzke, R. & Zimmermann, S. High velocity oxy-fuel flame spraying process and coating characteristics. Thermal Spray: Practical solutions for Engineering Problems. Berndt, C.C. (Ed.). Published by ASM International, Materials Park, Ohio-USA (1996), pp. 451–456.

[10] Li, M., Shi, D. & Christofides, P.D. Model-based estimation and control of particle velocity and melting in HVOF thermal spray. Chemical Engineering Science 59(2004), pp. 5647–5656.

[11] Dubsky, J. & Matějiček, J. Residual and applied stresses in thermally sprayed metallic and ceramic coatings, Thermal Spray 2002. Proceedings, International Thermal Spray Conference (ITSC 2002), Essen, 4–6 March 2002. Lugscheider, E. (Ed.). (2002), pp. 606–609.

[12] Allen, A.J., Long, G.G., Boukari, H., Ilavsky, J., Kulkarni, A., Sampath, S., Herman, H. & Goland, A.N. Microstructural characterization studies to relate the properties of thermal spray coatings to feedstock and spray conditions. Surface and Coatings Technology, 146–147(2001), pp. 544–552.

[13] Friis, M. & Persson, C. Control of thermal spray process by means of process maps and process windows. Journal of Thermal Spray Technology, 12, 1(2003), pp. 44–52.

[14] Nylén, P., Lemaitre, J. & Wigren, J. Sensitivity of four on-line diagnostic systems for plasma spraying. Thermal spray 2003: Advancing the science and applying technology. Moreau, C. & Marple, B. (Eds.). Published by ASM International, Materials Park, Ohio-USA (2003), pp. 1101–1106.

[15] Steffens, H.-D. & Duda, T. Enthalpy measurement of direct current plasma jets used for ZrO_2-Y_2O_3 thermal barrier coatings. Journal of Thermal Spray Technology, 9, 2(2000), pp. 235–240.

[16] Tucker, R.C. Jr. Integrated thermal spray systems – some practical considerations. Thermal spray 2001: New surfaces for a new millennium. Berndt, C.C., Khor, K.A. & Lugscheider, E.F. (Eds.). Published by ASM International, Materials Park Ohio, USA (2001), pp. 1261–1266.

[17] Hämäläinen, E., Vattulainen, J., Alahautala, T., Hernberg, R., Vuoristo, P. & Mäntylä, T. Imaging diagnostics in thermal spraying – "SprayWatch" system. Thermal Spray Surface Engineering via Applied Research, Proceedings, 1st International Thermal Spray Conference (ITSC 2000), Montreal, Quebec, Canada; 8–11 May 2000, pp. 79–83.

[18] Fincke, J.R., Swank, W.D., Bewley, R.L. & Haggard, D.C. Control of particle temperature, velocity, and trajectory in thermal spray process. Thermal spray 2003: Advancing the science and applying technology. Moreau, C. & B. Marple, B. (Eds.). Published by ASM International, Materials Park, Ohio-USA (2003), pp. 1093–1099.

[19] Moreau, C., Gougeon, P., Lamontagne, M., Lacasse, V., Vaudreuil, G. & Cielo, P. On-line Control of the Plasma Spraying Process by Monitoring the Temperature, Velocity and Trajectory of In-Flight Particles. Proceedings of the 7th National Thermal Spray Conference 20–24 June 1994, Boston, USA (1994), pp. 431–437.

[20] Fincke, J.R., Haggard, D.C. & Swank, W.D. Particle Temperature Measurement in the Thermal Spray Process. Journal of Thermal Spray Technology, 10, 2(2001), pp. 255–266.

[21] Vuoristo, P., Ahmaniemi, S., Nuutinen, S., Mäntylä, T., Hämäläinen, E., Arola, N. & Vattulainen, J. Optimisation and monitoring of spray parameters by a CCD camera based imaging thermal spray monitor. Thermal spray 2001: New surfaces for a new millennium. Berndt, C.C., Khor, K.A. & Lugscheider, E.F. published by ASM International, Materials Park Ohio, USA (2001), pp. 727–736.

[22] Lugscheider, E., Fischer, E., Koch, D. & Papenfuß, N. Diagnostics of in flight particle properties and resulting coating qualities on atmospheric plasma process, Thermal Spray 2001. New Surfaces for a New Millennium, Proceedings, International Thermal Spray Conference (ITSC 2001), Singapore; 28–30 May 2001, pp. 751–758.

[23] Bianchi, L., Blein, F., Lucchese, P., Vardelle, M., Vardelle, A. & Fauchais, P. Effect of particle velocity and substrate temperature on alumina and zirconia splat formation. Proceedings of the 7th National Thermal Spray Conference 20–24 June 1994, Boston, USA (1994), pp. 569–574.

[24] Fan, X., Gitzhofer, F. & Boulos, M. Investigation of alumina splats formed in the induction plasma process. Journal of Thermal Spray Technology, Vol. 7, No. 2, June 1998, pp. 197–204.

[25] Fauchais, P., Vardelle, A., Vardelle, M., Denoirjean, A., Pateyron, B. & El Ganaoui, M. Formation and layering of alumina splats: thermal history of coating formation, resulting stresses and coating microstructure. Thermal Spray 2001. New Surfaces for a New Millennium, Proceedings, International Thermal Spray Conference (ITSC 2001), Singapore; 28–30 May 2001, pp. 865–873.

[26] Fukanuma, H. & Ohmori, A. Behaviour of molten droplets impinging on flat surfaces, Effect of particle velocity and substrate temperature on alumina and zirconia splat formation. Proceedings of the 7th National Thermal Spray Conference 20–24 June 1994, Boston, USA (1994), pp. 563–568.

[27] Sampath, S. & Jiang, X. Splat formation and microstructure development during plasma spraying: deposition temperature effects. Materials Science and Engineering A304–306 (2001), pp. 144–150.

[28] Vardelle, M., Vardelle, A., Leger, A.C. & Fauchais, P. Dynamics of splat formation and solidification in thermal spraying process. Proceedings of the 7th National Thermal Spray Conference 20–24 June 1994, Boston, USA (1994), pp. 555–562.

[29] Sundararajan, G., Sivakumar, G. & Srinivasa Rao, D. The interrelationship between particle velocity and temperature, spalt formation and deposition efficiency in detonation sprayed alumina coatings. ITSC 2001: International Thermal Spray Conference 2001, Singapore; 28–30 May 2001, pp. 849–858.

[30] Hackett, C.M. & Settles, G.S. Independent control of HVOF particle velocity and temperature, Thermal Spray: Practical solutions for Engineering Problems. Berndt, C.C. (Ed.). Published by ASM International, Materials Park, Ohio-USA (1996), pp. 665–673.

[31] Lugscheider, E., Herbst-Dederichs, C. & Zhao, L. Particle behavior in a powder-laden HVOF jet. ITSC 2000: 1st International Thermal Spray Conference; Montreal, Quebec; Canada; 8–11 May 2000, pp. 501–508.

[32] Yamada, H., Kuroda, S., Fukushima, T. & Yumoto, H. Capture and evaluation of HVOF thermal sprayed particles by a gel target. ITSC 2001: International Thermal Spray Conference 2001, Singapore; 28–30 May 2001, pp. 797–-804.

[33] Sobolev, V.V., Guilemany, J.M. & Martin, A.J. Engineering Formulas for flattening of composite particles during thermal spraying. Thermal Spray, A united forum for scientific and technological advances, ASM international (1997), 653–656.

[34] Sobolev, V.V. & Guilemany, J.M. Formation of splats during thermal spraying of composite powder particles. Materials Letters 42(2000), pp. 46–51.

[35] Sampath, S., Jiang, X.Y., Matejicek, J., Prchlik, L., Kulkarni, A. & Vaidya, A. Role of thermal spray processing method on the microstructure, residual stress and properties of coatings: an integrated study for Ni-5 wt.%Al bond coats. Materials Science and Engineering A364(2004), pp. 216–231.

[36] Lugscheider, E., Herbst, C. & Zhao, L. Parameter studies on high-velocity oxy-fuel spraying of MCrAlY coatings. Surface and coatings technology 108–109(1998), pp. 16–23.

[37] Hanson, T.C. & Settles, G.S. Particle temperature and velocity effects on the porosity and oxidation of an HVOF corrosion-control coating. Journal of thermal spray technology 12, 3(2003), pp. 403–415.

[38] Planche, M.P., Normand, B., Liao, H., Rannou, G. & Coddet, C. Influence of HVOF spraying parameters on in-flight characteristics of Inconel 718 particles and correlation with the electrochemical behaviour of the coating. Surface and coatings technology 157(2002), pp. 247–256.

[39] Gil, L. & Staia, M.H. Influence of HVOF parameters on the corrosion resistance of NiWCrBSi coatings. Thin solid films 420–421(2002), pp. 446–454.

[40] Li, M. & Christofides, P.D. Multi-scale modelling and analysis of an industrial HVOF thermal spray process. Chemical engineering science 60 (2005), pp. 3649–3669.

[41] Li, M., Shi, D. & Christofides, P.D. Diamond jet hybrid HVOF thermal spray: gas-phase and particle behaviour modeling and feedback control design. Industrial and engineering chemistry research 43(2004), pp. 3632–3652.

[42] Shi, D., Li, M. & Christofides, P.D. Diamond jet hybrid HVOF thermal spray: rule-based modelling of coating microstructure. Industrial and engineering chemistry research 43(2004), pp. 3653–3665.

[43] Dolatabadi, A., Pershin, V. & Mostaghimi, J. Effect of flow regime on particle velocity in the high velocity oxyfuel (HVOF) [spraying] process, Thermal Spray 2002. Proceedings, International Thermal Spray Conference (ITSC 2002), Essen, 4–6 March 2002. Lugscheider, E. (Ed.). Publ: 40010 Dusseldorf, Germany; DVS-Verlag, for Deutscher Verband fur Schweissen und verwandte Verfahren; 2002, pp. 918–925.

[44] Hackett, C.M., Settles, G.S. & Miller, J.D. On the gas dynamics of HVOF thermal sprays. Journal of Thermal Spray Technology 3(3) Sept. 1994, pp. 299–304.

[45] Hearley, J.A., Little, J.A. & Sturgeon, A.J. The effect of spray parameters on the properties of high velocity oxy-fuel NiAl intermetallic coatings. Surface and coatings technology 123(2000), pp. 210–218.

[46] Ignatiev, M., Smurov, I. & Bertrand, P. Application of digital CCD camera for monitoring of particle-in-flight parameters in plasma and HVOF spraying, Thermal Spray 2002. Proceedings, International Thermal Spray Conference (ITSC 2002), Essen, 4–6 March 2002. Lugscheider, E. (Ed.). DVS-Verlag, for Deutscher Verband für Schweissen und verwandte Verfahren; Dusseldorf, Germany (2002), pp. 72–77.

[47] Bertrand, P., Smurov, I. & Ignatiev, M. Low cost industrial type diagnostic system for powder jet visualisation, particle-substrate interaction and coating growth, Thermal Spray 2002. Proceedings, International Thermal Spray Conference (ITSC 2002), Essen, 4–6 March 2002. Lugscheider, E. (Ed.). DVS-Verlag, for Deutscher Verband fur Schweissen und verwandte Verfahren; Dusseldorf, Germany; (2002), pp. 66–71.

[48] Arsenault, B., Legoux, J.G., Hawthorne, H., Immarigeon, J.P., Gougeon, P. & Moreau, C. HVOF process optimization for the erosion resistance of WC-12Co and WC-10Co-4Cr coatings. ITSC 2001: International Thermal Spray Conference 2001, Singapore; 28–30 May 2001, pp. 1051–1060.

[49] Devasenapathi, A., Shimizu, Y., Kazuhiko, S. & Minamida, T. Effect of spraying parameters on the microstructure of alumina coating sprayed by high velocity oxyfuel (HVOF) method. Nippon Yosha Kyokai Shi (Journal of Japan Thermal Spraying Society), 36, 1(1999), pp. 1–11.

[50] Lima, R.S. & Marple, B.R. Fro APS to HVOF spraying of conventional and nanostructured titania feedstock powders: a study on the enhancement of the mechanical properties. Surface and coatings technology (2004) article in press, available online (http://www.sciencedirect.com)

[51] Saravanan, P., Selvarajan, V., Rao D.S., Joshi, S.V. & Sundararajan, G. Influence of process variables on the quality of detonation gun sprayed alumina coatings. Surface and coatings technology 123(2000), pp. 44–54.

[52] Niemi, K., Vuoristo, P., Kumpulainen, E., Sorsa, P. & Mäntylä, T. Recent Developments in the Characteristics of Thermally Sprayed Oxide Coatings. Proceedings of 14th international thermal spray conference, 22–26 May 1995, Kobe, Japan (1995), p. 687–694.

[53] Liu, Y., Fischer, T.E. & Dent, A. Comparison of HVOF and plasma sprayed alumina/titania coatings-microstructure, mechanical properties and abrasion behaviour. Surface and Coatings Technology 167(2003), pp. 68–76.

[54] Kadyrov, V., Evdokimenko, Y., Kisel, V. & Kadyrov, E. Calculation of the limiting parameters for oxide ceramic particles during HVOF spraying. Proceedings of the 7th National Thermal Spray Conference 20–24 June, 1994, Boston, Massachusetts, USA (1994), pp. 245–250.

[55] Sordelet, D.J., Besser, M.F. & Anderson, I.E. Particle size effects on chemistry and structure of Al-Cu-Fe quasicrystalline coatings. Journal of thermal spray technology 5, 2(1996), pp. 161–174.

[56] Lang, C.I., Shechtman, D. & Gonzalez, E. Friction and wear properties of quasi-periodic material coatings. Bull. Mater. Sci., 22(1999), pp. 189–192.

[57] Sordelet, D.J., Kramer, M.J., Anderson, I.E. & Besser, M.F. Microstructural evaluation, oxidation and wear of Al-Cu-Fe quasicrystalline coatings. Proceedings of the fifth international conference of quasicrystals (1995), pp. 778–785.

[58] De Palo, S., Usmani, S., Sampath, S., Sordelet, D.J. & Besser, M. Friction and wear behaviour of thermally sprayed Al-Cu-Fe quasicrystalline coatings. Thermal Spray, A united forum for scientific and technological advances, ASM international (1997), pp. 135–139.

[59] Fleury, E., Lee, S.M., Kim, W.T. & Kim, D.H. Effects of air plasma spraying parameters on the Al-Cu-Fe quasicrystalline coating layer. Journal of Non-Crystalline Solids 278(2000), pp. 194–204.

[60] Sordelet, D.J., Besser, M.F. & Kramer, M.J. Thermal spray quasicrystalline coatings. Part 1: relationship among processing, phase structure and splat morphology. Proceedings of the 15th international thermal spray conference, 25–29 May 1998, Nice, France (1998), pp. 467–471.

[61] Kuroda, S. Properties and characterisation of thermal sprayed coatings – a review of recent research progress. Proceedings of the 15th international thermal spray conference, 25–29 May 1998, Nice, France (1998), pp. 539–550.

[62] De Palo, S., Usmani, S., Kishi, K., Sampath, S., Sordelet, D.J. & Besser M.F. Thermal spray quasicrystalline coatings. Part II: relationships among processing, phase assemblage and tribological response. Proceedings of the 15th international thermal spray conference, 25–29 May 1998, Nice, France (1998), pp. 705–710.

[63] Anderson, C.W. & Heffner, K.H. Precision gas bearing plasma sprayed aluminium oxide coating characterization. Proceedings of the international thermal spray conference, Orlando, USA 28 May–5 June 1992, pp. 695–704.

[64] Ramachandran, K., Selvarajan, V., Ananthapadmanabhan, P.V. & Sreekumar, K.P. Microstructure, adhesion, microhardness, abrasive wear resistance and electrical resistivity of the plasma sprayed alumina and alumina-titania coatings. Thin Solid Films, 315, (1998), pp. 144–152.

[65] Swindeman, C.J., Seals, R.D., Murray, W.P., Cooper, M.H. & White, R.L. An investigation of the electrical behaviour of thermally sprayed aluminium oxide, Practical solutions for engineering problems. Berndt, C.C. (Ed.). ASM International, Materials Park, Ohio-USA (1996), pp. 793–797.

[66] Shackelford, J.F. Materials science and engineering handbook. Third edition, CRC press, Boca Raton, Florida, USA (2001), p. 1949.

[67] Levin, I., Bendersky, L.A., Brandon, D.G. & Rühle, M. Cubic to monoclinic phase transformations in alumina. Acta Mater. 9(1997), pp. 3659–3669.

[68] Devi, M.U. On the nature of phases in Al2O3 and Al2O3-SiC thermal spray coatings. Ceramics international 30(2004), pp. 545–553.

[69] Niemi, K., Vuoristo, P., Mäntylä, T., Lugscheider, E., Knuuttila, J. & Jungklaus, H. Wear characteristics of oxide coatings deposited by plasma spraying, high power plasma spraying and detonation gun spraying. Proceedings of the 8th national thermal spray conference, 11–15 September 1995, Houston, USA (1995), pp. 645–650.

[70] Hannula, S.-P., Koskinen, J., Haimi, E. & Nowak, R. Mechanical properties of nanostructured materials. Encyclopedia of Nanoscience and Nanotechnology, 5. Nalwa, H.S. (Ed.). American Scientific Publishers. California, USA (2004), pp. 31–162.

[71] Mayo, M.J. High and low temperature superplasticity in nanocrystalline materials. Nanostruct. Mater. 9(1997), pp. 717–726.

[72] Mohamed, F.A. & Li, Y. Creep and superplasticity in nanocrystalline materials: current understanding and future prospects. Mater. Sci. Eng. 298A(2001), pp. 1–15.

[73] Sekino, T., Nakajima, T. & Niihara, K. Mechanical and magnetic properties of nickel dispersed alumina-based nanocomposite. Materials letters 29(1996), pp. 165–169.

[74] Oh S.-T., Sando M. & Niihara K. Processing and Properties of Ni-Co Alloy Dispersed Al_2O_3 Nanocomposites. Scripta Materialia 39(1998), pp. 1413–1418.

[75] Shaw, L.L., Goberman, D., Ren, R., Gell, M., Jiang, S., Wang, Y., Xiao, T.D. & Strutt, P.R. The dependency of microstructure and properties of nanostructured coatings on plasma spray conditions. Surface and coatings technology 130(2000), pp. 1–8.

[76] Gell, M., Jordan, E.H., Sohn, Y.H., Goberman, D., Shaw, L. & Xiao, T.D. Development and implementation of plasma sprayed nanostructured ceramic coatings. Surface and Coatings Technology 146–147(2001), pp. 48–54.

[77] Jordan, E.H., Gell, M., Sohn, Y.H., Goberman, D., Shaw, L., Jiang, S., Wang, M., Xiao, T.D., Wang, Y. & Strutt, P. Fabrication and evaluation of plasma sprayed nanostructured alumina-titania coatings with superior properties. Mater. Sci. Eng. 301(2001), pp. 80–89.

[78] Goberman, D., Sohn, Y.H., Shaw, L., Jordan, E. & Gell, M. Microstructure development of Al_2O_3-13wt.%TiO_2 plasma sprayed coatings derived from nanocrystalline powders. Acta Materialia, 50(2002), pp. 1141–1152.

[79] Sordelet, D.J & Dubois, J.M. Quasicrystals: Perspectives and potential applications. MRS Bulletin, November 1997, pp. 34–37.

[80] Besser, M.F. & Eisenhammer, T. Deposition and applications of quasicrystal coating. MRS Bulletin, November 1997, pp. 59–64.

[81] Tamari, S. & Aguilar-Chàvez, A. Optimum Design of Gas Pycnometers for Determining the Volume of Solid Particles. Journal of Testing and Evaluation 33, 2(2005), p. 4.

[82] Field, J.S. & Swain, M.V. A Simple Predictive Model for Spherical Indentation. J. Mater. Res. 8, 2(1993), p. 297.

[83] Parker, W. Flash Method of Determining Thermal Diffusivity, Heat Capacity and Thermal Conductivity. J. Appl. Phys. 32, 9(1961), p. 1679.

Appendix I of this publication is not included in the PDF version.
Please order the printed version to get the complete publication
(http://www.vtt.fi/inf/pdf/)

PUBLICATION II

Microstructural characterisation of thermally sprayed quasicrystalline Al-Co-Fe-Cr coatings

In: Journal of Alloys and Compounds 2003.
Vol. 354, No. 1–2, pp. 269–280.

ELSEVIER

Journal of Alloys and Compounds 354 (2003) 269–280

Journal of ALLOYS AND COMPOUNDS

www.elsevier.com/locate/jallcom

Microstructural characterisation of thermally sprayed quasicrystalline Al–Co–Fe–Cr coatings

E. Huttunen-Saarivirta[a,*], E. Turunen[b], M. Kallio[c]

[a]*Tampere University of Technology, Institute of Materials Science, P.O. Box 589, Fin-33101, Tampere, Finland*
[b]*VTT Technical Research Centre of Finland, Surface Engineering and Laser Processing, P.O. Box 1703, Fin-02044 VTT, Tampere, Finland*
[c]*VTT Technical Research Centre of Finland, Materials and Chemicals, Hermiankatu 8 G, P.O. Box 16071, Fin-33101, Tampere, Finland*

Received 20 November 2002; accepted 4 December 2002

Abstract

A microstructural characterisation was carried out for Al–Co–Fe–Cr feed powder and the coatings sprayed with a high velocity oxy-fuel method using different operation conditions. The aims of the study were to explore the structural development of thick Al–Co–Fe–Cr coatings and the influence of the spraying parameters on the microstructure of produced Al–Co–Fe–Cr coatings. X-ray diffractometry, scanning electron microscopy and analytical transmission electron microscopy were the techniques used in the phase identification and in the microstructural exploration of the study. The results show that Al–Co–Fe–Cr feed powder and the coatings sprayed with low and high operation temperature are composed of a dodecagonal quasicrystalline phase. The composition of this new dodecagonal phase approximately corresponds to that of the feed powder, being $Al_{70.6}Co_{12.5}Fe_{9.4}Cr_{7.5}$. The dodecagonal phase does not decompose during the spraying process. Instead, it orientates to form a lamellar coating structure. When a lower spraying temperature is used, the incomplete melting of powder particles introduces a partly orientated coating structure. Due to this incomplete melting of powder particles, porosity is also involved in these coatings. Higher spraying temperature, in turn, promotes oxidation, leading to the incorporation of an oxygen-containing film on the splat boundaries. While the feed powder and the coating deposited with a lower spraying temperature are one-phase quasicrystalline structures, the coating sprayed with a higher operation temperature is comprised of a dodecagonal phase and an oxygen-containing phase. This oxygen-containing phase is not pure aluminium oxide but contains all the elements present in the alloy.

Keywords: Transition metal alloys; Quasicrystals; Coating materials; TEM; SEM

1. Introduction

Quasicrystals are materials where a repeating periodicity in an atom arrangement exists together with a rotational symmetry forbidden for crystalline materials; fivefold, eightfold, tenfold and even twelvefold symmetries have been encountered in quasicrystals [1]. The first observation of a fivefold symmetry in a rapidly-solidified Al–Mn alloy in 1984 [2] triggered an intense theoretical study of quasicrystals. The examination of a new and exceptional structure of quasicrystals, the survey of their physical and mechanical properties and the development of theories explaining the observed qualities have been the central academic research topics during the last two decades. However, the focus of the research is currently shifting closer to the reality; much interest is nowadays concentrated on finding practical production techniques and applications for these materials.

The first method used to prepare quasicrystalline phases was melting followed by a rapid quenching using the melt spinning technique [2]. Nowadays the fabrication of quasicrystalline materials is possible by a number of different manufacturing methods making use of the variety of the solidification rates of melt [3,4], powder metallurgical processes [5–7] and thin film techniques [8–12]. Besides quasicrystals in bulk, powder or thin film form

*Corresponding author. Tel.: +358-3-365-2912; fax: +358-3-365-2330.
E-mail address: elina.huttunen-saarivirta@tut.fi (E. Huttunen-Saarivirta).

0925-8388/02/$ – see front matter
doi:10.1016/S0925-8388(02)01361-0

introduced by these synthesis methods, quasicrystalline coatings with greater thickness are pursued in order to get the full advantage of the attractive combination of surface characteristics associated with quasicrystalline materials: a low surface energy [13–15], a low coefficient of friction [14,16], a good corrosion resistance [13], a high hardness [1,17,18] and a good abrasive wear resistance [19]. Thermal spraying has been shown [20–25] to be a versatile method for producing thick quasicrystalline coatings with these qualities.

So far, the majority of studies on the thermally sprayed quasicrystalline coatings have concentrated on the different modifications of the ternary base alloys Al–Cu–Fe and Al–Ni–Co [21–27]. In this study, the quasicrystalline coatings of a quaternary alloy Al–Co–Fe–Cr are produced by a high velocity oxy-fuel (HVOF) spraying technique. Although the formation of a quasicrystalline structure in thin films of this alloy has been reported after heat treatments [28,29], no studies deal with the structural development of thick Al–Co–Fe–Cr coatings. Another unknown area is the influence of spraying parameters on the microstructure of Al–Co–Fe–Cr coatings deposited by thermal spraying.

The aim of this study is to extract this lack of scientific data on the formation of microstructure in Al–Co–Fe–Cr thermally sprayed coatings. In the current study, thermally sprayed quasicrystalline Al–Co–Fe–Cr coatings are produced from an Al–Co–Fe–Cr feed powder by the HVOF spraying technique with two different operation conditions. The phases in the feed powder and in the formed thick coatings are identified and the sensitivity of coating microstructure to the spraying conditions such as temperature is examined. X-ray diffractometry (XRD), scanning electron microscopy (SEM) and analytical transmission electron microscopy (ATEM) are used for the microstructural characterisation of Al–Co–Fe–Cr feed powder and HVOF sprayed coatings.

2. Experimental procedure

2.1. Preparation of coatings

Al–Co–Fe–Cr coatings were applied on low carbon steel substrates by a high velocity oxy-fuel (HVOF) spraying technique. HVOF spraying technique is a thermal spraying method, where the spray powder is fed to a gas flow of high pressure, and which yields coatings of low porosity and, thus, good surface properties [30]. In the present study, the spray powder was a commercial powder Christome BT1 manufactured by Saint-Gobain Advanced Ceramics SNMI, France. The composition of the powder, given by the manufacturer, was 52.8 wt.% Al, 20.4 wt.% Co, 15.3 wt.% Fe and 11.2 wt.% Cr, which corresponds to the composition 70.1 at.% Al, 12.4 at.% Co, 9.8 at.% Fe and 7.7 at.% Cr. The particle size of the powder ranged from 20 to 53 μm.

The coatings were sprayed using a HV-2000 spray gun by Praxair Surface Technologies (USA). The gun was operated by a Model 3440 console utilising a model 1262 volumetric powder feeder by Plasmatron Pvt. Ltd. (USA). A two-axis traverse unit with a rotating spindle of a 200 mm inner diameter was used to manipulate the gun and substrates during the coating deposition. The spray distance was 300 mm in the spraying experiments of the study. In the HVOF process, nitrogen was used as a carrier gas, along with hydrogen as a fuel gas. The coatings were sprayed under two different operation conditions, varying the flow of hydrogen and oxygen and their ratio. The gas flow ratio generally determines the temperature of the flame [30], the higher oxygen content promoting the higher flame temperature. This also applied to the HVOF spraying process of the study. The thickness of the HVOF sprayed coatings also varied as a result of different operating conditions. The spraying conditions used in the study and the resulting coating thicknesses are shown in Table 1.

Temperature of the sprayed particles was studied through the spraying diagnostics. SprayWatch 2i imaging system from Oseir Ltd. (Finland), designed for the quality control of industrial thermal spray processes, was used for the on-line measurements of in-flight particles' temperature in the spray. It has to be noticed that these temperature measurements conducted during the spraying experiments only introduced the surface temperature of powder particles. Due to the low thermal conductivity of the powder particles, however, the true temperature of the inner part of particles cannot be evaluated. For the same reason, the temperature difference measured between the surfaces of particles does not correspond to the true temperature difference between the inner parts of the particles. The surface temperature of powder particles, thus, only gives a rough approximation about the scale of temperature the powder particles reach during the spraying process. The observations on the microstructural characteristics of studied Al–Co–Fe–Cr coatings deposited under different operating conditions further support these suggestions about the greater temperature difference as measured between the powder particles sprayed with different gas flow conditions.

Table 1
HVOF spraying conditions and the resulting coating thicknesses

Coating	O_2 l/min	H_2 l/min	H_2/O_2 ratio	Surface temperature of powder particles, °C	Thickness, μm
A	235	665	2.83	1950	470
B	280	620	2.21	1980	250

2.2. Microstructural characterisation of coatings

The microstructural characterisation of Al–Co–Fe–Cr coatings was performed by X-ray diffraction (XRD) measurements, scanning electron microscopy (SEM) and analytical transmission electron microscopy (ATEM). XRD measurements were carried out using a model Diffrac 500 diffractometer by Siemens (Germany) and copper Kα radiation. The XRD analyses were performed with powdery samples. Thus, the studied coatings were stripped off their substrates and crushed into powdery form in a mortar. In addition to the powdery coating samples, the feed powder was characterised by XRD in order to reveal the possible phase transitions introduced by the coating process. The microstructure of the feed powder and the sprayed coatings was also studied with a scanning electron microscope model XL30 by Siemens (The Netherlands), equipped with an energy dispersive spectrometer (EDS) model DX-4 by EDAX International (USA). The cross-sectional samples were used in the SEM studies. The feed powder and the sprayed coatings were further examined by an analytical transmission electron microscope JEM 2010 by JEOL (Japan) equipped with a Noran Vantage energy dispersive spectrometer by ThermoNoran (The Netherlands). The ATEM was operated at an accelerating voltage of 200 kV. ATEM examination was conducted for powdery samples; the coating samples were prepared similarly as for the XRD analyses.

3. Results and discussion

3.1. XRD analysis

In the XRD analysis, the feed powder and the powdery samples of coatings A and B were characterised in order to identify the compounds and phases they are composed of. In addition to the phase qualification, the aim of the XRD measurements was to reveal the possible phase transitions introduced by the coating process.

Fig. 1 shows the XRD patterns for the Al–Co–Fe–Cr feed powder and the HVOF sprayed coatings A and B. For all these samples, the peak with the highest intensity appears at about 43.5° in 2θ scale. Comparing the trace from the feed powder (Fig. 1(a)) to the trace obtained from the HVOF sprayed coatings (Figs. 1(b) and (c)) reveals microstructural evolution to take place during spraying; the intensity of the highest-intensity-peak has increased during the spraying operation. The location of the peaks does not change prominently, thus, no reaction is proposed to take place. However, the number of peaks and the intensities related to them somewhat change during the spraying of the feed powder. For the feed powder, the number of peaks in the XRD spectrum totals almost ten. In contrast, only five distinguishable peaks can be noticed in the XRD patterns of the HVOF sprayed coatings; mainly the small peaks are erased from the XRD spectra due to spraying. These findings are proposed to be linked to the texture evolution. The microstructural development during the

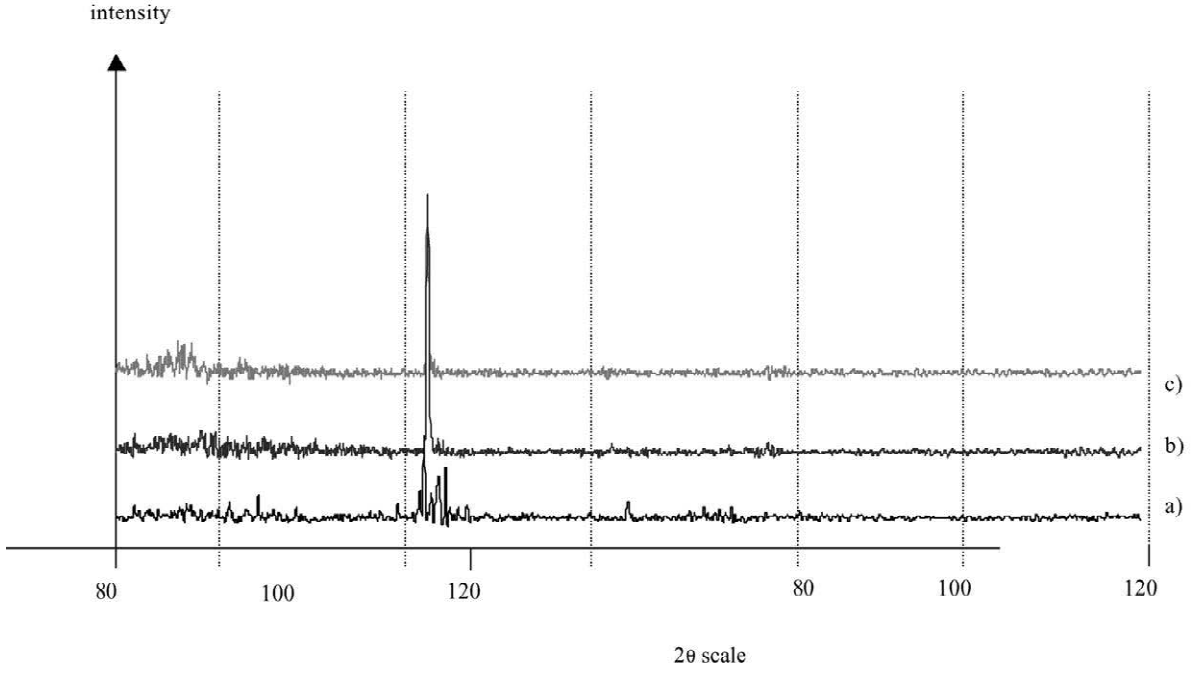

Fig. 1. XRD patterns for (a) Al–Co–Fe–Cr spray powder, (b) the Al–Co–Fe–Cr coating A sprayed with the lower spraying temperature, (c) the Al–Co–Fe–Cr coating B sprayed with the higher spraying temperature.

spraying is, accordingly, thought to be brought about by the orientation of grains during the spraying to yield texture into coatings. Besides, the small number of peaks observed in the XRD spectra of the feed powder and specially the HVOF sprayed coatings allows us to assume that only one or a maximum of two phases can create them.

The feed powder BT1 has earlier been analysed with XRD by Reyes-Gasga et al. [28,29]. They suggest the powder to be composed of Co_2O_3, $A1_2O_3$, Al_2Co_2, $A1_{86}Cr_{14}$ and $A1_{80}Cr_{20}$. From these compounds and alloys, $A1_{86}Cr_{14}$ and $A1_{80}Cr_{20}$ are quasicrystalline with fivefold rotational symmetry and, accordingly, icosahedrally structured. Applying this analysis of Reyes-Gasga et al. to the XRD patterns of the feed powder and the HVOF sprayed coatings A and B of this study indicates that they should mainly be composed of $A1_{86}Cr_{14}$ because the major peak in their XRD pattern corresponds to this quasicrystalline alloy. However, the smaller peaks of the coatings can not be connected to $A1_{86}Cr_{14}$ or any other of the named compounds or alloys. This fact as well as the perception that Fe is not included in any of the components suggested by Reyes-Gasga et al. [28,29] emerged; the feed powder and the coatings of the study are not composed of any of the compounds or alloys proposed by Reyes-Gasga et al. [28,29].

In thin films synthesised from the feed powder BT1, Reyes-Gasga et al. [28,29] observed a quasicrystalline decagonal phase $A1_{58}Cr_{20}O_{17}Fe_5$. However, knowing the existence and composition of this decagonal phase and the availability of numerous crystalline phases and intermetallic compounds for the system Al–Co–Fe–Cr, no matching of their JCDPS cards with the XRD spectra of feed powder BT1 and the HVOF sprayed coating A and B was obtained. Finally, a question about the contents of the JCDPS card files arose; what phases, compounds and alloys are really included in them? It appeared that from quasicrystalline materials, basically icosahedral phases are considered by the JCDPS card files. Octagonal, decagonal or dodecagonal phases, at least those related to Al–Co–Fe–Cr system, were ignored. It was, thus, considered whether the feed powder and the HVOF sprayed coatings of the present study could be octagonal, decagonal or dodecagonal; it was, at least, realised that they did not exhibit any known crystalline structure.

3.2. SEM studies

The aim of SEM studies was to answer questions about the coating microstructure and the phases present in the feed powder as well as in the HVOF sprayed coatings. The microstructure of the Al–Co–Fe–Cr feed powder and coatings deposited with different spraying temperatures was determined from the cross-sectional samples.

The feed powder consists of spherical particles, as shown in Fig. 2(a). SEM studies both in SE and BSE mode indicated powder particles to be composed of one phase only. This phase consisted of 71.0 at.% Al, 12.4 at.% Co, 9.2 at.% Fe and 7.5 at.% Cr. The composition of this phase, consequently, corresponds well with the powder composition given by the manufacturer.

Figs. 2(b) and (c) addresses the influence of spraying temperatures on the microstructure of Al–Co–Fe–Cr coatings. The microstructure of Al–Co–Fe–Cr coating A sprayed with lower spraying temperature is shown in Fig. 2(b). No perfectly lamellar structure, typical for thermally sprayed coatings, can be encountered in this coating, indicating an incomplete melting of the feed powder during the spraying process. This results in a rather high amount of porosity in the coating A as compared to the other studied coating. This porosity incorporated in coating A, in turn, results in thicker coatings. No marks of intense oxide layer formation on the surface of the powder particles during the spraying process utilising the lower operation temperature can be observed. As the spraying temperature rises, the lamellarity of coating structure increases, as can be assessed from Fig. 2(c). This is due to more efficient melting of the feed powder during the spraying event and it brings about a reduced amount of porosity in coating. The oriented lamellar structure is, thus, more pronounced in Al–Co–Fe–Cr coating B than in the coating A. Besides the tendency towards the build-up of a layered structure, the oxidation of powder particles is enhanced with an increasing spraying temperature, introducing oxide particles or even films into the HVOF sprayed coating B. The oxide particles are mostly located between the lamellas, as can be seen in Fig. 2(c). It is worth noting that there is no difference in the coating structure near the substrate and near the coating surface, thus, the coating structures were horizontally quite homogeneous.

The observations concerning the porosity as well as the presence of oxide particles and films in the Al–Co–Fe–Cr coatings were further confirmed with the elemental X-ray mapping. The elemental X-ray maps are collected for Al, Co, Fe, Cr and O for the studied coatings. The results of the elemental X-ray mapping for the coating A are shown in Fig. 3, while those for coating B are illustrated in Fig. 4. The X-ray maps indicate oxide particles to be composed of all the elements present in the powder (not only aluminium), since at least low elemental intensities are gained for all of them at the areas of great oxygen intensity. Moreover, in addition to this oxide formation, both the studied coatings comprise one phase only. This can be noticed from the even distribution of the mapped elements in the oxygen-free areas of the studied Al–Co–Fe–Cr coatings.

The composition of the phases present in Al–Co–Fe–Cr coatings was determined by the EDS analysis. As already

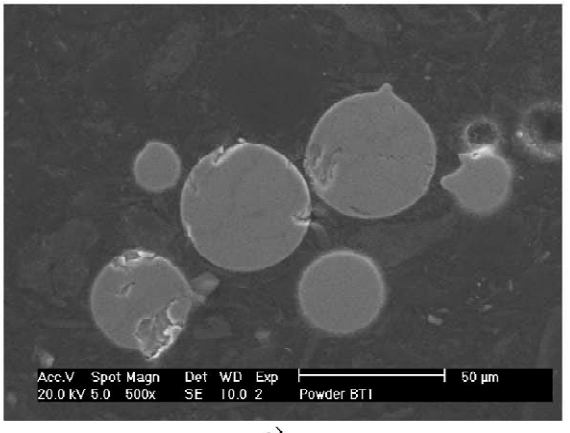

a)

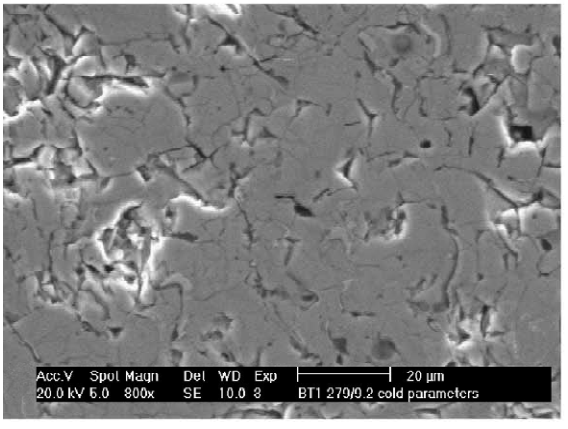

b)

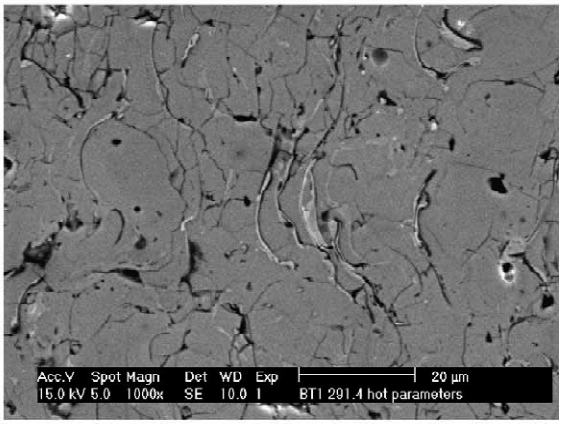

c)

Fig. 2. SEM photographs showing the microstructural details of Al–Co–Fe–Cr feed powder and HVOF sprayed coatings. (a) The morphology and microstructure of Al–Co–Fe–Cr feed powder BT1. (b) The microstructure of Al–Co–Fe–Cr coating A deposited with the lower spraying temperature. (c) The microstructure of Al–Co–Fe–Cr coating B deposited with the higher spraying temperature.

shown, coating A is mainly composed of one phase. The composition of this phase was determined to be 70.5 at.% Al, 12.5 at.% Co, 9.6 at.% Fe and 7.4 at.% Cr. The composition of this phase, accordingly, approximately corresponds to the composition of the feed powder. In the coating B, two main phases were identified. The composition of the major phase was 70.4 at.% Al, 12.5 at.% Co, 9.6 at.% Fe and 7.5 at.% Cr. The coating lamellas were built up of this phase. The other phase was principally located between the lamellas and contained a lot of oxygen. The oxide particle formation discussed above refers to the formation of this phase. The composition of this oxide phase was 41.4 at.% O, 47.8 at.% Al, 4.5 at.% Co, 3.2 at.% Fe and 3.1 at.% Cr. The oxide phase, thus, is somewhat enriched with aluminium as compared to the original composition of the feed powder. The oxide phase can still be considered as an oxidised form of the major phase, since not only aluminium but also the other elements oxidise during the spraying process. However, some oxide particles contained somewhat lower aluminium and higher alloying element concentrations. Cobalt concentrations as high as 23.5 at.% were measured. For iron and chromium, even 16.6 at.% and 11.6 at.% concentrations were determined, respectively. The rest of the phase was covered by aluminium and oxygen, the lowest aluminium content being 46.1 at.%. These oxide particles with lower aluminium content are suggested to carry out the compensation of the aluminium enrichment and the successive deficiency of alloying elements in the majority of oxide particles.

The earlier studies discussing the microstructure of thermally sprayed quasicrystalline Al–Cu–Fe coatings report the deficiency of Al during the spraying operation. This is due to the higher vapour pressure of Al as compared to the other two elements in Al–Cu–Fe feed powders [20,26,27]. Similarly in Al–Co–Fe–Cr feed pow-

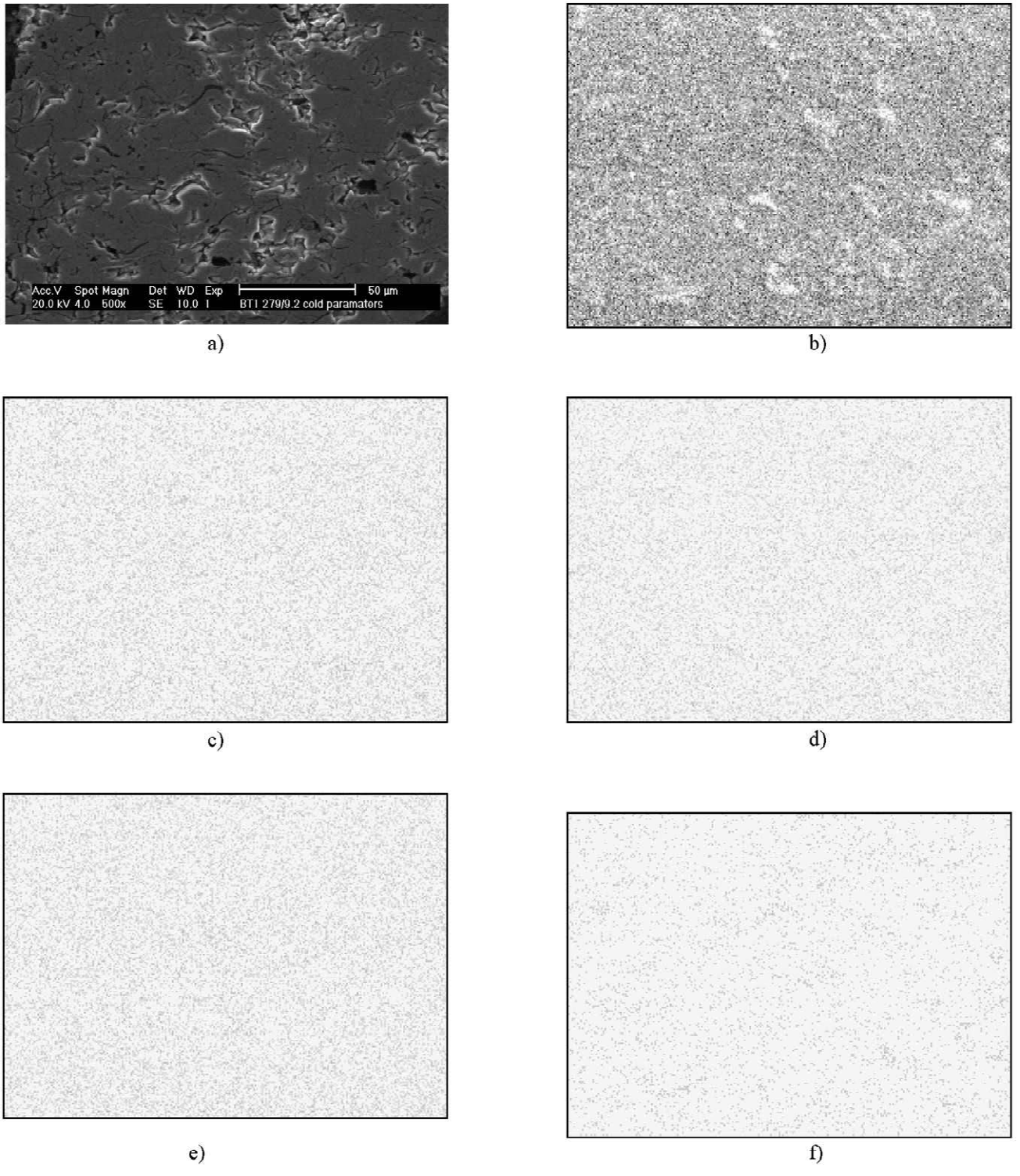

Fig. 3. The polished cross-section of the Al–Co–Fe–Cr coating A studied with the elemental X-ray mapping, (a) SEM micrograph showing the lamellar microstructure of the coating and the region for elemental mapping. (b) The aluminium map for the area. (c) The cobalt map for the area. (d) The iron map for the area. (e) The chromium map for the area. (f) The oxygen map for the area.

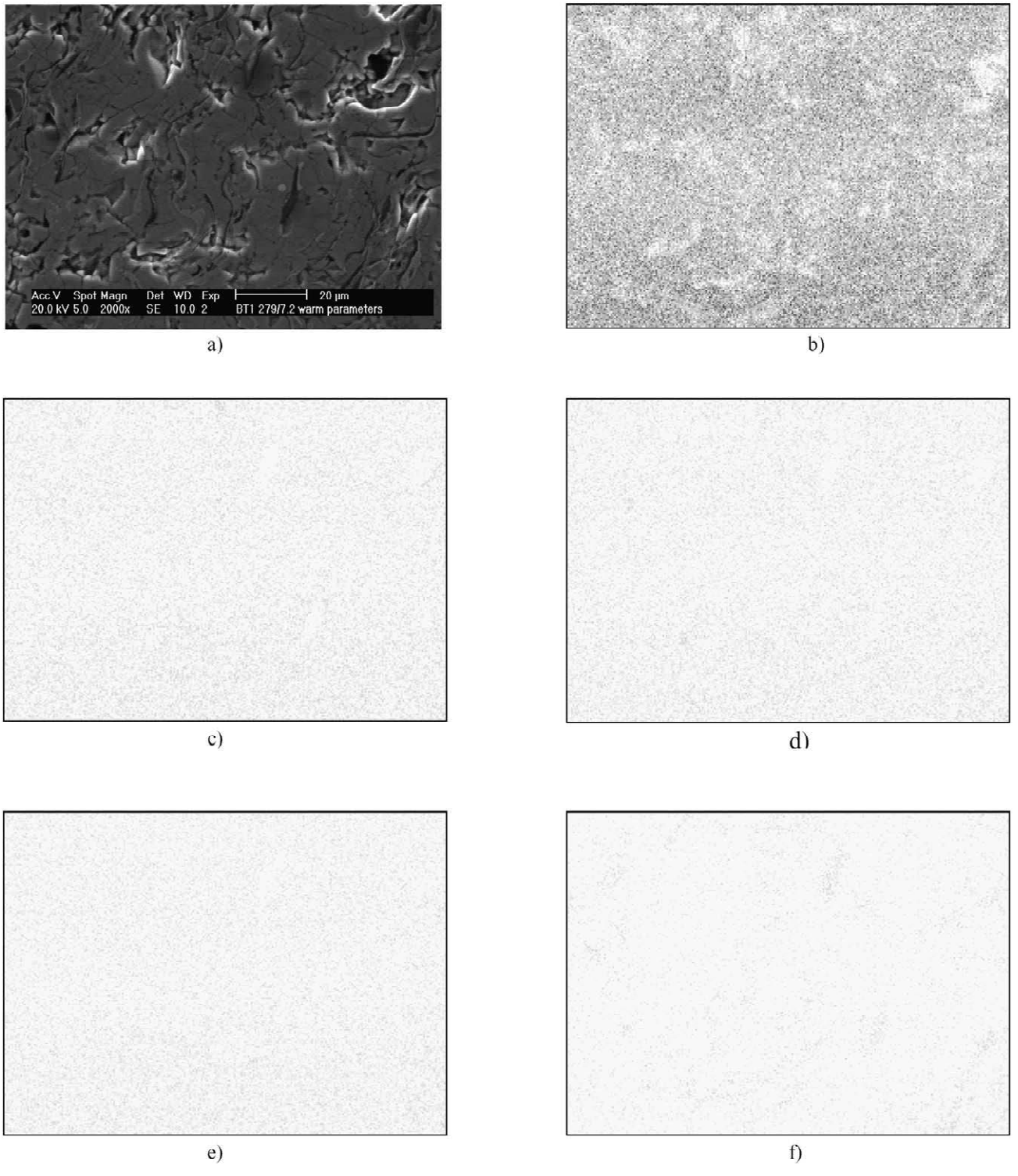

Fig. 4. The polished cross-section of the Al–Co–Fe–Cr coating B studied with the elemental X-ray mapping. (a) SEM micrograph showing the lamellar microstructure of the coating and the region for elemental mapping. (b) The aluminium map for the area. (c) The cobalt map for the area. (d) The iron map for the area. (e) The chromium map for the area. (f) The oxygen map for the area.

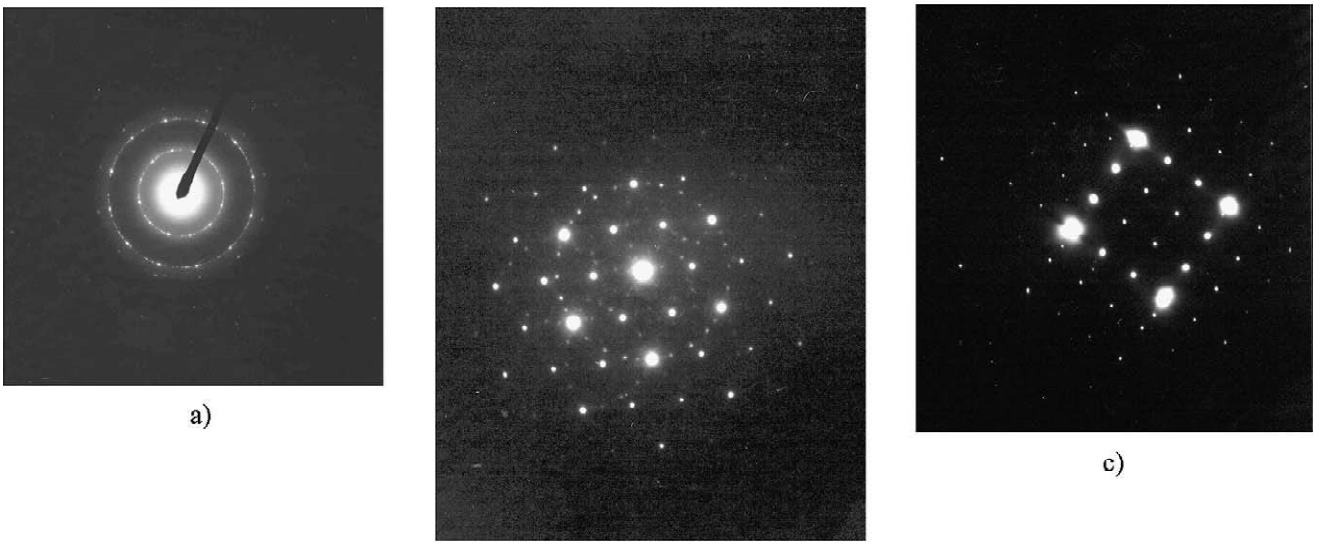

Fig. 5. Electron diffraction patterns of the dodecagonal quasicrystalline Al–Co–Fe–Cr phase taken along the (a) twelve-fold, (b) threefold and (c) twofold axes.

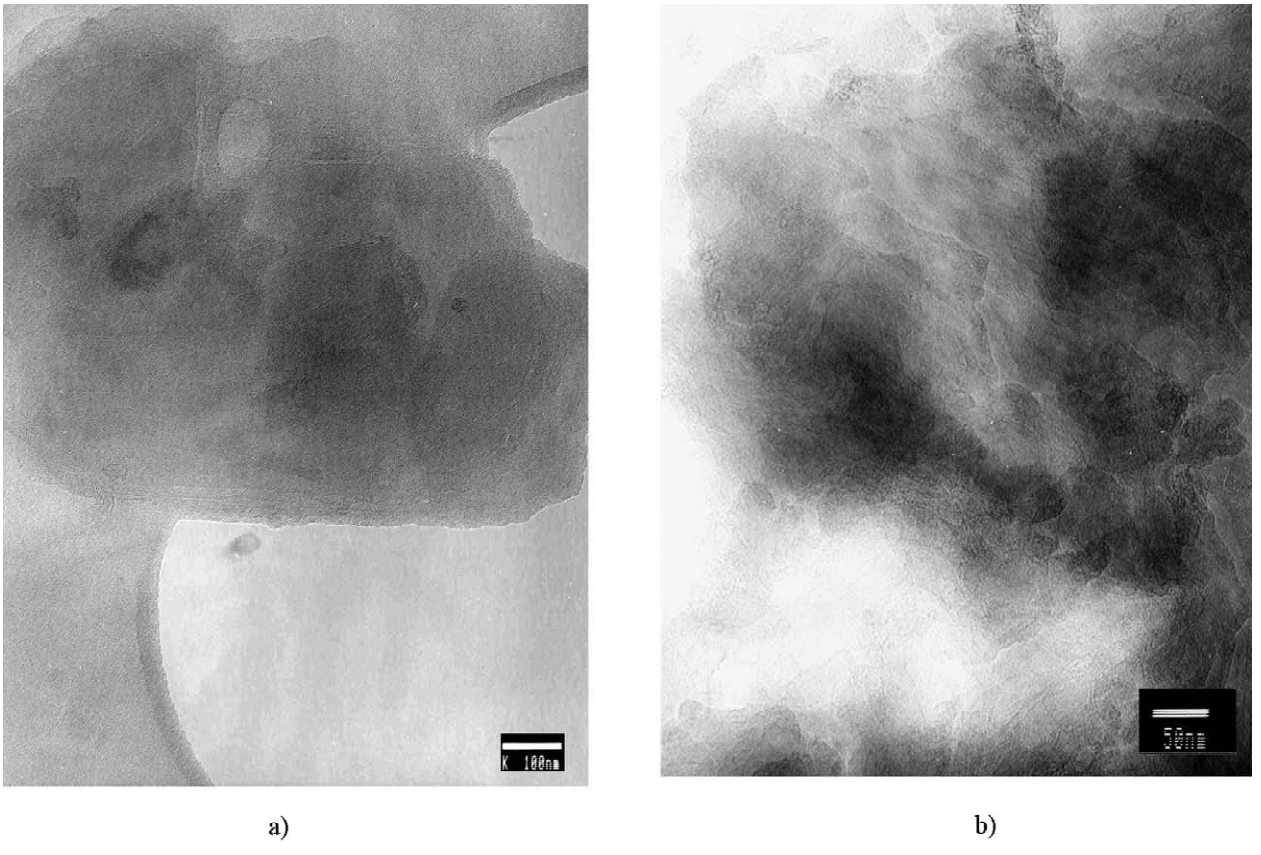

Fig. 6. (a) TEM bright field image of the feed powder particle showing the twelvefold symmetry. (b) TEM bright field image of the HVOF sprayed coating A showing the twelvefold symmetry. No defects or bend contours can be seen in the structure of this dodecagonal phase either in the feed powder or in the HVOF sprayed coatings. This is in agreement with the results of Sordelet et al. [27].

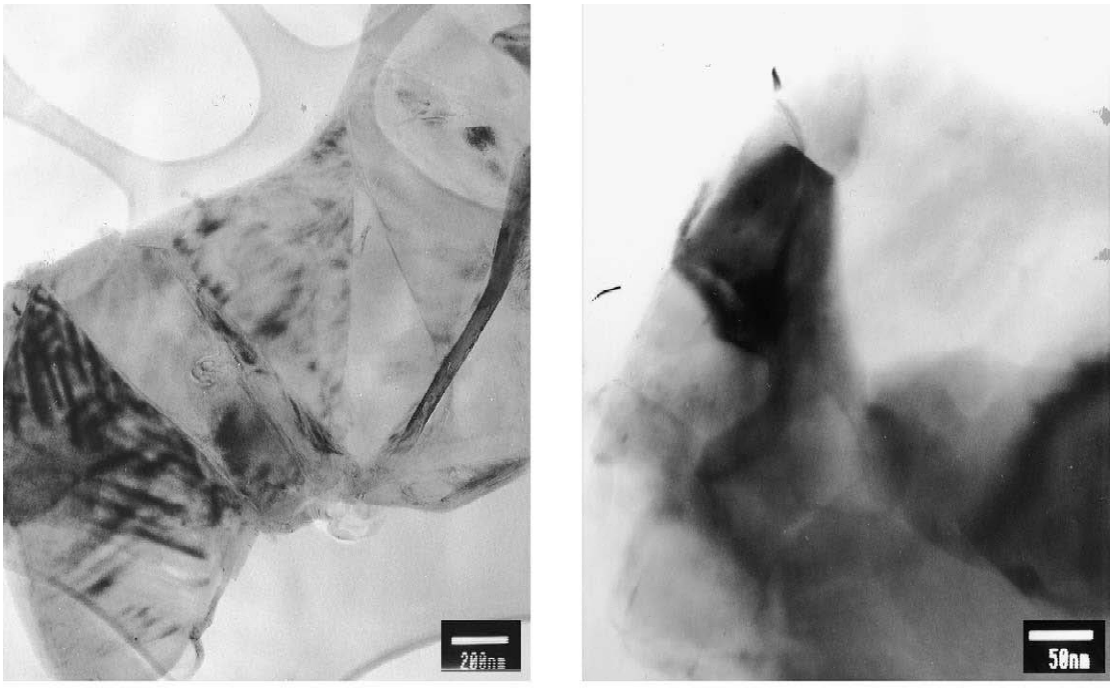

a) b)

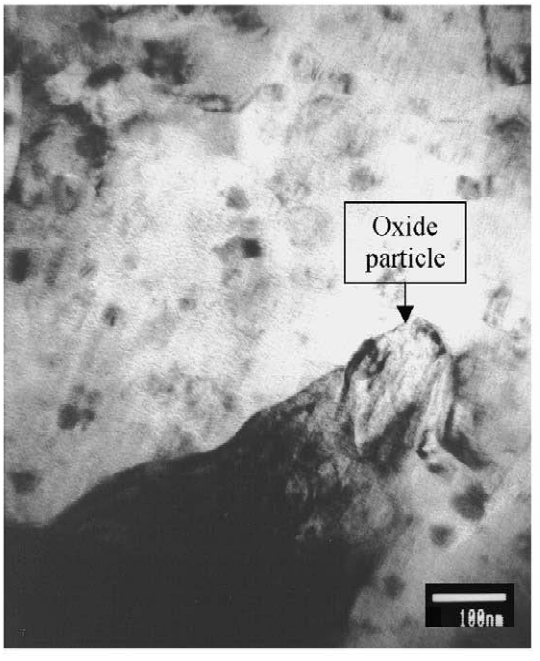

c)

Fig. 7. Microstructure of Al–Co–Fe–Cr coating B from different orientations. (a) TEM bright field image of the coating from the cross-sectional perspective. Micrograph taken with the electron beam parallel to the threefold axis. (b) TEM bright field image showing the coating structure from the top of the coating. Micrograph taken with the electron beam parallel to the twofold axis. (c) TEM bright field image showing the oxide particle in the coating structure. Micrograph taken with the electron beam parallel to the two-fold axis.

der of the present study, Al has a higher vapour pressure than the other elements. In this study, however, no such Al vaporisation was observed.

3.3. ATEM examination

The identification of the phases and their microstructure present in the feed powder and HVOF sprayed coatings was the main task of TEM studies. Also, the details of coating microstructure were of interest. TEM studies were carried out for the powdery samples; the feed powder was studied as such and the coating samples were crushed into a powdery form. The utilisation of the powdery samples instead of the cross-sections of coatings was due to the finding that the spraying process yields orientation into the coating structure [31], which may complicate the TEM studies.

TEM studies reveal the major phase in the feed powder and both of the HVOF sprayed coatings to be dodecagonal, since its diffraction pattern indicates a twelve-fold rotational symmetry. The indications of the presence of a quasicrystalline phase in studied structures due to XRD analysis were, thus, confirmed. Figs. 5(a)–(c) shows the twelve-fold, threefold and twofold zone axes patterns, respectively. The earlier studies of coating formation from the Al–Co–Fe–Cr powder have reported the formation of a decagonal quasicrystalline phase [28,29]. Instead, no observations of a dodecagonal phase have been announced. This finding of a new dodecagonal Al–Co–Fe–Cr phase greatly widens the family of dodecagonal quasicrystals, which has only embraced dodecagonal Co–Cu [32], Ta–Te [33], Ni–Cr [34], Ni–V and Ni–V–Si [35] alloys so far.

The microstructure of the feed powder particle with a twelvefold symmetry is shown in Fig. 6(a). A similar microstructure is retained in both of the coatings, too. Fig. 6(b) presents the section of the powder particle of coating A, exhibiting the twelvefold symmetry. It is worth noting that no defects can be seen in the structure of this dodecagonal phase either in the feed powder or in the HVOF sprayed coatings. This is in agreement with the results of Sordelet et al. [27]. Furthermore, the absence of phason strains, i.e. the sharpness of the diffraction spots, supports this finding.

Fig. 7 shows the microstructure of HVOF sprayed coating B from the cross-sectional perspective and from the top of the coating. As can be seen in Fig. 7(a), the coating lamellas consist of columnar grains extending through the lamella thickness. The columnar grains are approximately equiaxed on the plane parallel to the lamellas. In turn, the size of the grains somewhat varies throughout the coating structure; the diameter of the grains was generally 150–500 nm. This is also shown in Fig. 7(b).

Similarly to SEM studies, EDS analysis in TEM characterisation revealed no significant differences in the composition of the dodecagonal phase between the feed powder or the HVOF sprayed coatings. In the feed powder, the dodecagonal phase consisted of 64.5 at.% Al, 12.0 at.% Co, 8.9 at.% Fe, 7.5 at.% Cr and 7.1 at.% O. In the coating A, the dodecagonal phase contained 72.4 at.% Al, 10.2 at.% Co, 8.0 at.% Fe, 6.5 at.% Cr and 2.8 at.% O. The corresponding phase composition in the coating B was 72.2 at.% Al, 10.2 at.% Co, 8.0 at.% Fe, 5.8 at.% Cr and 4.4 at.% O. Accordingly, somewhat higher Al contents were received in TEM characterisation than in the SEM analyses. The main feature, however, to be taken into account is the involvement of oxygen in the EDS analysis of the dodecagonal phase. The presence of oxygen in the EDS analysis and in TEM analysis but not in SEM exploration indicates that the small and powdery TEM samples have oxidised due to their high surface area. Thus, oxygen can not be registered as a component element of the dodecagonal quasicrystalline phase, although it has earlier been described as a part of quasicrystalline Al–Cu–Fe–Cr–O structure [28,29].

In the feed powder and the HVOF sprayed coating A, no phases other than the dodecagonal one were encountered in the TEM studies. On the contrary, coating B, sprayed with higher operation temperature, contained an oxygen-containing minor phase together with the dodecagonal major phase. Particles of this oxygen-containing phase were predominantly located between the coating lamellas, as shown in Fig. 2(c), or even between the individual grains, as depicted in Fig. 7(c). The EDS analysis suggests the oxygen-containing phase to be composed of 48.0 at.% Al, 11.0 at.% Co, 8.2 at.% Fe, 6.2 at.% Cr and 26.7 at.% O. Similarly as in the SEM studies, also the Al-poor and alloying-element-rich version of the oxygen-containing phase was noticed in the TEM exploration of coating B. A concentration as low as 41.0 at.% was measured for aluminium in this Al-poor oxide, while cobalt concentrations as high as 21.0 at.%, iron contents as high as 15.1 at.% and chromium amounts as high as 12.7 at.% were measured. It is, still, worth noting that the amount of this Al-poor oxide is not high.

In the study of Sordelet et al. [26], the composition of the oxygen-containing phase was evaluated to be Al_2O_3. The results of the present study do not support this conclusion. Already the elemental X-ray maps recorded by SEM suggest the oxide-containing phase to be composed of all the elements present in the Al–Co–Fe–Cr alloy. Yet, no pure Al_2O_3 could be identified in XRD, SEM or TEM characterisation of the Al–Co–Fe–Cr coatings of the study. The results of TEM exploration also indicate the presence of all the alloy elements in the oxygen-containing phase. Besides, at the areas of high oxygen content, the dodecagonal quasicrystalline structure can still be resolved in the EDP. This promotes another theory of Sordelet et al. [27], where the oxygen is

presented to be present as a metallic oxide surface film on prior splat boundaries rather than as an interstitial solution or a precipitated oxide phase. However, more detailed studies are needed to characterise the structure of the oxygen-containing phase.

4. Conclusions

The microstructural characterisation was carried out for the Al–Co–Fe–Cr feed powder and the coatings sprayed with a HVOF method in order to explore the structural development of thick Al–Co–Fe–Cr coatings and the influence of the spraying parameters on the microstructure of produced Al–Co–Fe–Cr coatings. The results show that Al–Co–Fe–Cr feed powder and the coatings sprayed with lower and higher operation temperatures are all composed of a dodecagonal quasicrystalline phase. The composition of this new dodecagonal phase approximately corresponds to that of a feed powder, being $Al_{70.6}Co_{12.5}Fe_{9.4}Cr_{7.5}$. This finding of a new dodecagonal Al–Co–Fe–Cr phase greatly widens the family of existing dodecagonal quasicrystals, which, so far, has only embraced alloys Co–Cu, Ta–Te, Ni–Cr, Ni–V and Ni–V–Si.

The dodecagonal phase orientates during the spraying process. As a result, a lamellar coating structure forms with both used spraying temperatures. These lamellas are made up of columnar dodecagonal grains, which extend through the lamella thickness. However, the melting of powder particles and the subsequent build-up of an oriented lamellar structure is not complete when a lower spraying temperature is used, yielding porosity into the coating. Higher spraying temperature, in contrast, promotes oxidation, leading to the incorporation of an oxygen-containing film on splat boundaries. Thus, while feed powder and the coating deposited with a lower spraying temperature are one-phase structures, the coating sprayed with a higher operation temperature is comprised of a dodecagonal phase and an oxygen-containing phase. The oxygen-containing phase is not pure aluminium oxide but contains all the elements present in the alloy.

It should be noticed that among quasicrystalline powders the studied dodecagonal Al–Co–Fe–Cr powder was exceptionally easy to spray with a HVOF method due to its structural stability. No phase transformations typical for metastable quasicrystals were associated with the HVOF spraying of Al–Co–Fe–Cr powder at the studied temperatures. Similarly, no vaporisation of Al, typical for some less stable quasicrystalline powders, was observed for the Al–Co–Fe–Cr alloy. The spraying parameters were mainly observed to regulate the porosity and, thus, thickness as well as the amount of the oxidised splat boundaries of Al–Co–Fe–Cr coatings.

Acknowledgements

E. H.-S. expresses her sincere thanks to the Academy of Finland and Walter Ahlström Foundation for financing her research.

References

[1] D.J. Sordelet, J.M. Dubois, Mater. Res. Soc. Bull. 11 (1997) 34–37.
[2] D. Shechtman, I. Blech, D. Gratias, J.W. Cahn, Phys. Rev. Lett. 53 (1984) 1951–1953.
[3] A.P. Tsai, Mater. Res. Soc. Bull. 11 (1997) 43–47.
[4] K. Kimura, H. Yamane, T. Hashimoto, S. Takeuchi, Mat. Sci. Eng. A 99 (1988) 435–438.
[5] C. Suiyanarayana, Prog. Mater. Sci. 46 (2001) 1–184.
[6] F. Schurack, J. Eckert, L. Schultz, Mater. Sci. Eng. A 294–296 (2000) 164–167.
[7] J. Eckert, L. Schultz, K. Urban, Mater. Sci. Eng. A 133 (1991) 393–397.
[8] M. Takeda, S. Sakai, A. Kawasaki, Y. Hattori, M. Katoh, Mater. Sci. Eng. A 294–296 (2000) 842–845.
[9] R. Teghil, L. D'Alessio, M.A. Simone, M. Zaccagnino, D. Ferro, D.J. Sordelet, Appl. Surf. Sci. 168 (2000) 267–269.
[10] Y. Ding, D.O. Northwood, A.T. Alpas, Surf. Coatings Tech. 96 (1997) 140–147.
[11] A. Kanjilal, U. Tiwari, R. Chatterjee, Mater. Res. Bull. 37 (2002) 343–351.
[12] T. Grenet, F. Giroud, K. Loubet, A. Bergman, G. Safran, J. Labar, P. Barna, J.L. Joulaud, M. Capitan, J. Alloys Comp. 342 (2002) 2–6.
[13] C.J. Jenks, P.A. Thiel, Mater. Res. Soc. Bull. 11 (1997) 55–58.
[14] J.M. Dubois, Mater. Sci. Eng. A 294–296 (2000) 4–9.
[15] E. Belin-Ferré, J.M. Dubois, V. Fournée, P. Brunet, D.J. Sordelet, L.M. Zhang, Mater. Sci. Eng. A 294–296 (2000) 818–821.
[16] P. Brunet, L.M. Zhang, D.J. Sordelet, M. Besser, J.M. Dubois, Mater. Sci. Eng. A 294–296 (2000) 74–78.
[17] F. Audebert, R. Colaco, R. Vilar, H. Sirkin, Scr. Materialia 40 (1999) 551–557.
[18] B. Wolf, K.O. Bambauer, P. Paufler, Mater. Sci. Eng. A 298 (2001) 284–295.
[19] D.J. Sordelet, M.F. Besser, J.L. Logsdon, Mater. Sci. Eng. A 255 (1998) 54–65.
[20] M.F. Besser, T. Eisenhammer, Mater. Res. Soc. Bull. 11 (1997) 59–63.
[21] E. Fleury, Y.-C. Kim, J.-S. Kim, H.-S. Aim, S.-M. Lee, W.-T. Kim, D.-H. Kim, J. Mater. Res. Soc. 17 (2002) 492–501.
[22] D.J. Sordelet, M.F. Besser, J.L. Logsdon, Mater. Sci. Eng. A 255 (1998) 54–65.
[23] E. Fleury, Y.-C. Kim, J.-S. Kim, D.-H. Kim, W.-T. Kim, H.-S. Ahn, S.-M. Lee, J. Alloys Comp. 342 (2002) 321–325.
[24] D.J. Sordelet, S.D. Widener, Y. Tang, M.F. Besser, Mater. Sci. Eng. A 294–296 (2000) 834–837.
[25] S. De Palo, S. Usmani, S. Sampath, D.J. Sordelet, M. Besser, in: C.C. Berndt (Ed.), Thermal Spray: A United Forum for Scientific and Technological Advances, ASM International, Ohio, USA, 1997, pp. 135–139.
[26] D.J. Sordelet, M.F. Besser, I.E. Anderson, J. Thermal Spray Tech. 5 (1996) 161–174.
[27] D.J. Sordelet, M.J. Kramer, O. Unal, J. Thermal Spray Tech. 4 (1995) 235–244.
[28] J. Reyes-Gasga, A. Pita-Larranaga, M.P. Valles-Gonzalez, A. Sanchez-Pascual, Thin Solid Films 355–356 (1999) 506–512.
[29] J. Reyes-Gasga, A. Pita-Larranaga, G. Mondragon-Galicia, M.P. Valles-Gonzalez, A. Sanchez Pascual, Mater. Sci. Eng. A 294–296 (2000) 850–853.

[30] L. Pawlowski, The Science and Engineering of Thermal Spray Coatings, John Wiley & Sons, Chichester, England, 1995.
[31] X.Z. Li, L.D. Marks, J. Maciejewski, L. Fehrenbacher, J. Zabinski, J. O'Neill, Metall. Mater. Trans. A 33 (2002) 675–679.
[32] Z.F. Li, B.X. Liu, Nucl. Instr. Methods Phys. Res., B 178 (2001) 224–228.
[33] M. Uchida, S. Horiuchi, Micron 31 (2002) 493–497.
[34] T. Ishimasa, H.-U. Nissen, Y. Fukano, Phys. Rev. Lett. 55 (1985) 511–513.
[35] H. Chen, D.X. Li, K.H. Kuo, Phys. Rev. Lett. 60 (1988) 1645–1648.

PUBLICATION III

Influence of Cr alloying on the microstructure of thermally sprayed quasicrystalline Al-Cu-Fe coatings

In: Intermetallics 2003. Vol. 11, pp. 879–891.
Reprinted with permission from the publisher.

Available online at www.sciencedirect.com
SCIENCE DIRECT®
Intermetallics 11 (2003) 879–891
Intermetallics
www.elsevier.com/locate/intermet

Influence of Cr alloying on the microstructure of thermally sprayed quasicrystalline Al–Cu–Fe coatings

Elina Huttunen-Saarivirta[a,*], Erja Turunen[b], Marke Kallio[c]

[a]Tampere University of Technology, Institute of Materials Science, PO Box 589, Fin-33101 Tampere, Finland
[b]VTT Technical Research Centre of Finland, Surface Engineering and Laser Processing, PO Box 1703, Fin-02044 VTT, Finland
[c]VTT Technical Research Centre of Finland, Materials and Chemicals, Hermiankatu 8 G, PO Box 16071, Fin-33101 Tampere, Finland

Received 7 April 2003; accepted 8 May 2003

Abstract

The present work reports the structural development of Al–Cu–Fe and Al–Cu–Fe–Cr coatings deposited by the high velocity oxy-fuel thermal spraying process and the influence of Cr alloying on the phase selection of Al–Cu–Fe coatings at various deposition temperatures. The porosity levels of the Al–Cu–Fe and Al–Cu–Fe–Cr coatings of the study are demonstrated to be lower than those reported for corresponding plasma-sprayed coatings. The results show that high velocity oxy-fuel spraying technique produces Al–Cu–Fe coatings that are phase structurally similar to plasma-sprayed Al–Cu–Fe coatings reported in literature. Al–Cu–Fe coatings are composed of a crystalline β-AlFe phase and a quasicrystalline i-$Al_{65}Cu_{20}Fe_{15}$ phase as well as an oxidised form of either or both of these phases. Addition of Cr to Al–Cu–Fe alloys introduces coatings that are made up of the crystalline θ-Al_2Cu phase and two quasicrystalline phases, the i_1-$Al_{80}Cr_{13.5}Fe_{6.5}$ and i_2-$Al_{13}Cr_3Cu_4$ phases. The formation of these icosahedral phases in Al–Cu–Fe–Cr alloys has not been reported before, although the occurrence of quasicrystal approximants with compositions close to those of the i_1-$Al_{80}Cr_{13.5}Fe_{6.5}$ and i_2-$Al_{13}Cr_3Cu_4$ phases has been demonstrated. On the basis of our results we propose that the icosahedral phase structure is greatly stabilised by the Cr addition to Al–Cu–Fe alloys.

Keywords: A. Multiphase intermetallics; B. Phase identification; C. Coatings; D. Microstructure

1. Introduction

During the early 1980s, a new material group with a long-range orientational but no translational order emerged [1]. Until then, a dichotomy between amorphous and crystalline materials had prevailed in the realm encompassing the structure of materials. The discovery of these quasicrystalline materials exhibiting an atomic structure somewhere between that of amorphous and crystalline materials, thus, significantly widened the scope of the structural foundation of materials.

Up to now, quasicrystalline phases with fivefold, eightfold, tenfold or even twelvefold rotational symmetries have been observed in over a hundred different metal alloy systems. Besides being theoretically interesting due to their complicated atomic structure, the unique properties of quasicrystalline materials—high hardness [2,3], a low surface energy [4–6] accompanied by a low coefficient of friction [5,7], good corrosion [4] and wear [8] resistance, low electrical and thermal conductivity [9–13] and unusual optical properties [14], to name a few—make them tempting to many practical purposes, too. However, the utilisation of quasicrystalline materials in bulk form is often compromised by their brittleness [2,15,16]. Therefore, quasicrystalline materials with these extreme surface properties are at their best in coating applications, when used in combination with more ductile substrate materials, which, in turn, provide the bulk properties.

In tribological applications, Al–Cu–Fe and Al–Cu–Fe–Cr are the most often utilised quasicrystalline materials. They are generally used in the form of thick coatings, produced by plasma spraying [8,17–21]. In this study, Al–Cu–Fe and Al–Cu–Fe–Cr thick coatings are deposited by a high velocity oxy-fuel (HVOF) spraying technique. Besides this thermal spraying technique not very much used to yield quasicrystalline coatings, the

* Corresponding author. Tel.: +358-3-31152912; fax: +358-3-31152330.
E-mail address: elina.huttunen-saarivirta@tut.fi (E. Huttunen-Saarivirta).

0966-9795/03/$ - see front matter © 2003 Elsevier Ltd. All rights reserved.
doi:10.1016/S0966-9795(03)00097-9

novelty of the present study lies in its comparative approach of the HVOF spraying of two different alloy coating, Al–Cu–Fe and Al–Cu–Fe–Cr. Although the structural development of both of these alloys during the thermal spraying process have been studied individually, no earlier reports compare their microstructures systematically by taking the influence of alloying elements and spraying parameters into account. The paper was, accordingly, motivated by the limited amount of experimental studies concerning the effect of Cr alloying on the microstructure of Al–Cu–Fe alloys, although the formation of new phases as a result of Cr alloying of Al–Cu–Fe is theoretically known. The present paper addresses the influence of chromium alloying on the microstructure of HVOF sprayed quasicrystalline Al–Cu–Fe coatings in different spraying temperatures.

The objective of the study is to tackle some aspects, which have not been completed in the earlier studies on thermally sprayed Al–Cu–Fe and Al–Cu–Fe–Cr coatings. In this study, Al–Cu–Fe and Al–Cu–Fe–Cr coatings are produced by HVOF spraying technique to gain new information on their structural development under different spraying conditions. The formed coating microstructures are compared to existing literature on the microstructures of coatings produced by other thermal spraying methods. In addition to the thermal spraying technique effects, the study aims at clarifying the role of Cr alloying in the phase selection of Al–Cu–Fe coatings at various temperatures. X-ray diffractometry (XRD), scanning electron microscopy (SEM) and analytical electron microscopy (ATEM) are used for the microstructural characterisation of Al–Cu–Fe and Al–Cu–Fe–Cr feed powders and HVOF sprayed coatings.

2. Experimental

2.1. Preparation of coatings

Al–Cu–Fe and Al–Cu–Fe–Cr coatings were applied on low carbon steel substrates by a high velocity oxy-fuel (HVOF) spraying technique. The HVOF spraying technique is a thermal spraying method, where a spray powder is fed to the gas flow of high pressure and which yields coatings of low porosity and, therefore, of good surface properties [22]. In the present study, the spray powders were commercial powders Christome F1 and A1/S, corresponding to Al–Cu–Fe and Al–Cu–Fe–Cr powders, respectively. These powders were manufactured by Saint-Gobain Advanced Ceramics SNMI, France. The composition of the Al–Cu–Fe powder, given by the manufacturer, was 40.8 wt.% Al, 41.2 wt.% Cu, 17.0 wt.% Fe and 0.8 wt.% B, which corresponds to the composition 59.6 at.% Al, 25.5 at.% Cu, 12.0 at.% Fe and 2.9 at.% B. The particle size of this powder ranged from 20 to 45 μm. In turn, the composition of the Al–Cu–Fe–Cr powder, given by the manufacturer, was 54.1 wt.% Al, 17.8 wt.% Cu, 13.0 wt.% Fe and 14.9 wt.% Cr, which corresponds to the composition 71.5 at.% Al, 10.0 at.% Cu, 8.3 at.% Fe and 10.2 at.% Cr. The particle size of this powder ranged from 20 to 53 μm.

The coatings were sprayed using a HV-2000 spray gun by Praxair Surface Technologies (USA). The gun was operated by a Model 3440 console utilising a model 1262 volumetric powder feeder by Plasmatron Pvt.Ltd (USA). A two-axis traverse unit with a rotating spindle of a 200 mm inner diameter was used to manipulate the gun and the substrates during the coating deposition. The spray distance was 300 mm in the spraying experiments of the study. In the HVOF process, nitrogen was used as a carrier gas, along with hydrogen as a fuel gas. The coatings were sprayed under two different operation conditions, varying the flow of hydrogen and oxygen and their ratio. The gas flow ratio generally determines the temperature of the flame [22], the higher oxygen content promoting the higher flame temperature. This also applied to the HVOF spraying process of the study. The thickness of the HVOF sprayed coatings also varied in the spraying experiments. The spraying conditions used in the study and the coating thicknesses are shown in Table 1.

Temperature of the sprayed particles was studied through the spraying diagnostics. SprayWatch 2i imaging system from Oseir Ltd. (Finland), designed for the quality control of industrial thermal spray processes, was used for the on-line measurements of in-flight particles' temperature in the spray. It has to be noticed that these temperature measurements conducted during the spraying experiments only recorded the surface temperature of powder particles. Due to the low thermal conductivity of the powder particles, however, the true

Table 1
HVOF spraying conditions and the resulting coating thicknesses

Spray powder alloy	Coating	O_2 (l/min)	H_2 (l/min)	H_2/O_2 (ratio)	Surface temperature of powder particles (°C)	Thickness (μm)
Al–Cu–Fe	A	235	665	2.83	1983	310
Al–Cu–Fe	B	280	620	2.21	2015	280
Al–Cu–Fe–Cr	C	235	665	2.83	2003	289
Al–Cu–Fe–Cr	D	280	620	2.21	2011	284

temperature of the inner part of particles cannot be evaluated. For the same reason, the temperature difference measured between the surfaces of particles does not correspond to the true temperature difference between the inner parts of the particles. The surface temperature of powder particles, therefore, only gives a rough approximation about the scale of temperature the powder particles reach during the spraying process.

2.2. Microstructural characterisation of coatings

The microstructural characterisation of Al–Cu–Fe and Al–Cu–Fe–Cr coatings was performed by X-ray diffraction (XRD) measurements, scanning electron microscopy (SEM) and analytical transmission electron microscopy (ATEM). The XRD measurements were carried out using a model Diffrac 500 diffractometer by Siemens (Germany) and copper K_α radiation with the wavelength of 0.1540501 nm. The XRD analyses were performed with powder samples. Thus, the studied coatings were stripped off their substrates and crushed into powder form in a mortar. In addition to the powder coating samples, the feed powder was characterised by XRD in order to reveal the possible phase transitions introduced by the coating process. The microstructure of the feed powder and the sprayed coatings was also studied with a scanning electron microscope model XL30 by Philips (The Netherlands), equipped with an energy dispersive spectrometer (EDS) model DX-4 by EDAX International (USA). SEM examination was used for the coating thickness determination as well, the given coating thicknesses being average values from ten individual measurements. Cross-sectional samples were used in the SEM studies. The feed powder and the sprayed coatings were further examined by an analytical transmission electron microscope JEM 2010 by Jeol (Japan) equipped with a Noran Vantage energy dispersive spectrometer by ThermoNoran (The Netherlands). The ATEM was operated at an accelerating voltage of 200 kV. ATEM examination was conducted for powdery samples; the coating samples were prepared similarly as for the XRD analyses.

3. Results

3.1. Microstructural characterisation of Al–Cu–Fe coatings

Fig. 1 shows the XRD patterns for the Al–Cu–Fe feed powder and the HVOF sprayed coatings A and B. The Al–Cu–Fe spray powder (Fig. 1a) was detected to represent a two-phase structure, consisting of the

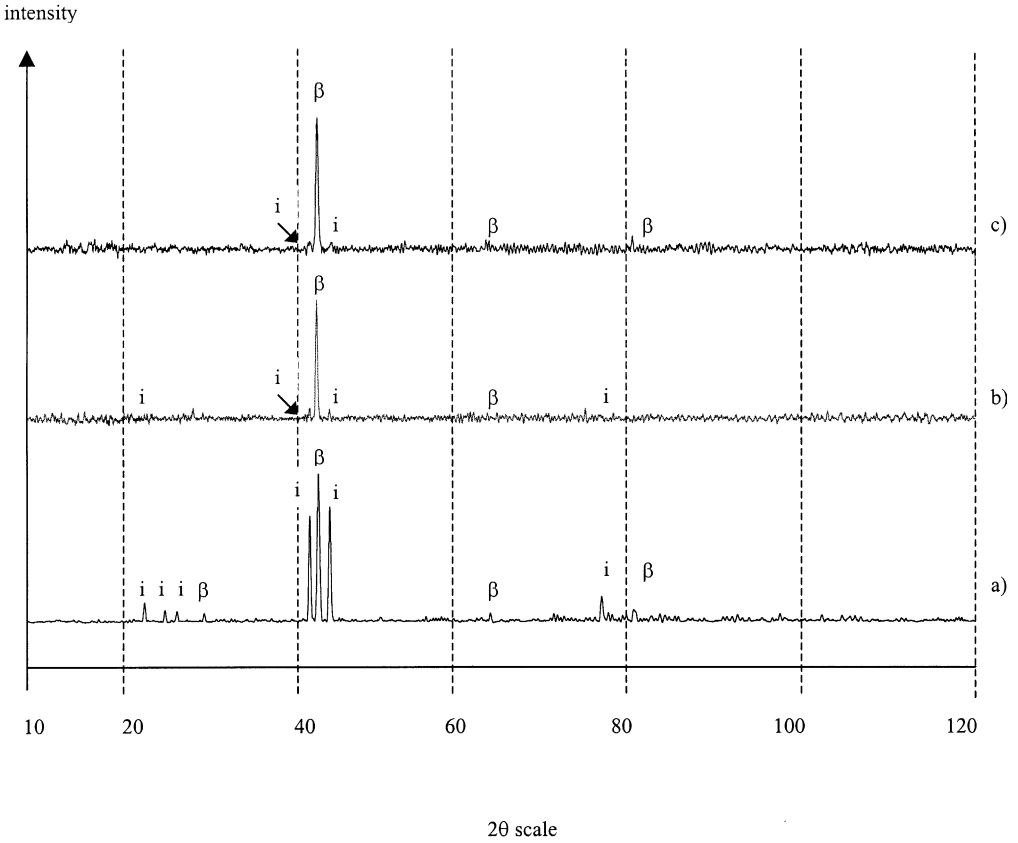

Fig. 1. XRD patterns for the (a) Al–Cu–Fe spray powder, (b) Al–Cu–Fe coating A sprayed with the lower spraying temperature, (c) Al–Cu–Fe coating B sprayed with the higher spraying temperature. i denotes the icosahedral $Al_{65}Cu_{20}Fe_{15}$ phase, β stands for the cubic AlFe phase.

quasicrystalline icosahedral i-$Al_{65}Cu_{20}Fe_{15}$ phase and the crystalline cubic β-AlFe phase. According to the manufacturer, the feed powder is almost completely quasicrystalline. However, the quantitative analysis of the amount of i-$Al_{65}Cu_{20}Fe_{15}$ and β-AlFe phases in the feed powder by comparing their peak heights in the XRD spectrum is very suspect due to the complex atomic structure and scattering phenomena associated with the quasicrystalline i-$Al_{65}Cu_{20}Fe_{15}$ phase. Due to this, the relative amount of these phases could not be evaluated on the basis of the XRD data.

The HVOF sprayed Al–Cu–Fe coatings A (Fig. 1b) and B (Fig. 1c) were composed of the same two phases as the feed powder, i-$Al_{65}Cu_{20}Fe_{15}$ and β-AlFe. Comparison of the XRD spectrum of Al–Cu–Fe coating A to that of Al-Cu-Fe coating B revealed them to be almost identical. The only registered differences were a somewhat higher intensity of peaks and their greater amount in the XRD trace of coating A, deposited with lower spraying temperature. As for the divergences between the XRD spectra of HVOF sprayed Al–Cu–Fe coatings A and B and that of the feed powder, in turn, more significant dissimilarities could be discovered. The relative intensity of i-$Al_{65}Cu_{20}Fe_{15}$ peaks was dramatically decreased during the spraying process, while that of β-AlFe peaks was not altered remarkably. Besides the lowered intensity of i-$Al_{65}Cu_{20}Fe_{15}$ peaks, their number was also reduced due to the spraying process, the lowest-intensity peaks being erased from the XRD spectra. These findings strongly suggest the formation of the β-AlFe phase to be promoted by the spraying process at the expense of the i-$Al_{65}Cu_{20}Fe_{15}$ phase.

The Al–Cu–Fe feed powder consisted of spherical particles, as shown in Fig. 2a. The overall composition of the feed powder was determined to be 56.3 at.% Al, 29.3 at.% Cu and 14.5 at.% Fe. Thus, the composition of the feed powder was slightly shifted towards lower aluminium contents from the composition given by the manufacturer. No boron was observed at all; this is clearly explained, however, by the thick beryllium window of the EDS detector. SEM studies indicated Al–Cu–Fe powder particles to be composed of two phases. The lighter phase accounted for the phase with lower aluminium content, which is the β-AlFe phase. Its composition was determined to be 58.8 at.% Al, 29.6 at.% Cu and 11.5 at.% Fe. The darker phase, in contrast, corresponded to the i-$Al_{65}Cu_{20}Fe_{15}$ phase, the composition of which was 63.9 at.% Al, 22.3 at.% Cu and 13.8 at.% Fe. According to the SEM studies, neither of the phases showed an overwhelming majority in the powder microstructure, but the phases were evaluated to be present in almost equal amounts.

Fig. 2b and c shows the microstructures of Al–Cu–Fe coatings A and B, respectively. Like the feed powder, the coatings were composed of two phases, i-$Al_{65}Cu_{20}Fe_{15}$ and β-AlFe. In both coatings A and B, the β-AlFe phase was the major phase. It was observed to construct the basic coating structure, since the coating lamellas were mainly composed of the β-AlFe phase. The composition of the β-AlFe phase somewhat deviated in the studied two coating structures. In the coating A, the composition of the β-AlFe phase was 51.0 at.%

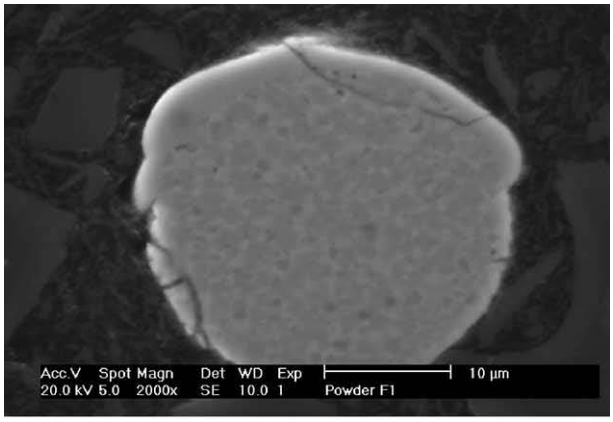

(a)

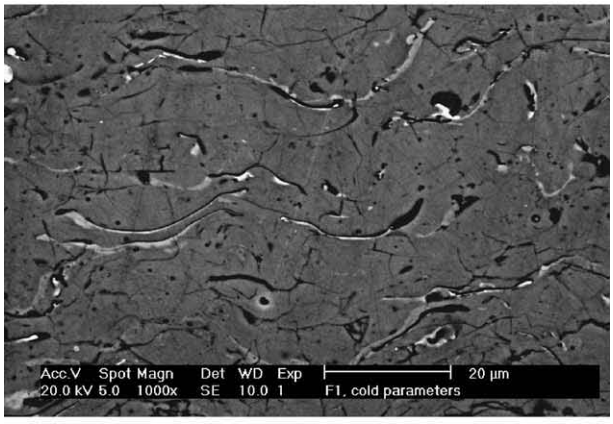

(b)

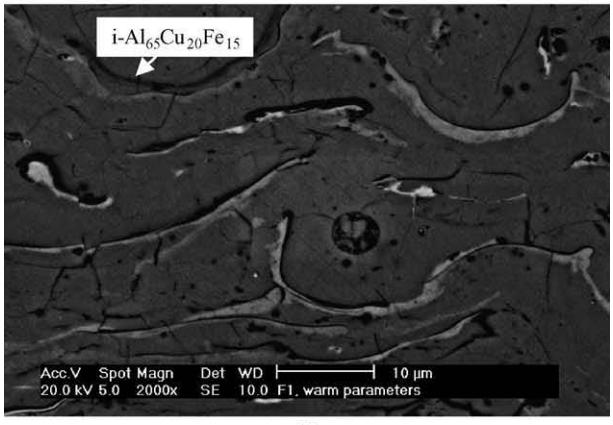

(c)

Fig. 2. SEM photographs showing the microstructural details of Al–Cu–Fe feed powder and HVOF sprayed coatings. (a) The morphology and microstructure of the Al–Cu–Fe feed powder F1. (b) The microstructure of the Al–Cu–Fe coating A deposited with the lower spraying temperature. (c) The microstructure of the Al–Cu–Fe coating B deposited with the higher spraying temperature.

Al, 32.1 at.% Cu and 16.9 at.% Fe, while in the coating B it was 43.6 at.% Al, 45.1 at.% Cu and 11.3 at.% Fe. In contrast, the composition of the minor quasicrystalline i-$Al_{65}Cu_{20}Fe_{15}$ phase was almost identical in the studied coatings; in the coating A it was 61.8 at.% Al, 26.0 at.% Cu and 12.2 at.% Fe, and in the coating B it was 61.5 at.% Al, 25.9 at.% Cu and 12.5 at.% Fe. The quasicrystalline i-$Al_{65}Cu_{20}Fe_{15}$ was often located near the coating lamella surfaces, as there the cooling rate is the highest. In addition to these two phases, i-$Al_{65}Cu_{20}Fe_{15}$ and β-AlFe, an oxygen-containing phase could be resolved between the coating lamellas. The phase was not pure aluminium oxide, but contained all the alloy elements. The oxygen-containing phase did not cause peaks in the XRD data, further confirming the absence of pure aluminium oxide. The composition of the oxygen-containing phase varied widely, from approximately 27 at.% O to 53 at.% O, with also varying amounts of other elements. Thus, based on the SEM studies, it cannot be said whether the oxidised phase forms from the β-AlFe phase or from the i-$Al_{65}Cu_{20}Fe_{15}$ phase or even from both of them.

Besides the phase structure, the influence of spraying temperature on the microstructure of Al–Cu–Fe coatings can be evaluated from Fig. 2b and c. The microstructure of Al–Cu–Fe coating A sprayed with lower spraying temperature is shown in Fig. 2b. All the powder particles were not completely melted during the spraying process. Accordingly, a perfectly lamellar and dense coating structure was not formed. Instead, porosity was incorporated in the coating. When the higher spraying temperature was utilised, the feed powder particles were more efficiently melted, leading to a reduced level of porosity in coating B. Higher spraying temperature was therefore noticed to promote the formation of somewhat denser coating structure as the lower spraying temperature. Similarly, higher spraying temperature was observed to favour the oxide layer build-up on lamella boundaries. It is worth noting that although oxidation generally occurs due to increased spraying temperature, quite a heavy oxidation of Al–Cu–Fe spray powder took place during the deposition process independently of which spraying temperature was used. However, the oxide layers were thicker, when higher deposition temperature was employed.

In the ATEM characterisation, the results of XRD and SEM examinations concerning the structure of Al–Cu–Fe coatings A and B were confirmed. The powder particles, in turn, could not be properly studied by ATEM due to their relatively large size and, accordingly, great thickness. Fig. 3 shows the microstructure of the Al–Cu–Fe coating A studied by ATEM. The coating lamellas are clearly distinguished in Fig. 3a and b, as the light areas of oxygen-containing phase separate individual lamellas. The lamellas were mainly composed of the β-AlFe phase grains, the diameter of which generally varied in the range from 30 to 140 nm (Fig. 3c). This rather small grain size was reflected in the occurrence of rings in the electron diffraction pattern (Fig. 3d). Still, greater grains of the β-AlFe phase also existed in the coating structure (with their electron diffraction patters constituting of spots, as demonstrated in Fig. 3e). Besides the presence of the crystalline β-AlFe phase, the quasicrystalline i-$Al_{65}Cu_{20}Fe_{15}$ phase was identified in the structure of coating A. The grains of the icosahedral i-$Al_{65}Cu_{20}Fe_{15}$ phase were revealed by TEM studies to be mainly located near the lamella boundaries (Fig. 3a, b and f). These observations also hold for the Al–Cu–Fe coating B.

In addition to the microstructural features of the studied coatings, ATEM exploration also provided information on their phase compositions. In the Al–Cu–Fe coating A, the composition of the major β-AlFe phase was found to be 55.5 at.% Al, 35.1 at.% Cu and 9.4 at.% Fe. In the coating B, in contrast, the β-AlFe phase contained 57.4 at.% Al, 29.6 at.% Cu and 13.0 at.% Fe. As for the quasicrystalline i-$Al_{65}Cu_{20}Fe_{15}$ phase, in the coating A it was made up of 62.7 at.% Al, 26.3 at.% Cu and 11.0 at.% Fe. In the coating B, the corresponding composition was 64.7 at.% Al, 24.0 at.% Cu and 11.3 at.% Fe. Besides the composition of these main phases of the coatings, that of the oxygen-containing lamella-boundary phase could be determined. On average, it contained 53.0 at.% Al, 13.7 at.% Cu, 6.4 at.% Fe and 27.0 at.% O.

3.2. Microstructural characterisation of Al–Cu–Fe–Cr coatings

Fig. 4a shows the XRD results of the Al–Cu–Fe–Cr initial powder, where two different icosahedral phases, $Al_{80}Cr_{13.5}Fe_{6.5}$ and $Al_{13}Cr_3Cu_4$ (denoted by i_1 and i_2, respectively), were found to coexist together with a minor tetragonal θ-Al_2Cu phase. Marks of a decagonal quaternary phase could also be identified. These phases observed in the XRD curve of the feed powder perfectly match with the phase structure reported by the powder manufacturer. In the XRD spectrum, the peaks of the icosahedral phases were mostly superimposed. However, the major peak in the XRD pattern of the feed powder corresponds to the major peak of $Al_{13}Cr_3Cu_4$, suggesting it to be the major phase.

The XRD patterns of the HVOF sprayed coatings C and D (Fig. 4b and c) reveal their microstructure to be still composed of the same phases as the feed powder. However, the phase fractions were somewhat changed during the spraying process. Coating C, sprayed with lower operation temperature, showed almost equal peak heights for icosahedral phases i_1-$Al_{80}Cr_{13.5}Fe_{6.5}$ and i_2-$Al_{13}Cr_3Cu_4$ (Fig. 4b). Only the major peak of the tetragonal θ-Al_2Cu phase was visible in the XRD spectrum of the coating C, indicating its decreased quantity as

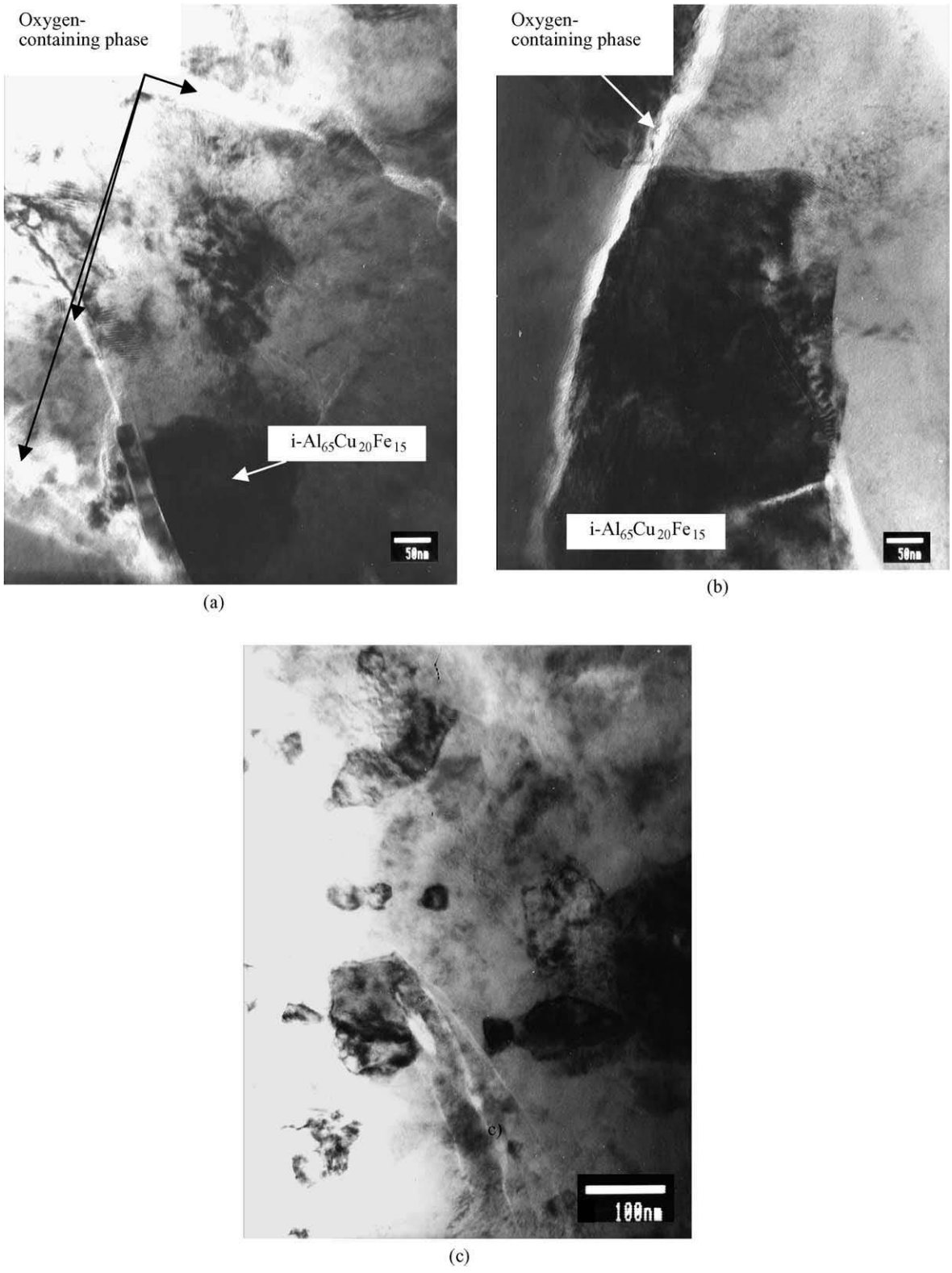

Fig. 3. Microstructure of the Al–Cu–Fe coating A sprayed with the lower spraying temperature. (a) TEM bright field (BF) image showing the coating structure from the cross-sectional perspective. Micrograph taken with the electron beam parallel to the fivefold axis of the dark grain (shown in the bottom of the figure). (b) TEM BF image showing the coating structure from the cross-sectional perspective and the icosahedral particle in the vicinity of lamella boundary. Micrograph taken with the electron beam parallel to the fivefold axis of the dark grain (shown in the bottom of the figure). (c) TEM BF image showing the grain size of the β-AlFe grains. (d) Electron diffraction pattern of the β-AlFe phase. Rings can be seen in the electron diffraction pattern, indicating a small grain size. (e) Electron diffraction pattern of the β-AlFe phase, B = [−111]. (f) Electron diffraction pattern of the icosahedral i-$Al_{65}Cu_{20}Fe_{15}$ phase, taken along the fivefold axis.

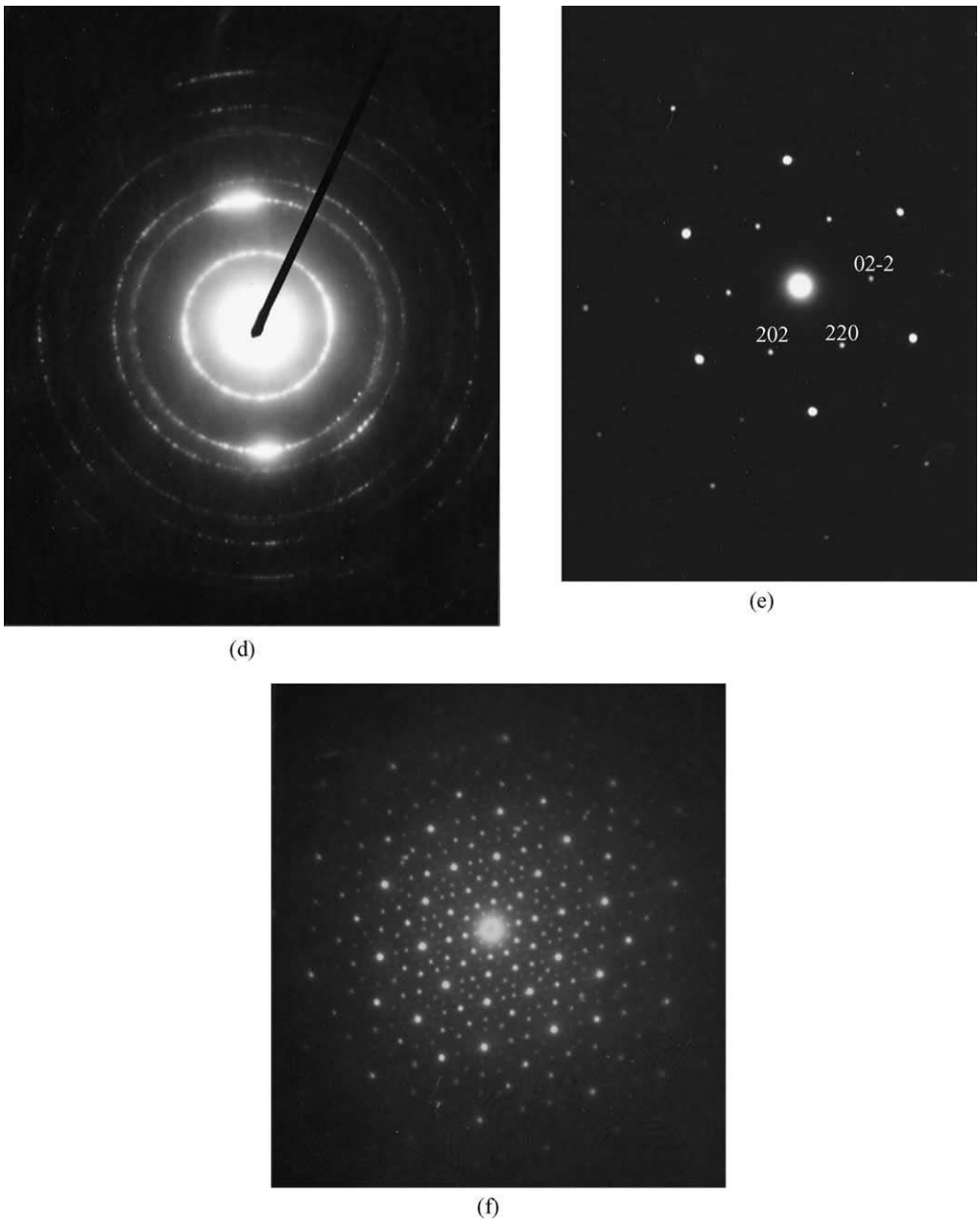

Fig. 3. (continued).

compared to the feed powder. When the spraying temperature was further increased to deposit the coating D, no marks of tetragonal θ-Al_2Cu phase could be identified in the XRD pattern (Fig. 4c), but the coating contained the icosahedral phases only. As a result of this high-temperature spraying process, the peak heights of the icosahedral phases were also changed, the major peak of the coating D corresponding to the major peak of i_1-$Al_{80}Cr_{13.5}Fe_{6.5}$.

Similarly to the Al–Cu–Fe feed powder, the Al–Cu–Fe–Cr initial powder consisted of spherical particles, as shown in Fig. 5a. The overall composition of the feed powder was determined to be 69.6 at.% Al, 10.5 at.% Cu, 9.1 at.% Fe and 10.8 at.% Cr. Thus, the composition of Al–Cu–Fe–Cr feed powder was also slightly shifted towards lower aluminium contents from the composition given by the manufacturer, like perceived for Al–Cu–Fe powder. SEM studies indicated Al–Cu–Fe–Cr powder particles to be composed of two phases: the lighter minor phase and the darker matrix. The lighter phase in the SEM photograph (Fig. 5a) corresponds to the θ-Al_2Cu phase, the composition of which was 69.7 at.% Al, 13.2 at.% Cu, 8.3 at.% Fe and 8.8 at.% Cr. The darker areas, however, were found in the elemental X-ray mapping to be made up of small copper- and iron-rich areas. Their exact boundaries could

not be determined, thus, not allowing a detailed compositional analysis. The average composition of these darker icosahedral areas, nevertheless, was 71.0 at.% Al, 6.7 at.% Cu, 10.2 at.% Fe and 12.2 at.% Cr.

A three-phase microstructure of the Al–Cu–Fe–Cr coating C can be seen in Fig. 5b, where the SEM photograph of the coating C is shown. The white areas account for the minor θ-Al_2Cu phase. The composition of this θ-Al_2Cu phase was 59.7 at.% Al, 13.3 at.% Cu, 14.1 at.% Fe and 12.9 at.% Cr. The light grey areas correspond to the copper-rich icosahedral phase i_2-$Al_{13}Cr_3Cu_4$, the composition of which was 69.0 at.% Al, 13.4 at.% Cu, 8.9 at.% Fe and 8.8 at.% Cr. The dark grey areas represent the iron-rich i_1-$Al_{80}Cr_{13.5}Fe_{6.5}$ phase. The composition of this phase was 69.2 at.% Al, 11.3 at.% Cu, 9.3 at.% Fe and 10.3 at.% Cr. In the structure of coating D, in turn, only the icosahedral phases, i_1-$Al_{80}Cr_{13.5}Fe_{6.5}$ and i_2-$Al_{13}Cr_3Cu_4$, could be well distinguished, as shown in Fig. 5c. In the coating D, these two phases were compositionally even closer to each other than in the coating C. The composition of the i_1-$Al_{80}Cr_{13.5}Fe_{6.5}$ phase, seen darker in the SEM photograph, was 68.6 at.% Al, 11.2 at.% Cu, 9.7 at.% Fe and 10.5 at.% Cr. In contrast, the composition of the lighter i_2-$Al_{13}Cr_3Cu_4$ phase was 67.9 at.% Al, 11.0 at.% Cu, 9.8 at.% Fe and 11.3 at.% Cr. The reason for the negligible compositional difference between these two phases in the coating D is suggested to be the disappearance of the θ-Al_2Cu phase at the expense of remaining icosahedral phases.

As for the influence of spraying temperature on the microstructure of Al–Cu–Fe–Cr coatings, Fig. 5b and c provides some information. As for Al–Cu–Fe coatings, higher spraying temperature tends to promote the formation of somewhat denser coatings. As compared to the Al–Cu–Fe coatings, however, the level of porosity present in coating structure seems to be somewhat greater for the Al-Cu-Fe-Cr coatings. This is explained by the greater melting point of the Al–Cu–Fe–Cr feed power compared to that of the Al–Cu–Fe feed powder.

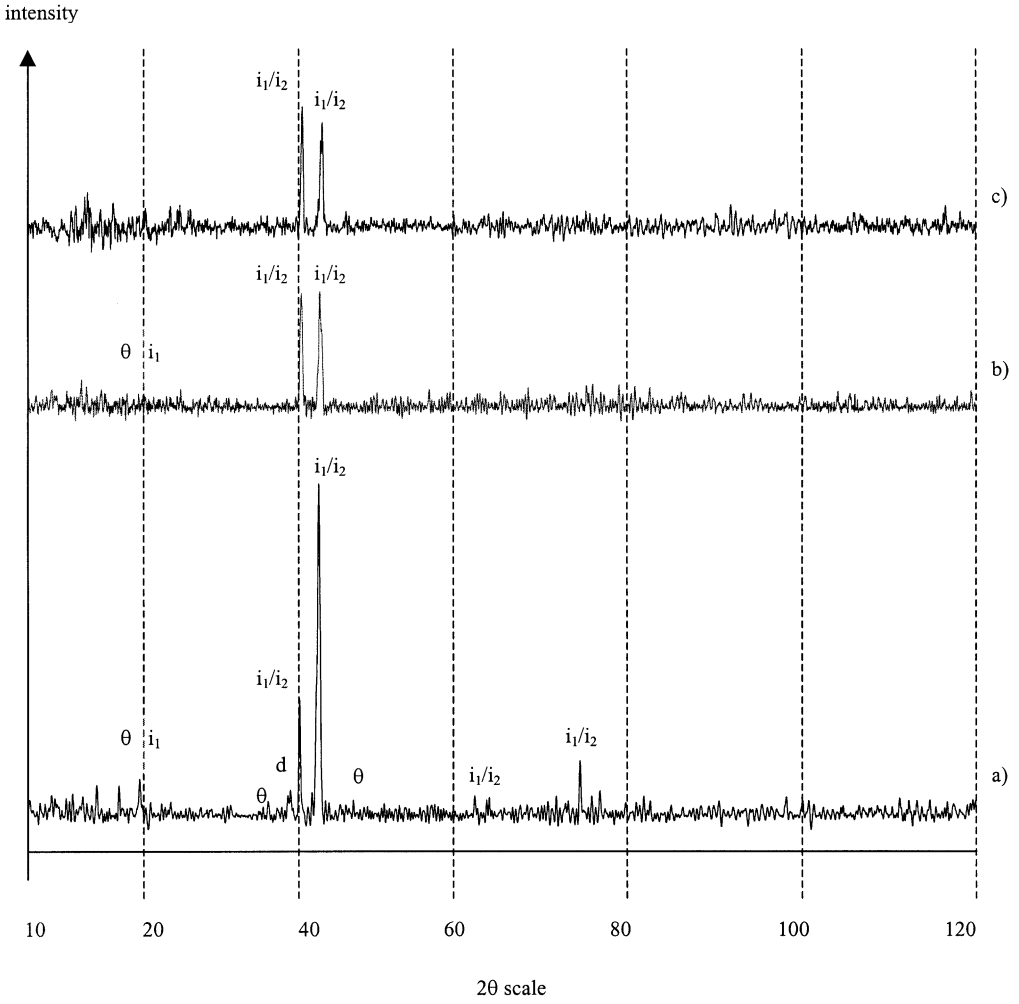

Fig. 4. XRD patterns for the (a) Al–Cu–Fe–Cr spray powder, (b) Al–Cu–Fe–Cr coating C sprayed with the lower spraying temperature, (c) Al–Cu–Fe–Cr coating D sprayed with the higher spraying temperature. i_1 denotes the icosahedral $Al_{80}Cr_{13.5}Fe_{6.5}$ phase, i_2 denotes the icosahedral $Al_{13}Cr_3Cu_4$ phase, θ stands for the tetragonal Al_2Cu phase and d stands for the decagonal phase in the Al–Cu–Fe–Cr system.

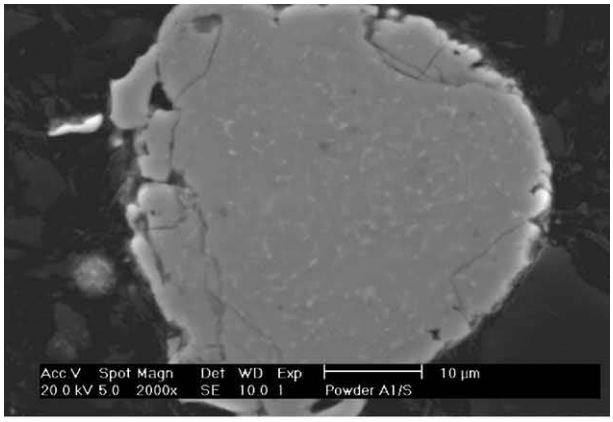

(a)

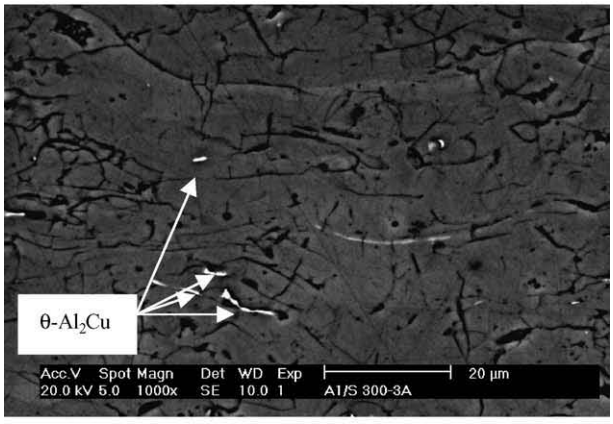

(b)

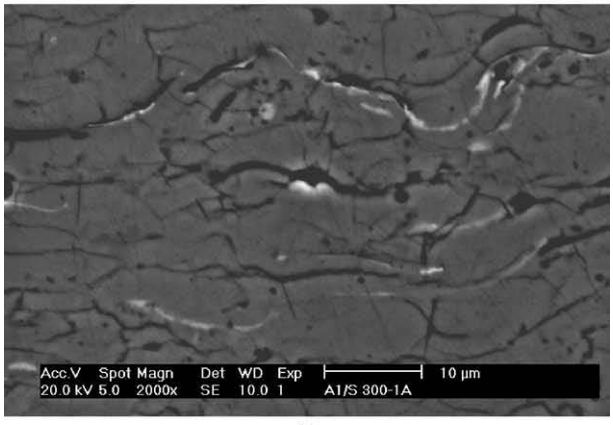

(c)

Fig. 5. SEM photographs showing the microstructural details of the Al–Cu–Fe–Cr feed powder and the HVOF sprayed coatings. (a) The morphology and microstructure of the Al–Cu–Fe–Cr feed powder F1. (b) The microstructure of the Al–Cu–Fe–Cr coating C deposited with the lower spraying temperature. (c) The microstructure of the Al–Cu–Fe–Cr coating D deposited with the higher spraying temperature.

The greater melting point of the Al–Cu–Fe–Cr feed power as compared to that of the Al–Cu–Fe feed powder was evidenced by differential thermal analysis (more detailed study of differential thermal analysis results is beyond the scope of the present study). It can, thus, be concluded that the Al–Cu–Fe–Cr powder particles were not melted completely during the spraying process. It is also worth noting that no oxidation was found to take place during the spraying process of the Al–Cu–Fe–Cr feed powder, independently of the spraying parameters. This contrasts sharply with the observations made for the Al–Cu–Fe coatings. Based on these results, it is suggested that the microstructure of the Al–Cu–Fe–Cr coatings is less sensitive to small changes in spraying temperature than the microstructure of the Al–Cu–Fe coatings.

ATEM studies were conducted for the Al–Cu–Fe–Cr feed powder and coatings C and D. However, due to the heavy charging of the feed powder under the electron beam, the microstructure of the feed powder could not be analysed with TEM. The coating particles were also charged in some degree, but the charging was not as intense as for the feed powder.

Fig. 6a shows the microstructure of the Al–Cu–Fe–Cr coating C viewed from the top of the coating. As can be noticed, the coating lamellas consisted of rather equiaxed grains of various sizes. This also applies to coating D. Both coating structures were found in ATEM examination to be composed of two different icosahedral phases (Fig. 6b and c). ATEM examination revealed the crushed coating particles to be mainly composed of either of these icosahedral phases. Both of them occurred seldom in the same particle. However, it is worth noting that no tetragonal θ-Al_2Cu phase could be encountered in either of the coating structures in ATEM studies.

The major phase in the coating C was detected to be the icosahedral phase i_1-$Al_{80}Cr_{13.5}Fe_{6.5}$ with the composition of 74.7 at.% Al, 10.1 at.% Cu, 7.4 at.% Fe and 7.8 at.% Cr. The electron diffraction pattern of this i_1-$Al_{80}Cr_{13.5}Fe_{6.5}$ phase from the fivefold axis is shown in Fig. 6b. The minor phase was the i_2-$Al_{13}Cr_3Cu_4$ phase, the composition of which was 66.5 at.% Al, 13.5 at.% Cu, 9.5 at.% Fe and 10.5 at.% Cr. The electron diffraction patterns of this i_2-$Al_{13}Cr_3Cu_4$ phase from five- and threefold axes are shown in Fig. 6c and d, respectively. In the coating D, in contrast, the icosahedral i_2-$Al_{13}Cr_3Cu_4$ phase was observed to be the major phase, with the composition of 60.5 at.% Al, 15.8 at.% Cu, 11.5 at.% Fe and 12.3 at.% Cr. The icosahedral i_1-$Al_{80}Cr_{13.5}Fe_{6.5}$ phase was the minor phase in the coating D. It exhibited a composition of 73.0 at.% Al, 10.5 at.% Cu, 7.9 at.% Fe and 8.5 at.% Cr.

4. Discussion

4.1. Microstructure of HVOF sprayed Al–Cu–Fe and Al–Cu–Fe–Cr coatings in the light of earlier coating studies

As compared to earlier studies on thermally sprayed Al–Cu–Fe coatings, deposited by plasma spraying, the phase structure of the studied HVOF sprayed Al–Cu–

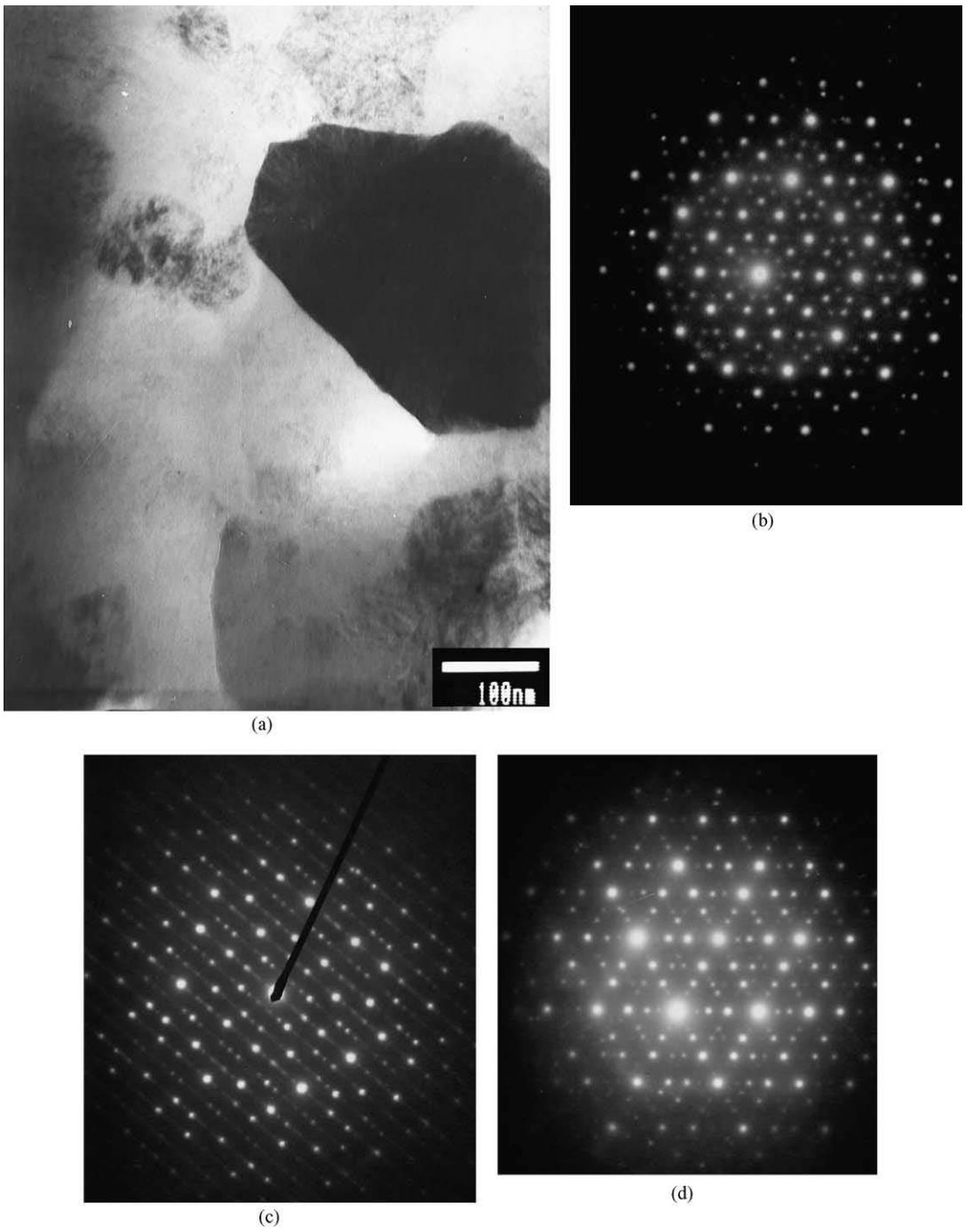

Fig. 6. Microstructure of the Al–Cu–Fe–Cr coating C sprayed with the lower spraying temperature. (a) TEM bright field image showing the coating structure from the top of the coating. Micrograph taken with the electron beam parallel to the fivefold axis of the dark grain. (b) Electron diffraction pattern of the major icosahedral i_1-$Al_{80}Cr_{13.5}Fe_{6.5}$ phase, taken along the fivefold axis. (c) Electron diffraction pattern of the minor icosahedral i_2-$Al_{13}Cr_3Cu_4$ phase, taken along the fivefold axis. (d) Electron diffraction pattern of the minor icosahedral i_2-$Al_{13}Cr_3Cu_4$ phase, taken along the threefold axis.

Fe coatings shows quite similar features. The HVOF sprayed coatings of the study are made up of the crystalline β-AlFe phase and the quasicrystalline i-$Al_{65}Cu_{20}Fe_{15}$ phase, which is in agreement with the earlier studies [8,17–19,23]. Only in one study [19], the formation of the λ-$Al_{13}Fe_4$ phase has been encountered in Al–Cu–Fe coatings in addition to the β-AlFe and i-$Al_{65}Cu_{20}Fe_{15}$ phases. Furthermore, oxygen has been detected both in the coatings of the present study and those reported in the earlier studies. Still, no pure aluminium oxide can be found in the HVOF sprayed Al–Cu–Fe coatings in this study or in the plasma-sprayed coatings of other studies. Oxygen is, therefore, incorporated in the coating structure rather as an oxidised form

of alloy present at lamella boundaries than a precipitated pure aluminium oxide phase [19].

Only Sordelet et al. [19] have earlier determined the composition of the phases present in thermally sprayed Al–Cu–Fe coatings. According to Sordelet et al., the average compositions of the neighbouring grains of the β-AlFe and i-$Al_{65}Cu_{20}Fe_{15}$ phases were 65.7 at.% Al, 21.9 at.% Cu and 12.5 at.% Fe and 73.9 at.% Al, 7.3 at.% Cu and 18.9 at.% Fe, respectively. The β-AlFe phase of the present study shows much higher amount of Cu as compared to the results of Sordelet et al. Similarly, the i-$Al_{65}Cu_{20}Fe_{15}$ phase of the coatings of this study is enriched in Cu as compared to that in the coatings of Sordelet et al. The composition of the feed powder is quite equal in our study and in the study of Sordelet et al., so it cannot be treated as a reason for the compositional difference of the coating phases. Besides, the Fe contents of the phases studied by us and by Sordelet et al. are of the same magnitude, suggesting that an excessive Al vaporisation cannot be a cause for the high Cu content of the coating phases of the present study. It is, however, important to keep in mind that the composition and volume ratio of coexisting phases as well as the spraying conditions all influence the composition of phases building the coating structure. As mentioned in the previous chapter, in the coatings of Sordelet et al., the λ-$Al_{13}Fe_4$ phase co-exists with the β-AlFe and i-$Al_{65}Cu_{20}Fe_{15}$ phases, while the coatings of the present study only contain the β-AlFe and i-$Al_{65}Cu_{20}Fe_{15}$ phases.

In addition to this compositional difference of the coating phases, the porosity level of the HVOF sprayed coatings of this study does not match with the earlier reported porosity levels in plasma- sprayed coatings. Based on the visual evaluation of the SEM photographs of the studied Al–Cu–Fe coatings, their porosity level is well below 10%. In plasma sprayed coatings, in contrast, porosities well above 10% are reported [17]. However, HVOF spraying generally introduces less porosity in coatings than plasma spraying, which is suggested to be the main reason for the difference in porosity level between the coatings of the study and those examined in earlier studies.

For the Al–Cu–Fe–Cr coatings of this study, the comparative data is mainly composed of earlier studies on the plasma-sprayed coatings [20,21] with one study concerning also HVOF sprayed coatings [24]. On one hand, according to Kong et al. [20], the as-sprayed coatings show a mixture of quasicrystalline and crystalline phases. Fleury et al. [24] have obtained similar results. They have specified these quasicrystalline phases to be icosahedrally and decagonally structured, while the crystalline phases refer to the quasicrystal approximant phases, the λ-$Al_{13}Fe_4$ phase and the β-AlFe phase. On the other hand, Dubois et al. [21] and Sordelet et al. [25] have shown that thermally sprayed Al–Cu–Fe–Cr coatings are only composed of quasicrystalline icosahedral and decagonal phases, with oxide particles present in the splat boundaries. This icosahedral phase is reported to be made up of 63.1 at.% Al, 24.6 at.% Cu, 11.6 at.% Fe and 0.7 at.% Cr. The composition of the icosahedral phase indicates it to be the one also occurring in the ternary Al-Cu-Fe system, i.e. the i-$Al_{65}Cu_{20}Fe_{15}$ phase. No exact composition of the quaternary decagonal phase, in contrast, is described [21]. The HVOF sprayed Al–Cu–Fe–Cr coatings of the present study, however, do not show the formation of any of the above-mentioned crystalline or quasicrystalline phases. In our study, the quasicrystalline i_1-$Al_{80}Cr_{13.5}Fe_{6.5}$ and i_2-$Al_{13}Cr_3Cu_4$ phases are encountered. The only crystalline phase found in our coatings is the θ-Al_2Cu phase. The marked differences between the icosahedral phases found in the coatings of this study and the earlier ones are suggested to be explained by the limited amount of data available for the Al–Cu–Fe–Cr quaternary system. The above-mentioned coating studies seem to comprise the majority of known literature on the Al–Cu–Fe–Cr quasicrystalline alloys. No proper phase diagrams, for example, exist for the system Al–Cu–Fe–Cr. Furthermore, the build-up of the decagonal phase is reported [21] to be heavily cooling-rate-dependent. The absence of this decagonal phase in our Al–Cu–Fe–Cr coatings is explained by a rather low cooling rate caused by the employment of low carbon steel substrates, the thermal conductivity of which is not sufficiently high (if compared for example to aluminium).

4.2. Influence of Cr alloying on the microstructure of HVOF sprayed Al–Cu–Fe coatings

Based on the Al–Cu–Fe phase diagram sketched by Faudot et al. [26], the feed powder of the observed composition of 56.3 at.% Al, 29.3 at.% Cu and 14.5 at.% Fe falls within the two-phase range of the β-AlFe and i-$Al_{65}Cu_{20}Fe_{15}$ phases, with somewhat equal phase amounts. The coexistence of these phases in the HVOF sprayed coatings of the study is, thus, in agreement with theory. Unfortunately, the corresponding information is not available for the Al–Cu–Fe–Cr system. It is, however, known that in Al–Cu–Fe–Cr alloys, quaternary icosahedral and decagonal phases as well as quaternary polymorphous quasicrystal approximants may exist. Also, a ternary icosahedral phase and many binary crystalline phases can be encountered in the Al–Cu–Fe–Cr system. Nevertheless, both reported icosahedral phases refer to the icosahedral phase existing also in the Al–Cu–Fe ternary system, the i-$Al_{65}Cu_{20}Fe_{15}$ phase, which may contain less than one percent Cr. In addition, the binary crystalline phases are the same as for the ternary Al–Cu–Fe system [21]. Our interest, therefore, lies mainly on the crystalline approximant structures of quasicrystals. The quasicrystal approximant phases in the Al–Cu–Fe–Cr alloys are determined to be

orthorhombically structured, with the alloying element concentrations varying from 5.0 at.% to 15.7 at.% Cu, from 10.0 at.% to 11.3 at.% Fe and from 7.1 at.% to 12.5 at.% Cr [21].

In this study, it is shown that the alloying of Al–Cu–Fe with Cr introduces two new ternary icosahedral phases, the i_1-$Al_{80}Cr_{13.5}Fe_{6.5}$ and i_2-$Al_{13}Cr_3Cu_4$ phases. In this study, the composition of the i_1-$Al_{80}Cr_{13.5}Fe_{6.5}$ phase is determined to be approximately 73.9 at.% Al, 10.3 at.% Cu, 7.7 at.% Fe and 8.2 at.% Cr. The composition of the i_2-$Al_{13}Cr_3Cu_4$ phase, in turn, is 63.5 at.% Al, 14.7 at.% Cu, 10.5 at.% Fe and 11.4 at.% Cr. These compositions are very close to those of the crystalline approximant phases reported by Dubois et al. [21]. Keeping in mind the fact that in the connection of the icosahedral i-$Al_{65}Cu_{20}Fe_{15}$ phase, the quasicrystal approximant phases form as a result of the annealing of a metastable quasicrystalline structure [27], it is suggested that there might be some structural relation between the new icosahedral phases identified in the HVOF sprayed coatings of the study and the approximant phases reported by Dubois et al. [21]. Nevertheless, it is sure that the addition of Cr to the Al–Cu–Fe alloy neither destabilises the icosahedral phase nor promotes the formation of the decagonal phase, as suggested by Dong and Dubois [28]. Instead, new icosahedral phases are introduced as a result of Cr addition to the Al–Cu–Fe alloy.

As for the structural characteristics of studied coatings, Cr addition to the Al–Cu–Fe alloy stabilises the quasicrystalline icosahedral phase yielding an almost completely quasicrystalline structure in the Al–Cu–Fe–Cr coatings, instead of a mostly crystalline structure of the Al–Cu–Fe coating. This stabilising influence of Cr alloying on the Al–Cu–Fe coating structure is also reflected in the negligible oxidation of the Al–Cu–Fe–Cr alloy during the spraying process as compared to the extensive oxidation of the Al–Cu–Fe alloy. Accordingly, the Al–Cu–Fe coatings contain oxide layers on the lamella boundaries. This build-up of an oxide layer on the splat boundaries has been shown to be typical for Al–Cu–Fe coatings [18,19], but also for Al–Cu–Fe–Cr [25] and for example for Al–Co–Fe–Cr [29] coatings as a result of a high-temperature spraying process. However, the oxidation of Al–Cu–Fe–Cr alloy during the coating process has been reported for coatings comprising of icosahedral and decagonal phases, the icosahedral one referring to the i-$Al_{65}Cu_{20}Fe_{15}$ phase existing in the ternary Al–Cu–Fe system, too. On the basis of the results obtained in this study, we suggest that the new icosahedral phases in the quaternary Al–Cu–Fe–Cr system, the i_1-$Al_{80}Cr_{13.5}Fe_{6.5}$ and i_2-$Al_{13}Cr_3Cu_4$ phases, are structurally more stable than the i-$Al_{65}Cu_{20}Fe_{15}$ phase and the quaternary decagonal phase existing in Al–Cu–Fe–Cr alloys. This structural stability introduces negligible oxidation during the HVOF spraying of the Al–Cu–Fe–Cr feed powder and the nearly oxide-free Al–Cu–Fe–Cr coating.

It is worth noting that as a result of spraying temperature change, no change in the influence of Cr alloying on the microstructure or phase selection of the Al–Cu–Fe coatings is introduced. The only notable difference brought about by the increased spraying temperature in the Al–Cu–Fe–Cr coatings is a minor shift in the volume ratio of the formed phases. In the Al–Cu–Fe–Cr coatings, the amount of the chromium-rich i_2-$Al_{13}Cr_3Cu_4$ phase somewhat increases as a result of higher spraying temperature, at the expense of the i_1-$Al_{80}Cr_{13.5}Fe_{6.5}$ phase and the remaining θ-Al_2Cu phase. No change in the oxidation behaviour can be observed in the Al–Cu–Fe–Cr coatings due to the raised spraying temperature. In the Al–Cu–Fe coatings, in turn, higher spraying temperature yields somewhat less quasicrystalline i-$Al_{65}Cu_{20}Fe_{15}$ phase as compared to the lower spraying temperature. The amount of the oxidised lamella boundaries simultaneously multiplies.

5. Conclusions

In this study, Al–Cu–Fe and Al–Cu–Fe–Cr thick coatings were deposited under different spraying conditions by a HVOF spraying technique to gain information on the influence of chromium alloying on the microstructure of HVOF sprayed quasicrystalline Al–Cu–Fe coatings in different spraying temperatures. The results obtained may be summarised as follows:

1. HVOF sprayed Al–Cu–Fe coatings are build up of lamellas of the crystalline β-AlFe phase. Individual particles of the quasicrystalline i-$Al_{65}Cu_{20}Fe_{15}$ phase exist between coating lamellas. Furthermore, the lamella boundaries are covered by an oxide layer. This oxide is not pure aluminium oxide but an oxidised form of either or both of the main phases. Due to the increased spraying temperature, the amount of the quasicrystalline phase is somewhat reduced and that of the oxide phase increased.
2. HVOF sprayed Al–Cu–Fe–Cr coatings are made up of the crystalline θ-Al_2Cu phase and two icosahedral phases, the i_1-$Al_{80}Cr_{13.5}Fe_{6.5}$ and i_2-$Al_{13}Cr_3Cu_4$ phases. As a result of the raised spraying temperature, the θ-Al_2Cu phase disappears, increasing the relative amount of the Cu-rich i_2-$Al_{13}Cr_3Cu_4$ phase. Coating lamellas are found to be composed of the icosahedral phases so that in one crushed coating particle, only either of these phases is detected. No oxide layer forms at the coating lamella surfaces.
3. HVOF spraying technique yields Al–Cu–Fe and Al–Cu–Fe–Cr coatings that are structurally

almost identical to those reported in literature, although they have been produced by plasma spraying. However, HVOF spraying introduces less porosity in coatings as plasma spraying. The porosity levels of the Al–Cu–Fe and Al–Cu–Fe–Cr coatings of the study were, thus, lower than those reported for plasma-sprayed coatings.

4. The present study provides new and complementary information on the phases occurring in a quaternary Al–Cu–Fe–Cr system. In addition to the icosahedral i-$Al_{65}Cu_{20}Fe_{15}$ phase, which also appears in the Al–Cu–Fe system, the icosahedral i_1-$Al_{80}Cr_{13.5}Fe_{6.5}$ and i_2-$Al_{13}Cr_3Cu_4$ phases exist in the Al–Cu–Fe–Cr alloys. The composition of the i_1-$Al_{80}Cr_{13.5}Fe_{6.5}$ phase is approximately 73.9 at.% Al, 10.3 at.% Cu, 7.7 at.% Fe and 8.2 at.% Cr, while that of the i_2-$Al_{13}Cr_3Cu_4$ phase is 63.5 at% Al, 14.7 at.% Cu, 10.5 at.% Fe and 11.4 at.% Cr. Earlier, the phases with these compositions are referred to be crystalline approximant phases of quasicrystals.
5. Cr addition to the Al–Cu–Fe coatings neither destabilises the icosahedral phase nor promotes the formation of the decagonal phase, as earlier suggested. Instead, new icosahedral phases are introduced as a result of the Cr addition to the Al–Cu–Fe alloy. It can, thus, be suggested that the icosahedral phase structure is stabilised by the Cr addition to the Al–Cu–Fe alloys.

Acknowledgements

E. H.-S. is deeply indebted to the Academy of Finland and Walter Ahlström Foundation for financing her research.

References

[1] Shechtman D, Blech I, Gratias D, Cahn JW. Phys Rev Lett 1984; 53:1951.
[2] Sordelet DJ, Dubois JM. Mater Res Soc Bull 1997;11:34.
[3] Wolf B, Bambauer KO, Paufler P. Mater Sci Engng 2001; A298:284.
[4] Jenks CJ, Thiel PA. Mater Res Soc Bull 1997;11:55.
[5] Dubois JM. Mater Sci Engng 2000;A294-296:4.
[6] Belin-Ferré E, Dubois JM, Fournée V, Brunet P, Sordelet DJ, Zhang LM. Mater Sci Engng 2000;A294-296:818.
[7] Brunet P, Zhang LM, Sordelet DJ, Besser M, Dubois JM. Mater Sci Engng 2000;A294-296:74.
[8] Sordelet DJ, Besser MF, Logsdon JL. Mater Sci Engng 1998; A255:54.
[9] Rapp Ö. Mater Sci Engng 2000;A294-296:458.
[10] Kimura K, Yamane H, Hashimoto T, Takeuchi S. Mater Sci Engng 1988;A99:435.
[11] Archambault P, Janot C. Mater Res Soc Bull 1997;11:48.
[12] Bilusic A, Pavuna D, Smontara A. Vacuum 2001;61:345.
[13] Bilusic A, Smontara A, Lasjaunias JC, Ivkov J, Calvayrac Y. Mater Sci and Engng 2000;A294-296:706.
[14] Eisenhammer T, Mahr A, Haugeneder A, Assmann W. Solar Energy Mater Solar Cells 1997;46:53.
[15] Kang SS, Dubois JM. Phil Mag 1992;A66:151.
[16] Urban K, Feuerbacher M, Wollgarten M. Mater Res Soc Bull 1997;11:65.
[17] Fleury E, Lee SM, Kim WT, Kim DH. J Non-Crystalline Solids 2000;278:194.
[18] Sordelet DJ, Besser MF, Anderson IE. J Thermal Spray Technol 1996;5:161.
[19] Sordelet DJ, Kramer MJ, Unal O. J Thermal Spray Technol 1995;4:235.
[20] Kong J, Zhou C, Gong S, Xu H. Surf Coatings Technol 2003; 165:281.
[21] Dubois JM, Proner A, Bucaille B, Cathonnet Ph, Dong C, Richard V, et al. Annales de Chimie-Sciences des Materiaux France 1994;19:3.
[22] Pawlowski L. The science and engineering of thermal spray coatings. Chichester, UK: John Wiley & Sons; 1995.
[23] De Palo S, Usmani S, Sampath S, Sordelet DJ, Besser M. Thermal spray. A united forum for scientific and technological advances. Ohio, USA: ASM; 1997 p. 135.
[24] Fleury E, Kim YC, Kim JS, Kim DH, Kim WT, Ahn HS, et al. J Alloys Compounds 2002;342:321.
[25] Sordelet DJ, Widener SD, Tang Y, Besser MF. Mater Sci Engng 2000;A294-296:834.
[26] Faudot F, Quivy A, Calvayrac Y, Gratias D, Harmelin M. Mater Sci Engng 1991;A133:383.
[27] Edagawa K, Waseda A, Kimura K, Ino H. Mater Sci Engng 1991;A134:939.
[28] Dong C, Dubois JM. J Mater Sci 1991;26:1647.
[29] Huttunen-Saarivirta E, Turunen E, Kallio M. J Alloys Compounds 2003;254:269.

PUBLICATION IV

On the role of particle state and deposition procedure on mechanical, tribological and dielectric response of high velocity oxy-fuel sprayed alumina coatings

In: Materials Science and Engineering 2005.
Accepted for publication.

On the role of particle state and deposition procedure on mechanical, tribological and dielectric response of high velocity oxy-fuel sprayed alumina coatings

E. Turunen, T. Varis, S.-P. Hannula*[1]
VTT Industrial Systems, Espoo, Finland

A. Vaidya, A. Kulkarni, J. Gutleber, S. Sampath, H. Herman,
State University of New York, Stony Brook, NY, USA

* Corresponding author: Tel: +358-20-722 5425, Fax: +358-20-722 7069
Email: erja.turunen@vtt.fi
Address: VTT, P.O.Box 1703, FI-02044 VTT, Finland

[1] S-P. Hannula is a joint professor of Helsinki University of Technology and VTT Industrial Systems

Key words: *Thermal spray, HVOF, process optimization, diagnostic, alumina, mechanical properties, thermal and electrical properties*

Abstract

It is well known that the high velocity oxy-fuel based thermal spray process impart high density and reduced porosity in coatings compared to those produced by other ambient thermal spray processes. The benefits of HVOF have largely remained in the domain of metals and cermets and limited investigations have been carried out in ceramic coatings. The ability to produce high density ceramic coatings (e.g. alumina) offers potential in high performance applications in the field of wear, corrosion resistance, and dielectric coatings. However, due to extreme operational limits of the HVOF process, the fundamentals of process-structure-property relationships are not fully understood.

In this paper, we report an integrated approach to establish processing-microstructure-property correlations in order to optimize coatings for such

applications. This approach involves diagnostic studies, microstructure development and its resultant influence on properties of high velocity oxy-fuel (HVOF) sprayed alumina coatings. The diagnostic studies were aimed to investigate the effects of fuel gas/oxygen ratio and amount of total gas flow on the particle temperature and velocity. Furthermore, splats and coatings were deposited to investigate the relationship between diagnostic data, melting behavior and droplet substrate interactions. Such a comprehensive study, coupled with property measurements of the coatings, demonstrates critical operational variables among deposition procedure, coating microstructure and the deposit properties.

Introduction

Thermal sprayed ceramic coatings, such as alumina, zirconia and cordierite, offer a cost-effective alternative to modify the component surface properties and are widely applied as thermal barrier and wear resistance coatings. Typical wear resistance applications range from large pipes and paper machine rolls to smaller objects such as fiber guides and sleeves [1, 2]. Thermal sprayed ceramic coatings also show interesting electrical properties and can be considered to offer an economical solution as dielectric coatings in a variety of thick film and insulated metal substrate based electronics applications [3]. Extensive development work on plasma sprayed coatings has being carried out [2, 3], but recent studies have shown that HVOF is capable of depositing dense ceramic coatings [4–6]. The high velocity operational regime promotes an overall dense structure and. is considered an important benefit in numerous applications involving requirements for corrosion and wear as well as electrical insulation resistance. The HVOF process, being an enhanced combustion process, allows for acceptable deposition efficiencies of ceramic particles through axial injection of feedstock powders. However, due to the lower flame temperatures achievable when deposited by HVOF as compared to the plasma spray process; this form of thermal spray has yet to be successfully utilized for the production coatings [6]. Advanced characterization has revealed the difference in pore structure between air plasma sprayed (APS) and HVOF sprayed alumina coatings observed previously, showing the existence of lamellar/globular porosity for APS coatings compared to inter-pass layered porosity for HVOF coatings [7, 8]. This "sandwich structure" of the HVOF coating, where the porosity is concentrated on the inter-pass layer boundaries can

partly explain the difference in properties observed for HVOF sprayed alumina in comparison with APS sprayed alumina.

On-line diagnostic is an effective tool to comprehend issues between different spray parameters and particle behavior in the flame. Although a number of published studies exist for the plasma spray process diagnostics, there has been limited focus on the high velocity processes [9–12]. In these studies it has been shown that altering the gas flows and mixing ratios, i.e. the ratio of fuel to oxygen, will influence both the flame temperature and velocity, thereby influencing flame-particle interactions and coating development.

The studies presented in this paper focus on gaining a systematic understanding of the influence of processing conditions (fuel gas/oxygen ratio, total gas flow and particle flux) on microstructure development in HVOF alumina coatings. The effects of fuel gas/oxygen ratio on the melting level of the particle, total gas flow and particle flux in terms of coating thickness per pass on the properties of the coatings are presented in this paper. In-flight diagnostics, coupled with single splat studies, provide insights into particle behavior in the combustion zone and upon impact, thus allowing comprehension and establishment of salient processing-microstructure-property relationships.

In addition to process studies, experiments were carried out to deliberate to change the microstructure development process in order to examine the role of spray pass interfaces on various physical, thermal and electrical properties of the HVOF coatings. Past studies [7, 8] have shown that in HVOF process the high flattening ratio enables high density of deposits with low surface roughness, however, a new category of interfacial defects are observed in the interpass region as the torch travels in and out of the substrate. Studies have shown these interpass morphologies play a dominant role in through thickness thermal conductivity and interface fracture. In this study, attempts were made to produce such interpass interfaces of different density. Such integrated studies not only shed light into microstructure-property relationships but offer additional strategies for design and process optimization.

Experimental procedure

Spray test setup: Coating deposition and spray diagnostics were accomplished with a Praxair HV-2000 spray gun, fitted with 22 mm and 19 mm combustion chambers allowing for varying process parameters. Nitrogen was selected to be used as a carrier gas, and propylene (C_3H_6) and hydrogen (H_2) as fuel gases. A two-axis traverse unit with a rotating spindle was used to manipulate the gun and substrates during coating deposition. Feedstock powder was Praxair Al-1110HP, 99.3% Al_2O_3, with a nominal size of -22/+5 μm. Such a small particle size is required in the case of HVOF in order to provide sufficient heating of the material to ensure melting and efficient deposition.

Diagnostics: In-flight diagnostics were carried out at different spray conditions to measure the particle velocity, temperature and diameter using the Tecnar DPV-2000 system. Measurement distance was varied between 150 and 200 mm. The DPV-2000 uses infrared pyrometer along with a dual slit optical device to perform measurements on individual particles [13]. The instrument relies on the basic principle, where a hot particle passes through the measurement volume, emits energy into the sensor head in the form of a two-peak signal due to the double slit geometry of the photomask in front of the lens. Since the physical distance between the slits (~210 μm) as well as the time between signal peaks are known, the velocity of the particle can be determined. The particle temperature is measured using a dual color optical pyrometer, which references the temperature based on energy emission at two discrete wavelengths. The diameter of a particle is estimated by the time integral of the complete signal normalized for velocity. Additionally, the sensor head is mounted on an X–Y traverse unit, which permits mapping of the spray plume.

Splat test: Single splats were collected onto polished stainless steel plates by spraying a single pass with low powder feed rate. Splats collected were observed by optical microscopy, to determine the extent of melting of the alumina particles. While the temperature data from diagnostic tests, based on the emissivity of a particle in-flight, provides the surface temperature of the particle, single splats enhance our understanding on the particle state. In case of a material with high melting point and less residence time in the flame (owing to high velocity), such as alumina, the surface temperature will not reveal the melting of the core of the particles.

Coating preparation: Coatings were sprayed onto the steel plates with size of 25 mm × 50 mm × 2 mm for microstructural and property characterization and 50 mm × 100 mm × 2 mm for electrical breakdown studies. The microstructural development was controlled through traverse rate of the gun and rotational speed of the carousel, thus obtaining a certain thickness/pass. The aim of the spray tests was to generate coatings with the same total thickness by varying layer thickness per pass and amount of passes. The powder feed rate was between 10.5 g/min and 13.6 g/min. Spray distance was varied between 150 and 200 mm. The parameter combinations were similar for the splat and coating deposition.

Coating characterization: Microstructural characterization of the coatings was carried out under a Scanning Electron Microscope (SEM). The SEM used was a LEO 1550 model with a Schottky Field Emission gun, a standard Secondary Electron detector, an in lens Secondary Electron detector and a Back Scattered electron detector. Freestanding deposits were evaluated for porosity content using a Helium pycnometry technique. The skeletal density of the coating in this measurement is measured by volume of gas (Helium) displaced by a known mass of substance.

Thermal properties: Thermal conductivity measurements were carried out on a 12.5 mm (0.5") diameter disk, coated with carbon on both surfaces, using a Holometrix laser flash* thermal diffusivity instrument. In this test, the sample is irradiated uniformly on one side using a single laser beam pulse (1.06 μm wavelength). The temperature rise on the other side is recorded as a function of time using an HgCdTe infrared detector (2–5.5 μm wavelengths). The recorded temperature-rise data, with allowance for the measured sample thickness, are used to calculate the thermal diffusivity directly. Knowledge of the bulk density, together with the thermal diffusivity and specific heat, allows determination of the thermal conductivity [14].

Mechanical properties: Elastic modulus measurements were carried out on polished top-surfaces of the coatings bonded to the substrate. In this technique, depth-sensitive indentation method extracts the materials properties using the contact response of a small volume of material. In the present study, a spherical indenter was used. Continuous measurements of load/displacement curves were performed with a Nanotest 600 (Micro Materials Limited, Wrexham Technology Park, Wrexham, LL 137YP, UK) instrument using a 1.56 mm (1/16") WC-Co spherical indenter with a maximum load of 10N. The instrument enables a basic

load/displacement curve to be obtained, or multiple partial load/unload cycles to be performed. The load-displacement records were evaluated based on the Oliver and Pharr method [15] where the elastic modulus was determined from the elastic recovery part of the unloading curve.

Wear properties: The abrasive tests were performed using a rubber wheel and a quartz-sand abrasion tester according to ASTM G65. Samples were pressured against rubber wheel by using static normal force of 45 N. Sliding velocity was 1.2 m/s and sliding distance 2140 m. The abrasive sand for this test was rounded quartz particles with average size of 245 μm, and the sand mass flow was 270 g/min.

Electrical properties: Dielectric properties were measured using a HP 4294A Impedance Analyzer. Using parallel plate principles, the dielectric behavior was observed from 40 Hz to 100 MHz, the values at 10 kHz and 1 MHz are reported here.

Electrical strength of the coatings was tested according to IEC 60243-1 C1.9.1 by increasing the voltage up to the breakdown. Brass electrode, ∅25 mm, was used over the coating, and larger brass electrode, ∅75 mm, was placed under the specimen. The voltage was increased linearly from zero up to flashover by the rate of rise 0.03–0.05 kV/s.

Results

Diagnostics: Figure 1 and Figure 2 summarize findings of the diagnostic study from altering gas mixture, total gas flow and oxygen/fuel gas ratio. In Figure 3 is summarized the effect of different barrel lengths and stand off distances on the particle velocity-temperature behavior. The total gas throughput from the gun has a strong influence on the gas velocity and temperature for a given gas mixture ratio. For the experiments conducted, it was found that highest temperatures for propylene were obtained using a fuel gas/oxygen ratio of 0.30. In the case of hydrogen as fuel gas, highest temperature was obtained by using a ratio of 2.48 for the explored parametric space: Details of the influence of these parameter settings on the particle velocity and temperature are discussed later.

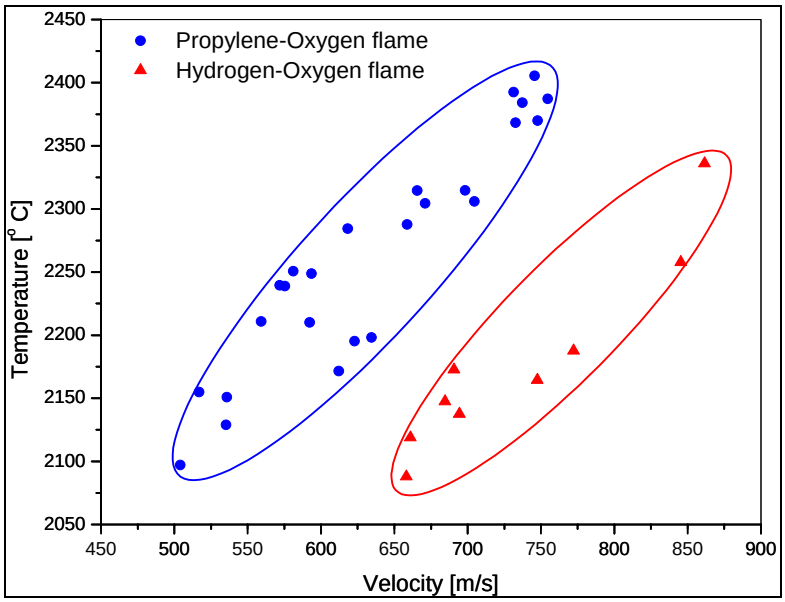

Figure 1. A first order process map for HVOF alumina depicting the range of particle temperatures and velocities for two fuel oxygen mixtures.

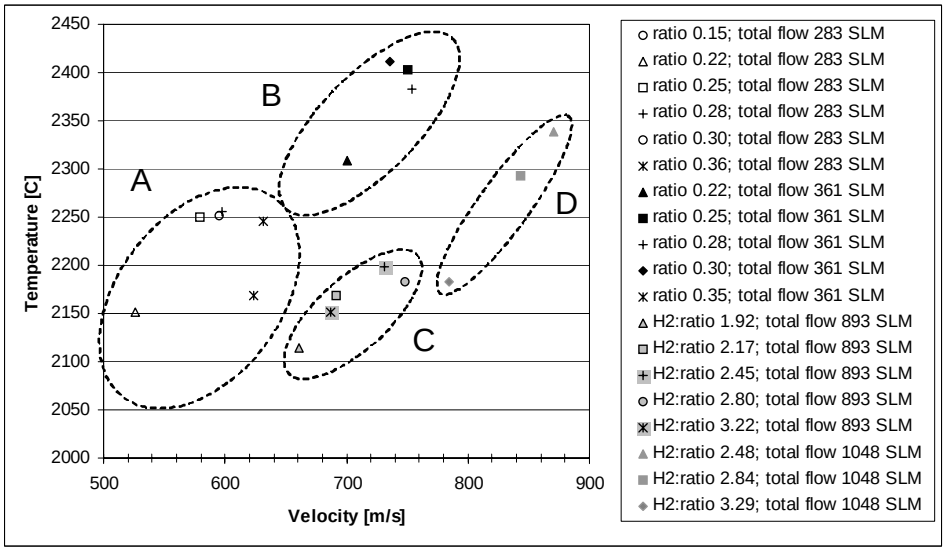

Figure 2. Process diagnostic data for different spray parameter combinations: Effect of total gas flow and gas flow ratio.

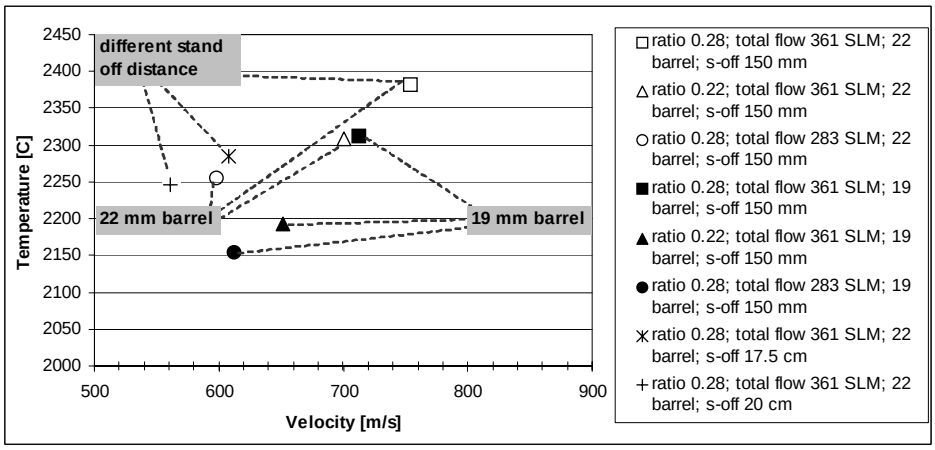

Figure 3. Process diagnostic data for different spray parameter combinations: Effect of barrel size and standoff distance.

Splat tests: Six spray parameter combinations were selected because of their influence on the single splats. The spray parameters used are listed in Table 1. Splats were produced to investigate the melting behavior of the particles. Wide range of splat morphologies observed is shown in Figure 4.

Table 1. Selected spray parameters and corresponding measured diagnostic data.

	Ratio C_3H_6/O_2	Total flow [l/min]	Stand off [mm]	T [°C]	v [m/s]
1	0.28	361	150	2390 ± 251	755 ± 120
2	0.22	361	150	2310 ± 204	700 ± 78
3	0.28	283	150	2210 ± 201	592 ± 86
4	0.28	361	200	2211 ± 159	560 ± 105
	Ratio H_2/O_2	Total flow [l/min]	Stand off [mm]	T [°C]	v [m/s]
5	2.48	1048	150	2339 ± 213	870 ± 124
6	2.17	893	150	2168 ± 170	692 ± 89

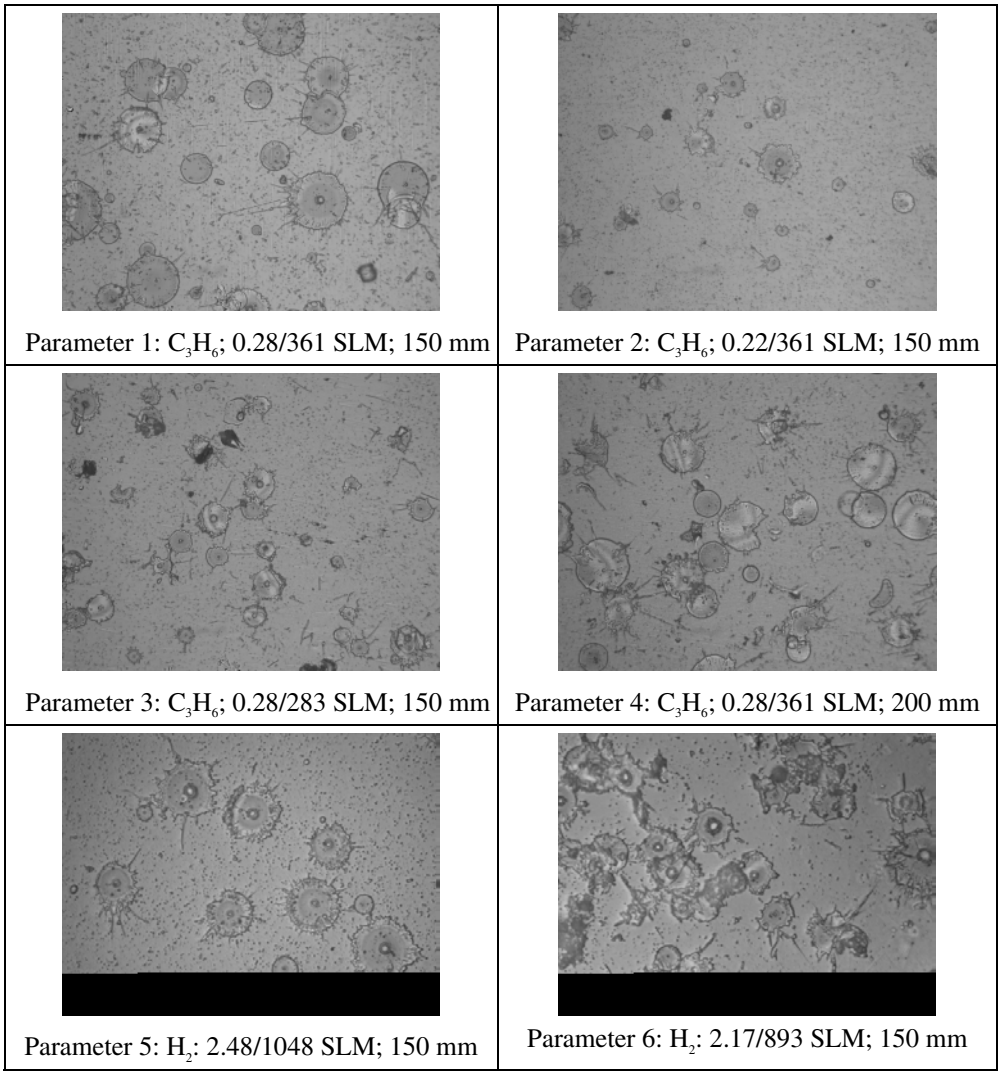

Figure 4. Micrographs depicting morphology of the splats collected at different spray parameters.

Deposition parameters: Coatings were sprayed with different fuel gas/oxygen ratios as listed in Table 2. All conditions from splat studies were selected. With condition 1 and 5, two variations of coatings were prepared varying thickness per layer. Total thickness was kept between 450–715 μm. Thickness per pass of the coating 'H' was found to be low due to poor deposition efficiency.

Table 2. Processing conditions for coating deposition.

	Ratio C_3H_6/O_2	Total flow [l/min]	Stand off [mm]	Thickness [µm]	Thickness/ pass [µm]
A	0.28	361	150	550	7.6
B	0.28	361	150	450	22.6
C	0.22	361	150	680	9.7
D	0.28	283	150	522	12.4
E	0.28	361	200	715	11.9
	Ratio H_2/O_2	**Total flow [l/min]**	**Stand off [mm]**	**Thickness [µm]**	**Thickness/ pass [µm]**
F	2.48	1048	150	620	4,8
G	2.48	1048	150	591	13,1
H	2.17	893	150	559	1,7

Coating characterization: A preliminary microstructural evaluation of the coatings was carried out using scanning electron microscopy (SEM). Microstructural details were examined looking at fractured surfaces, top surfaces and polished cross-sections. Figure 5 shows the top surface and fractured surface microstructures of coatings A, B and F. The top surfaces and the fractured surfaces of all the coatings look very similar. However, microcracking of the splats is observed on the top surface in each case in contrast to the single splat studies. A high magnification image is presented of the fractured surface showing well-adhered splats, indicative of complete melting (at least those that became part of the deposit). Figure 6 shows polished cross-section of the three coatings (A, B and F). The low magnification images show dense coatings with fine porosity while the corresponding high magnification images show detailed coating buildup. The formation of interpass porosity (corresponding to thickness per pass sprayed during processing) is observed for each of the three coatings.

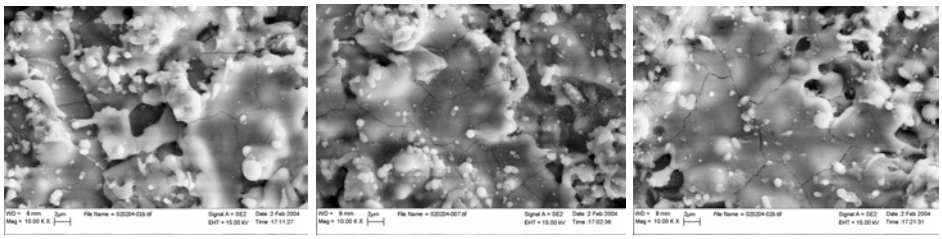

Coating A Coating B Coating F

Top surface

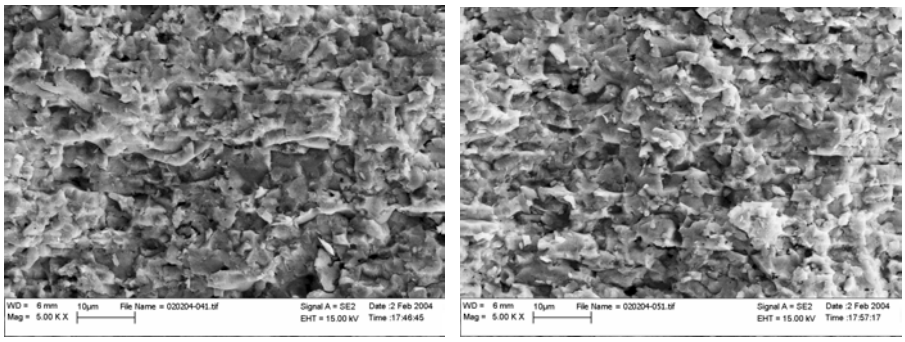

Coating A Coating F

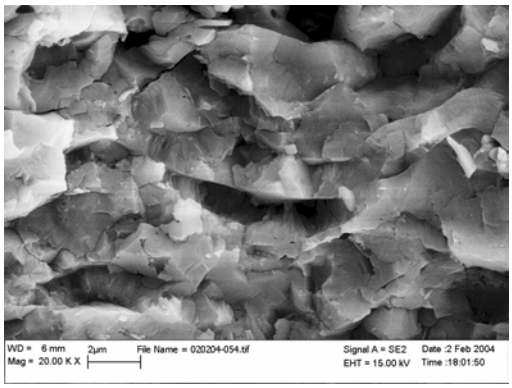

Coating F

Fractured cross-section

Figure 5. Top surface and fractured cross-section images of alumina coatings.

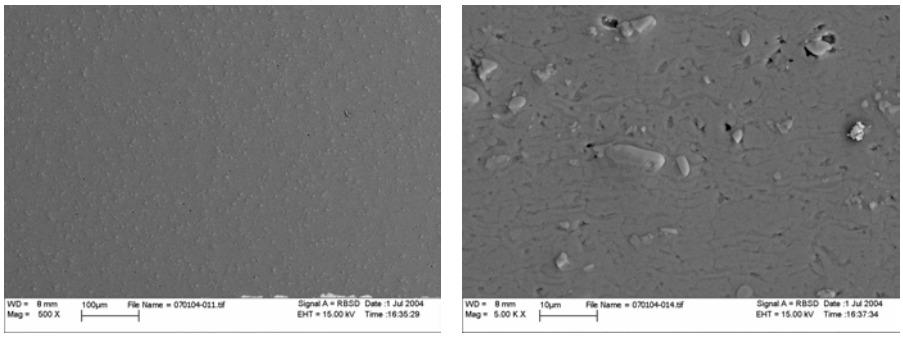

Coating A

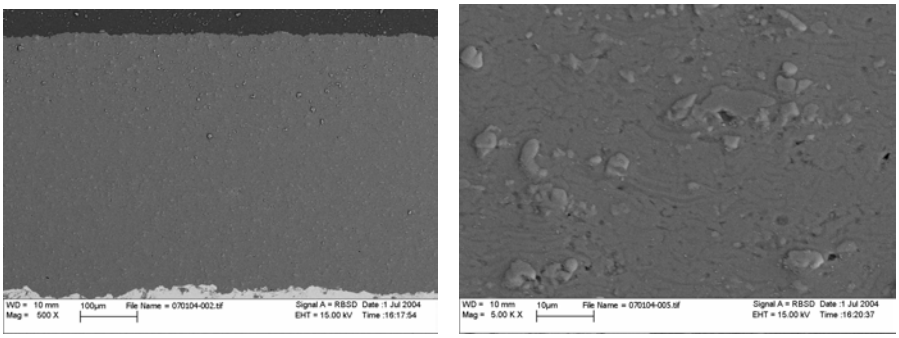

Coating B

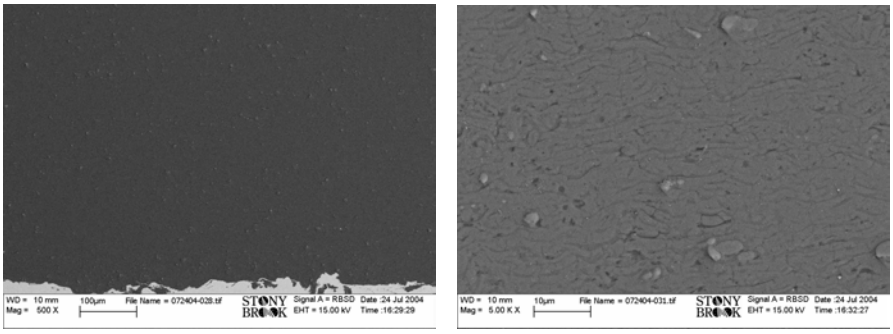

Coating F

Figure 6. Polished cross-section of alumina coatings, (A) low magnification images (500x) and (B) high magnification images (5000x).

Mechanical and thermal properties: Coatings were tested to compare the effect of different spray conditions and amount of interpass layering on the coating properties. In Table 3, density and elastic modulus for each coating is presented.

Not surprisingly, by using the hottest propylene and hydrogen parameters, highest density is obtained. As expected, density decreases as the melting status decreases.

Table 3. Density, Elastic Modulus and thermal conductivity of the coatings.

Sample	Density [g/cm³]	Elastic modulus [GPa]	Thermal conductivity [W/mK]
A	3.72	97 ± 6	3.88
B	3.70	100 ± 3	4.41
C	3.61	90 ± 4	3.74
D	3.65	99 ± 5	3.83
E	3.60	85 ± 2	3.58
F	3.72	100 ± 3	4.15
G	3.70	90 ± 5	3.86
H	3.66	97 ± 5	3.63

The variation in thermal conductivity for the eight coatings is also presented in Table 3. The overall thermal conductivity range was from 3.58 to 4.41. Similar to elastic modulus, thermal conductivity is lowest for the coating 'E' (sprayed at 200 mm standoff distance). Figure 7 (a) shows the thermal conductivity of the samples A–E plotted against number of interfaces normalized/mm for the coatings.

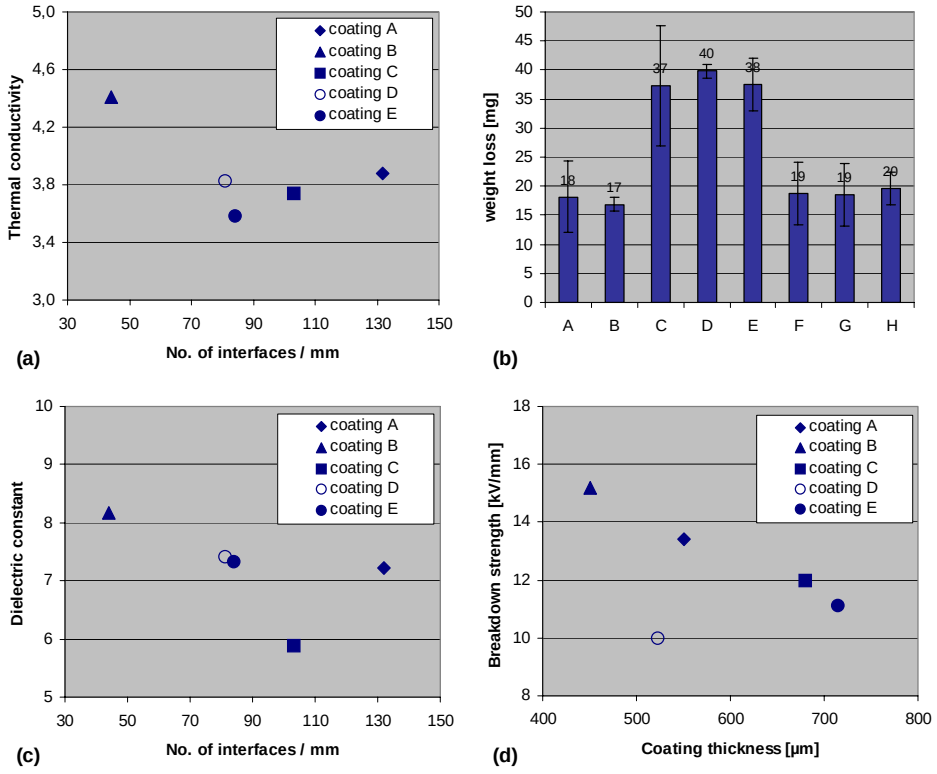

Figure 7. Mechanical, thermal and electrical properties of the coatings (a) Thermal conductivity, (b) Abrasive wear, (c) Dielectric constant, (d) Electrical breakdown strength as a function of coating thickness.

Electrical properties: The dielectric values were measured at 10 kHz and 1 MHz. Figure 7 (c) shows the dielectric behavior at 10 kHz for the samples A–E plotted against number of interfaces normalized/mm for the coatings. The dielectric constant varied from 5.9 to 8.2. An identical trend was observed when using 1 MHz. A clear correlation between number of interfaces and dielectric constant was again found. As the number of interpass interfaces increased, the dielectric constant was reduced.

The electrical breakdown studies were also performed for the coatings A–F. In the case of inhomogeneous thermal spray coatings, the breakdown always occurs at the "weak spot". It has been studied that mechanisms involved in the breakdown are mainly based on the corona discharge, which typically occur in the surrounding

medium such as voids and cracks. If electrical discharge and formation of the complete failure path is the main mechanism, the coating is damaged. Breakdown can partly operate in combination with thermal mechanism, in which case cumulative heating develops local paths with high electric field intensities. In this case, no definitive damage of the coating occurs [16].

Dielectric breakdown measured for the coatings sprayed by using propylene is presented versus thickness in Figure 7 (d). In all cases, electric arc occurred directly under the brass electrode. Upon repeated measurements at the same spot, only the main breakdown spot was left outside the electrode. Same values were obtained, which suggests that cracking and/or formation of major failure paths within coating under the test electrode does not occur. A small region (dia. 0.1–0.4 mm) was damaged within the main spot during breakdown.

Discussion

Diagnostics: The resulting 'Process map' for alumina in the temperature (T) – velocity (V) space is depicted in Figure 1. It must be noted that the operating range of the gas flows and fuel to oxygen ratios are quite different for the two mixtures. Two clear regions of different T and V arise from the use of different fuel gases. The hydrogen – oxygen mixtures typically resulted in greater velocity of the particles. Within each fuel gas, the effect of gas chemistry on the flame and resulting particle condition was examined by varying parameters such as fuel gas to oxygen ratios, total gas flow rates and different standoff distances. Conventional limits of gas ratios and flows were exceeded to obtain a wide velocity-temperature range.

A closer look at the effect of total gas flows and gas ratios is provided in Figure 2. It summarizes findings of the diagnostic study from altering total gas flow and oxygen/fuel gas ratio. In this figure, (A) and (B) refer to the zones of velocity and temperature achieved by using a gas mixture of propylene and oxygen while maintaining a total gas flow of 283 l/min and 361 l/min respectively. On the whole, there is a strong correlation between the velocity and temperature since the two total flow rate zones are separated quite clearly. A similar effect can be seen from (C) and (D) which are the values for hydrogen – oxygen gas mixtures with total flow rates of 893 l/min and 1048 l/min. Within each group of conditions, there is a

systematic variation of particle condition depending on the operating parameters. This variation is examined in detail in Figure 8.

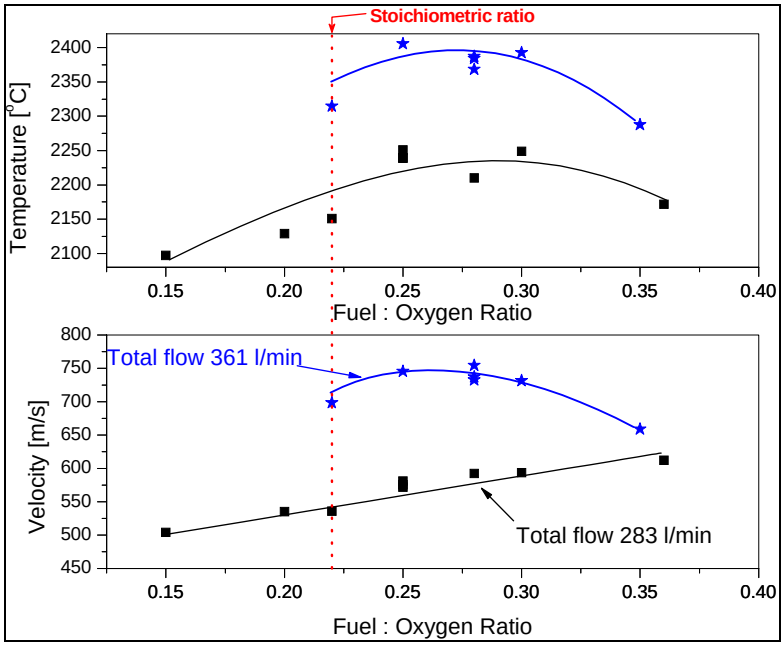

Figure 8. Variation in particle temperature and velocity as a function of fuel to oxygen ratio and total gas flow rates.

Figure 8 depicts the variation in particle temperature and velocity as a function of the fuel to oxygen ratio for two different total gas flow rates. Clearly, the total gas throughput through the gun has a strong influence on the gas velocity and temperature at a given ratio. The temperature increase in going from low to high flow rate seems to be uniform across all ratios. The change in particle velocity is not so uniform. In case of the high total flow rate condition, the velocity maximum coincides with the temperature maximum at a value of 0.30 i.e. the gas mixture had to be set to a fuel rich condition to achieve the maximum temperature for a fixed gas flow rate. For the lower flow rate conditions, the velocity values do not show a clear maximum. The values at stoichiometric ratio (0.22 as marked with the line) were found to be much lower than the maximum values recorded. The total gas flow could not be exceeded beyond 361 l/min due to safety and equipment considerations. It is expected that if the total gas flow was increased continuously, there would not be accompanying rise in temperature beyond an optimum point.

The velocity of particles is predominantly affected by the momentum of gases. Therefore, it would be more reasonable to evaluate temperature and velocity changes with respect to the total mass flow rate of the gases (since the nozzle opening is fixed, the increase in mass flow rate would correspond to an increase in the momentum of gases flowing through the torch). Such a comparison is provided in Figure 9. As can be seen, there is an almost linear increase in both velocity and temperature for a given ratio as the total mass flow rate of gases is increased (sample line drawn at common ratio value at all mass flows). Safety issues limited the range of mass flows that could be examined but it can be hypothesized that at sufficiently high mass flow rates, there will be a saturation or decrease in temperature due to incomplete combustion.

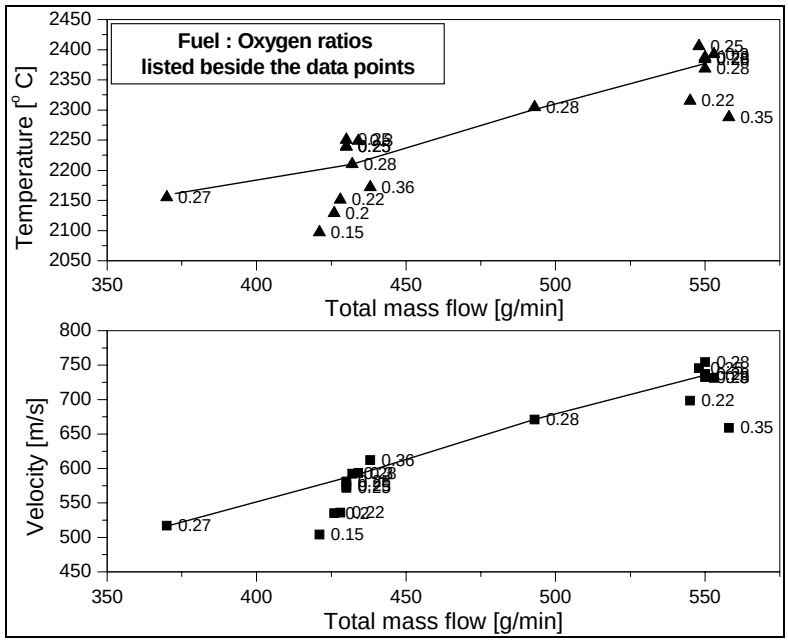

Figure 9. Velocity and temperature change as a function of total mass flow rate and ratio.

When using hydrogen, similar trends with lower temperatures but higher velocities were recorded. This is consistent with what has been reported before [12]. By increasing the amount of oxygen, particle temperature was seen to increase initially, but before the stoichiometric point, maximum value was obtained and subsequently there was a decrease in temperature.

Effect of using a longer and shorter combustion chamber (22 mm and 19 mm) and the effect of changing spray distance are shown in Figure 3. Comparing performance of combustion chambers, it is seen clearly that the length has a significant effect on the particle temperature but not on the velocity. A longer length of the nozzle seems to allow for better combustion of gases and heat transfer to the particles thereby raising the temperature, but velocity is governed more by the throughput of gases.

The effect of standoff distance on particle conditions was examined for three different spray distances. As seen in Figure 3, the highest velocity and temperature point is that measured at shortest spray distance (150 mm), the one with medium values at 175 mm and the lowest velocity and temperature point at 200 mm. Over the range of spray distances studied, temperature drop is not very significant (5%), but the change in velocity is (25%). The particles at longer distance have longer dwell times due to decrease in velocity as well as the longer spray distance. This results in better melting of the particles and is reflected in the splat formation as discussed below. It should be mentioned that with increasing spray distance, the divergence of spray plume also increases. This leads to a wider 'footprint' during coating and a change in thickness per pass of the deposit.

Splat tests: Different temperature-velocity points were selected to investigate of the particle surface temperature on the melting behavior of particle. It is evident that the particle wetting and flattening is dependent on the particle conditions in the flame. The best wetting was obtained for the parameter 1 producing highest Tp, Vp with maximum melting behavior. By decreasing particle temperatures and velocities, the largest particles were insufficiently melted and bounce away from the substrate (parameter 2).

Effect of particle flight time in the flame was demonstrated with parameters 3 and 4. With these two parameters, the data obtained from diagnostic measurements were identical but at different stand off distances. However, as discussed earlier particles melting efficiency was higher for those at extended stand off distance (parameter 4). This is evident from Figure 3 where the splat shape and splat density difference is seen. Splats set condition 5 and 6 were sprayed by using hydrogen as a fuel gas with two different total gas flows and ratios. Diagnostic studies showed that parameter set 5 gives slightly lower maximum particle temperatures, but higher velocities. Condition 6 was selected for comparison of lower and higher particle

temperature and velocity to the melting stage of the particle. Melting is good with both hydrogen parameters. In general the H2 condition resulted in a larger degree of fragmentation compared to the propylene conditions (comparing parameters 1 and 4). This is attributed to increased particle velocities.

Coating characterization: The intrinsic properties of the individual splats and their buildup in formation of the coating are affected by the in-flight feedstock-particle properties within the flame (i.e., their temperature, velocity, size, and degree of melting). From the high magnification images (Figure 6) the distinct features, corresponding to thickness per pass sprayed during processing, are observed in all three coatings. The coatings were deposited with different conditions (A with 7.6 μm per pass, B with 22.6 μm per pass and F with 4.8 μm per pass). This is evident in the high magnification images where maximum numbers of interfaces are observed for the coatings F and A as compared to coating B. This will influence coating properties as discussed below.

Mechanical properties: Decrease in density of the thermal sprayed coatings compared to the bulk density is a combination of the interlamellar pores, globular pores and cracks. However, the HVOF coating shows well-adhered splats with finer porosity compared to the plasma sprayed coatings [8]. The lower surface roughness for the top surface of the HVOF coating (compared to plasma spray) results from the use of a finer powder, from enhanced splat flattening, and from the smooth surface of the individual splats collected [3].

Clear correlation between diagnostic studies and melting stages of the particles obtained from the single splats can be observed. Highest density values are obtained with the hottest propylene and hydrogen parameters. Elastic modulus measured for the coatings correlates well with this observation, having highest modulus for the coatings having highest density. However, overall no strong differences in elastic modulus were observed. The low modulus of coating 'C' can be attributed to the low fuel/oxygen ratio compared to others. The coating 'E' showed the lowest modulus of all since it is sprayed at 200 mm standoff distance, compared to 150 mm for all others. This again correlates well with the lower particle velocity at increased standoff distances.

Wear resistance of the coatings also correlates with the particle state, and especially with the melting stage of the particles. Coatings deposited using hottest parameters,

had the best abrasive wear resistance. In the case of hydrogen, the effect of the total gas flow rate or the gas ratio is not that strong as compared to the coatings manufactured by using propylene.

A clear correlation between number of interfaces and dielectric constant was found. The behavior was similar to the thermal conductivity. In the case of high deposition rate (Coating 'B' with 22.6 μm per pass) there exist very few interfaces, thus giving highest thermal conductivity among all coatings. Coating A is sprayed with exactly same condition, but the thickness per layer is 7.6 μm per pass decreasing thermal conductivity of the coating. For all other coatings, there exist increasing amount of porosity between layers due to interpass layering effect, thus lowering the thermal conductivity. Spray parameters and flattening rate of the splats also effect the thermal conductivity. For coating 'E' having highest porosity due to the longer standoff distance the lowest thermal conductivity is measured.

Lower deposition rate leads to larger number of interpass interfaces, resulting in a lower dielectric constant. The interpass region can be treated as air gap resulting in a composite capacitor with alumina and air. Modeling work is underway to develop a constitutive relationship between this composite microstructure and dielectric properties.

The breakdown strength strongly depends on the coating thickness and follows the same trend as those reported in the literature for thermal spray coatings [3]. Breakdown voltages measured are presented in the Figure 7 (d) and are as follows for the various samples: a) 7.3 kV, b) 6.7 kV, c) 8.2 kV, d) 5.3 kV, e) 8.0 kV, f) 9.6, g) 9.4, and h) 9.4. It can be assumed that formation of the critical failure path is not linearly dependent on the coating thickness. After certain threshold value is exceeded, formation of the critical failure path is faster. Partly this is introduced by increased vertical cracking when coating thickness is increased. However, when results are normalized with coating thickness, better values are obtained for the thinner coatings.

These studies have shown that a combination of particle parameters and deposit build-up strategies can be used to manipulate and control coating properties. Establishing process-particle state correlations concurrently with microstructure-property relationships will ultimately enable new design strategies for coatings.

Conclusions

An integrated study with respect to processing, microstructure and properties of HVOF alumina was undertaken to understand each aspect of this chain. A spectrum of temperature velocity regimes can be obtained by varying process parameters such as fuel gas mixtures, fuel gas/oxygen ratio and total gas flow resulting in a range of melting states for the particles along with different kinetic energies. It is observed that a wider melting spectrum is demonstrated by the propylene – oxygen system. This can have implications for both – a larger control domain for the particles (and thus coating properties) if the process is controlled, or a wider variability in properties if the process control is inadequate.

It has been shown that the particle temperature and the melting state control the deposit efficiency and the build-up rate while the flattening behavior is dominated by particle kinetic energy.

The coating density and mechnical properties are strongly affected by particle velocity when complete melting is achieved. The particle state in the case of HVOF is very sensitive to the standoff distance and is found to be an influential parameter controlling microstructure and properties.

It has been noted that in HVOF the inter-pass interfaces play a dominant role in thermal, electrical and tribological properties. This is attributed to the large flattening degree of HVOF splats compared to their plasma spray counterparts. This introduces an additional degree of freedom with respect to property control. By varying coating build-up rate (through a combination of feedrate and robotic trajectory management), different interpass porosity structures were created in the coating. Clear correlations were obtained between nature of pore architecture with the thermal and dielectric behavior.

Such systematic and integrated studies enable a science based approach to coating development and optimization and ultimately provide a foundation for coating integrated component design.

Acknowledgement

This work was sponsored by the MRSEC program of the National Science Foundation under award DMR – 0080021 and by TEKES, National Technology Agency of Finland.

References

[1] Damani, R.J. & Makroczy, P. Heat treatment induced phase and microstructural development in bulk plasma sprayed alumina. Journal of the European Ceramic Society 20(2000), pp. 867–888.

[2] Ramachandran, K., Selvarajan, V., Ananthapadmanabhan, P.V. & Sreekumar, K.P. Microstructure, adhesion, microhardness, abrasive wear resistance and electrical resistivity of the plasma sprayed alumina and alumina-titania coatings. Thin Solid Films, 315(1998), pp. 144–152.

[3] Swindeman, C.J., Seals, R.D., Murray, W.P., Cooper, M.H. & White, R.L. Proceedings of the 9th National Thermal Spray Conference; Practical Solutions for Engineering Problems, ASM, Cincinnati, OH, USA, October 7–11, 1996, pp. 793–797.

[4] Thorpe, M.L. & Richter, H.J. A Pragmatic Analysis and Comparison of HVOF Processes. J. Therm. Spray Technol. 1, 2(1992), pp. 161–170.

[5] Sturgeon, A.J., Harvey, M.D.F., Blunt, F.J. & Dunkerton, S.B. Proceedings of 14th International Thermal Spray Conference. Current status and future trends, High Temperature Society of Japan, Kobe, Japan, May 22–26, 1995, pp. 669–673.

[6] Dent, A.H., Patel, A., Gutleber, J., Tormey, E., Sampath, S. & Herman, H. High velocity oxy-fuel and plasma deposition of BaTiO3 and (Ba,Sr)TiO3. Materials Science and Engineering B87(2001), pp. 23–30.

[7] Kulkarni, A., Sampath, S., Goland, A., Herman, H. & Dowd, B. Computed microtography studies to characterize microstructure-property correlations in thermal sprayed alumina deposits. Scripta mater. 43(2000), pp. 471–476.

[8] Kulkarni, A., Gutleber, J., Sampath, S., Goland, A., Lindquist, W.B., Herman, H., Allen, A.J. & Dowd, B. Studies of the microstructure and properties of dense ceramic coatings produced by high-velocity oxygen-fuel combustion spraying. Materials Science and Engineering A369(2004), pp. 124–137.

[9] Ignatiev, M., Smurov, I. & Bertrand, P. Proceedings of International Thermal Spray Conference. (ITSC 2002), DVS, Essen, Germany, March 4–6, 2002, pp. 72–77.

[10] Hearley, J.A., Little, J.A. & Sturgeon, A. J. The effect of spray parameters on the properties of high velocity oxy-fuel NiAl intermetallic coatings. Surface and Coatings Technology 123(2000), pp. 210–218.

[11] Arsenault, B., Legoux, J.G., Hawthorne, H., Immarigeon, J.P., Gougeon, P. & Moreau, C. HVOF process optimization for the erosion resistance of WC-12Co and WC-10Co-4Cr coatings. International Thermal Spray Conference 2001, Singapore; 28–30 May 2001, pp. 1051–1060.

[12] Lugscheider, E., Herbst, C. & Zhao, L. Parameter studies on high-velocity oxy-fuel spraying of MCrAlY coatings. Surface and Coatings Technology 108–109(1998), pp. 16–23.

[13] Blain, J., Nadeau, F., Pouliot, L., Moreau, C., Gougeon, P. & Leblanc, L. An Integrated Infrared Sensor System for On-Line Monitoring of Thermally Sprayed Particles. Proceedings, 10th International Conference on Surface Modification Technologies, SMT-10, Singapore, 2–4 Sept. 1996, pp. 677–686.

[14] Parker, W.J., Jenkins, R.J., Butler, C.P. & Abbott, G.L. Flash Method of Determining Thermal Diffusivity, Heat Capacity and Thermal Conductivity. J. Appl. Phys. 32, 9(1961), p. 1679.

[15] Oliver, W.C. & Pharr, G.M. An Improved Technique for Determining Hardness and Elastic Modulus Using Load and Displacement Sensing Indentation Experiments. J. Mater. Res. 7(1992), pp. 1564–1583.

[16] Kim, H.-J., Odoul, S., Lee, C.-H. & Kweon, Y.-G. The electrical insulation behaviour and sealing effects of plasma sprayed alumina-titania coatings. Surface and Coatings Technology 140(2001), pp. 293–301.

PUBLICATION V

Parameter optimization of HVOF sprayed nanostructured alumina and alumina-nickel composite coatings

In: Surface & Coatings Technology 2005.
Accepted for publication.

Available online at www.sciencedirect.com
SCIENCE DIRECT
Surface & Coatings Technology xx (2005) xxx – xxx
SURFACE & COATINGS TECHNOLOGY
www.elsevier.com/locate/surfcoat

Parameter optimization of HVOF sprayed nanostructured alumina and alumina–nickel composite coatings

Erja Turunen[a,*], Tommi Varis[a], Tom E. Gustafsson[a], Jari Keskinen[b], Teppo Fält[c], Simo-Pekka Hannula[a,c]

[a]VTT Industrial Systems, Espoo, VTT, P.O. Box 1703, FIN-02044 VTT, Finland
[b]VTT Processes, Tampere, Finland
[c]Helsinki University of Technology, Physical Metallurgy and Materials Science, Espoo, Finland

Received 16 February 2005; accepted in revised form 9 May 2005

Abstract

The use of a dense ceramic layer as an environmental barrier is often limited due to the differences in coefficient of thermal expansion (CTE) between the coating and steel substrate and poor mechanical strength of the ceramic layer. Nanocrystalline composite materials have been recognized to have special mechanical properties, especially improved fracture toughness in bulk form. In this paper, efforts in transferring the same type of improvements into a thermal spray coating have been made. Development of high velocity oxy-fuel (HVOF) spraying of nanocrystalline Al_2O_3- and Al_2O_3–Ni-coatings, where up to ten percent of nickel has been added in order to toughen the coating, is described. Spray parameters were optimized for HV-2000 HVOF spraying system based on the on-line diagnostics and single splat studies. Parameters were selected aiming at different melting stages of the powder. The resulting microstructure of the coatings and effect of it on the coating properties is discussed.

Keywords: Thermal spraying; HVOF; Process optimization; Diagnostic; Alumina; Nanofraction; Mechanical properties

1. Introduction

Thermal spraying is an effective and low cost method to apply thick coatings to change surface properties of the component. Coatings are used in a wide range of applications including automotive systems, boiler components, power generation equipment, chemical process equipment, aircraft engines, pulp and paper processing equipment, bridges, rollers and EAF electrodes in steel mills, concrete reinforcements, orthopedics and dental, land-based and marine turbines, ships, etc.

Ceramic coatings offer an interesting alternative to produce a protective layer over a steel structure due to their excellent chemical, corrosion and thermal resistance. Plasma spraying is the most widely used method to produce a thick ceramic coating. Recently it has been shown that HVOF process can produce much denser coatings and hence better environmental protection capacity than plasma sprayed coatings [1–3].

Poor mechanical strength as well as mismatches in coefficient of thermal expansion (CTE) often limits the use of dense ceramic coatings on metals. However, increasing porosity would decrease the protection capability of the coating. It is already recognized that nanocrystalline materials have special mechanical properties. Typically the strength of crystalline materials is increased with decreasing grain size and materials with small grain size often exhibit also superplastic behavior at elevated temperature. Nanocrystallinity has a positive influence on toughness of ceramic materials especially if alloyed with nanophased metals [4–6]. Furthermore, hardness and wear properties of coatings are usually improved. There are several recent reviews on mechanical properties of nanocrystalline materials [7–9].

* Corresponding author. Tel.: +358 20 722 5425; fax: +358 9 463 118.
E-mail address: erja.turunen@vtt.fi (E. Turunen).

0257-8972/$ - see front matter © 2005 Elsevier B.V. All rights reserved.
doi:10.1016/j.surfcoat.2005.05.018

The main effort that has been made so far in the field of nanostructured thermal spray materials has focused on the development of HVOF sprayed metallic or cermet coatings and atmospheric plasma spraying (APS) sprayed ceramic coatings [10,11]. The ceramic coating research is mainly focused on development of APS alumina–titania coatings, which possess superior toughness and adhesion along with high wear and spallation resistance [12–15].

Due to the higher kinetic energy, shorter dwell time of particles in the flame and lower flame temperature compared to the plasma spray, HVOF offers an interesting combination to produce dense coatings with less phase transformations [16]. However, thermal spraying is a very complex process including a number of variables. Particle melting stage and possible phase transformations during particle flight in the thermal spray flame must be controlled, as well as coating build up mechanism including splat interface and stress stages. Different tools have been developed in order to better understand the deposit formation and its relationship to the coating properties. These tools are currently presented under a concept of "Process Map" [17]. It can be considered to have two different meanings aiming either a) the optimization and mapping of different in-flight process conditions of particles producing different melting stages for particles or b) explaining the effect of different splat structures and substrate conditions on the final structure and properties of the deposited coating. These two maps have lately been named as "First order map" and "Second order map" [17].

In order to produce a coating with desired properties, e.g. with high fracture strength, it is not sufficient to control only material structure inside one lamella. Interaction between lamellae, stress stages of the final coating, adhesion to the substrate and cracking must be also controlled. These different phenomena which influence the final quality of the coating are depicted schematically in Fig. 1.

In this work the HVOF coating process for producing nanocrystalline Al_2O_3- and Al_2O_3–Ni-coatings is described. Focus is on the process control, lamellae microstructure, lamellae interaction and their effect on mechanical coating properties, such as hardness, wear resistance and fracture toughness.

2. Experimental procedure

2.1. Spray powder development

Various ways to produce ceramic nanocomposite powders exist. In the present work the synthesis of Al_2O_3 powder with and without Ni-nanoparticles was carried out using boehmite (AlO(OH)) as a starting media. The process is initiated by diluting $Ni(NO_3)_2$ to ethanol and then adding AlO(OH). The amounts are chosen to give the required Ni/Al_2O_3 ratio. After drying the resulting powder is calcined at 500 °C for 2 h to obtain NiO–γ-Al_2O_3. Both nickel oxide and alumina are as nanosized particles.

After calcinations nanopowder particles were agglomerated into larger agglomerates by spray drying. After agglomeration the powder was heat treated in argon containing hydrogen to reduce NiO to metallic nickel and to transform γ-alumina to α- or θ-alumina and to sinter particles together. The temperature used was 1100 °C for 3 h. The temperature was limited to this due to the limitations in the furnace equipment. For some powder batches heat treatment and reduction were performed simultaneously in

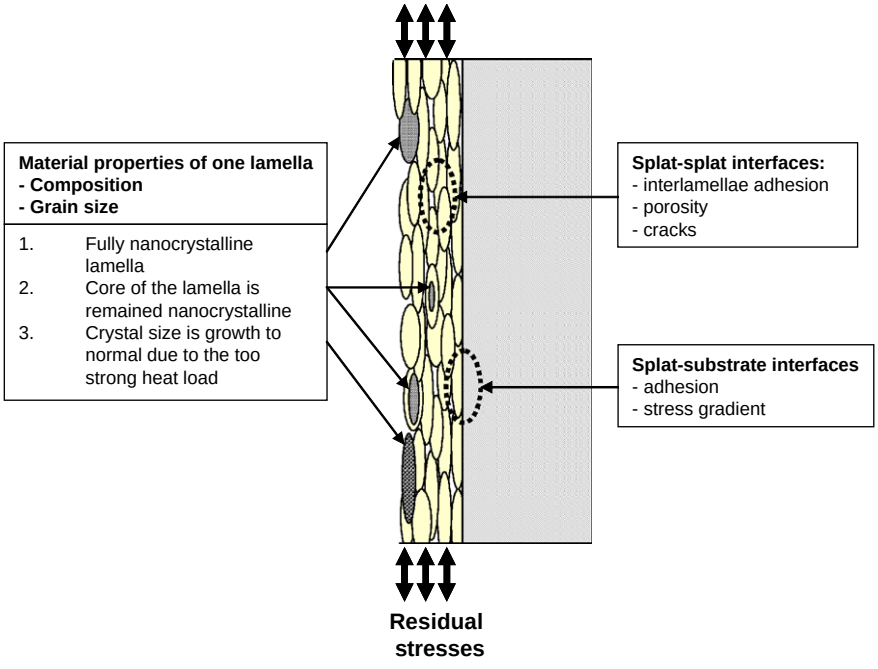

Fig. 1. Factors effecting on the properties of thermally sprayed coating.

hydrogen containing atmosphere. Two powders were produced having nickel content of 2 vol.%, and 5 vol.%, respectively.

Pure nanostructured alumina powders were also manufactured from boehmite. Boehmite was agglomerated by spray drying, heat treated to alumina and finally sintered. This process was similar to the one used for Ni containing alumina. Praxair Al-1110HP Al_2O_3 powder was used as reference material having grain size in the micrometer range.

2.2. Thermal spray test setup

Coatings were deposited using Praxair HV-2000 spray gun fitted with 22-mm combustion chambers. Nitrogen was selected for a carrier gas along with hydrogen as a fuel gas. As known from previous studies use of hydrogen results in a narrower process window in terms of velocity and temperature range as compared to propane or propylene [3]. This causes less variation in particle melting stage between different spray conditions. In the current work it was essential to maximize splat interface and therefore, despite the fact of smaller process window, hydrogen was selected as a fuel gas.

A two-axis traverse unit was used to manipulate the gun during coating deposition. Use of Thermico CPF-2HP powder feeder ensured sufficient powder feed rate also for trial powders, which had a non-optimal size distribution having particles smaller than 5 μm in diameter and consequently poor flow capability.

2.3. Online diagnostic studies

Online diagnostics using Spraywatch 3i equipment were carried out at different spray conditions to measure the particle velocity and temperature. Distance of the camera from the spray gun was equal with standoff distance during coating manufacturing being 150 and 200 mm. The measurement is based on the two-colour pyrometry and a fast CCD camera [18]. In diagnostic tests, the total gas flow rate was kept constant and the amount of hydrogen and oxygen was varied to obtain different gas ratios from 2.0 to 2.85. Besides the gas ratio, total gas flow and standoff distance were varied. Two total gas flow rates, 1050 l/min and 890 l/min, were used. Standoff distances of the spray gun from the substrate plate were either 150 or 200 mm.

2.4. Single splat studies

Single splats were collected onto preheated (200 °C) stainless steel substrates in order to study the melting level of the particles in different spray conditions. Splats were produced by spraying with a low powder feed rate over polished steel plates through a special shutter system. By using a shutter system, flame contacted with the steel plate only for some milliseconds, and single splats could be collected within the flame diameter. While temperature data from diagnostic tests, based on emissivity of particle in-flight, provides only the surface temperature of the particle, single splats enhance our understanding on the overall melting stage of a particle. In a case of a material with high melting point and short dwell time in the flame, the surface temperature will not always give the information of the melting through the whole particle.

2.5. Coating deposition

Coatings were sprayed onto grit blasted carbon steel plates having a size of $25 \times 50 \times 2$ mm. Traverse speed of the gun was 0.2 m/s, and approximately 13 μm thickness per pass was deposited. These samples were used for microstructural and property characterization. The spray parameter combinations were similar for the splat and coating deposition and were selected based on the measured on-line diagnostic data.

2.6. Characterization

The crystal structures of the powders and the coatings were characterized by X-ray diffraction (XRD) using Cu-Kα and Mo-Kα radiation. Powder agglomerate size was determined by using Lecotrac — LT100 particle size analyzer. Electron microscopy using JEOL JSM-6400 (SEM) combined with PGT PRISM 2000 X-ray analyzer, LEO982 Gemini (FEG–SEM), and Philips CM 200 (FEG–STEM) combined with Noran Voyager X-ray analyzer were used to study the splats and coating microstructures and to characterize micro-cracking and nickel distribution on fracture surface.

Splats produced with selected spray conditions were studied in detail for their size and thickness. Image analysis and direct length measurements (ImagePro®, Graftek) from images 1260×922 pixels) were applied to measure the diameter of the splats. The SEM was calibrated in X and Y directions with a reference grid (12.5 μm reference distance). The error in length measurements was less than ±3%. The thickness of the splats was derived from X-ray spectra acquired with three acceleration voltages (18, 25, and 33 kV) with constant microscope parameters and X-ray detection geometry. Splat thickness was calculated from Fe-K_α and Al-K_α intensity K-ratios (I_x/I_{std}) as a function of acceleration voltages using a simulation program (X-film®, Synergie[4]) to find the best fit between theoretical curves and experimental data points.

Hardness of the coatings was determined by Vickers micro hardness method using a mass of 300 grams. Instrumented nanoindentation with a Nanotest 550 instrument equipped with a 0.79 mm ball indenter was used to characterize the elasto-plastic properties of the coating. Calculation of elastic modulus was made by using the method developed by Field and Swain [19,20]. Wear resistance of the coatings was evaluated by rubber wheel abrasion test according to standard ASTM G 65-91.

3. Experimental results

3.1. Powder microstructure

After agglomeration and sintering powders were analyzed to confirm the grain size and phase structure of the particles before HVOF spray tests. Powders were analyzed by XRD to consist θ- and α-alumina and nanosized Ni-particles. Powder fraction was measured to be between 2 and 26 μm. Detailed information of the produced powders and a reference powder are presented in Table 1. Typical morphology and cross-section for the particle is presented in Fig. 2.

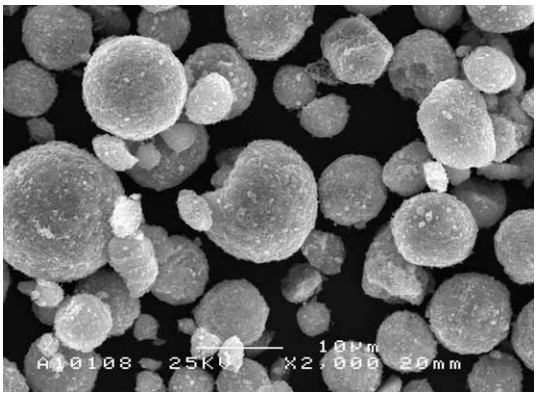

Fig. 2. Typical morphology for the n-Al_2O_3 agglomerates.

3.2. On-line diagnostics

Over 20 different spray conditions were studied where gas ratio of hydrogen and oxygen was varied. Table 2 gives the main trends observed in the measurements.

3.3. Splat studies

Single splats were sprayed on stainless steel at all process conditions using the reference powder. It was found that maximum velocity obtained in condition C is not optimal due to the larger fragmentation of the splat. This will produce small, solidified droplets in the coating, which will disturb the interlamellar adhesion. More detailed analyse were carried out for spray conditions A, B and D. The SEM images of the collected splat populations, and splat outlining by image analysis for size measurements, as well as the structure of corresponding coating cross-section for each spray condition are presented in Fig. 3. Sixteen (16) splats per plate were analyzed in detail for their diameter and thickness.

The average thickness was found to be 0.55 μm for condition A, 0.76 μm for condition B, and 0.48 μm for condition D. Results confirm the visual observations and diagnostic data, showing lowest flattening at condition B due to the lowest particle temperature and velocity. Flattening of the particles increased (thickness decreased) with increasing particle velocity and temperature being highest for condition D. The medians of the splat diameters were 19.25 μm for condition A, 18.8 μm for condition B, and 19.8 μm for condition D. The trend was opposite to that of diameters as expected. Diameter was smallest with the condition B where splat thickness was highest. In all cases, the largest particles have not attached to the substrate. Partly, this is assumed to be caused by the polished surface, and partly by the semi-molten state of the larger particles.

3.4. Coating microstructure

Coatings were deposited from all powders listed in Table 1, using spray conditions A, B and D. Based on the splat tests, spray conditions A and D were expected to be the potential ones to produce good, well adhering coatings. Condition B was selected in order to study the effect of the lower particle velocity and less flattening of the particles on the coating microstructure and properties.

Coating microstructure was studied and analyzed from the polished cross sections of the coatings by SEM in BEI mode, which ensures good contrast for studying flattening rate of the particles and adhesion of the lamellas.

Microstructural analysis based on the microscopy of the coating cross sections showed that coatings A and D, produced a much denser coating structure than spray condition B. The same trend was observed for all spray materials. Densest structures were obtained by using spray condition D. Microstructures for the reference materials with each condition are presented in Fig. 3.

Relative contents of α and γ phases as measured by XRD for ref-Al_2O_3 were 15% and 85% for coating A, 14% and 86% for coating B, and 4% and 96% for coating D. Again a good correlation between diagnostic studies and splat studies was found. A large difference in the alpha content was found between coatings A and D. Despite the higher particle surface temperature in condition A the particle velocity is also higher. Due to this, the dwell times of the particles are shorter in the flame and less melting occurs. This is manifested by the on average less flat single splats as

Table 1
Spray powders for the HVOF experiments

Powder	Material code	Manufacturer and method	Agglomerate size [μm]	Crystal size	Phase structure
Al-1110	ref-Al_2O_3	Praxair, fused and crushed	5–22	Conventional	alpha
Boehmite	n-Al_2O_3	VTT, agglomerated and sintered	2–25	Nano range	alpha
Boehmite	n-Al_2O_3–2% Ni	VTT, agglomerated and sintered	4–23	Nano range	theta
Boehmite	n-Al_2O_3 –5% Ni	VTT, agglomerated and sintered	2–26	Nano range	theta

Table 2
Diagnostic data for different spray conditions

Spray condition	Ratio H_2/O_2	Total flow [l/min]	Standoff [mm]	T [°C]	v [m/s]
A	2.85	1050	150	2050±5	1025±25
B	2.85	1050	200	1989±6	874±69
C	2.48	1050	150	2040±3	1073±34
D	2.00	1050	150	1990±4	1014±7
E	2.85	890	150	2027±5	1003±14

well as by the higher alpha alumina content in the final coating.

For n-Al_2O_3, α/γ ratio was 9%/91% for coating A, 8%/82% for coating B, and 3%/97% for coating D. These results correspond well to the results obtained from the single splat studies. Due to the agglomerated structure of n-Al_2O_3 particles compared to the fused and crushed reference powder, the melting is higher even with spray condition B.

A coating microstructure inside one lamella was studied by high-resolution SEM. A high resolution SEM image of the fracture surface of n-Al_2O_3 coating (D) is shown in Fig. 4. Alumina grains having dimensions in a range of hundreds nanometers are observed. It should be noted that the fine structure seems to have been retained in spite of extensive melting of the powder in the HVOF process and only a small amount of α-Al_2O_3 in the structure.

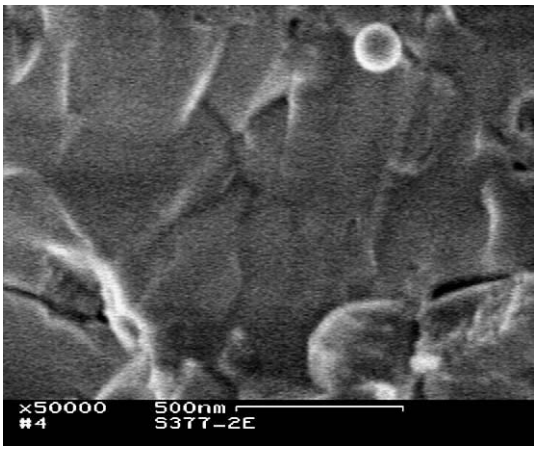

Fig. 4. An FEG–SEM micrograph of a fracture surface of n-Al_2O_3–HVOF coating.

The distribution of nickel in the polished cross sections of the samples as revealed by the back-scattered electron imaging is shown in Fig. 5(a) to (f). These micrographs indicate that nickel is partly deposited into the splat boundaries, i.e. interlamellarily. Especially in the case of 5% of nickel alloy, clear interlamellar deposits of nickel can been observed. A fraction of nickel seems to remain within the lamellae in the nano scale, while some of the nickel is transferred to the interlamellar boundaries, and some is lost in the HVOF spray process. The total nickel content as

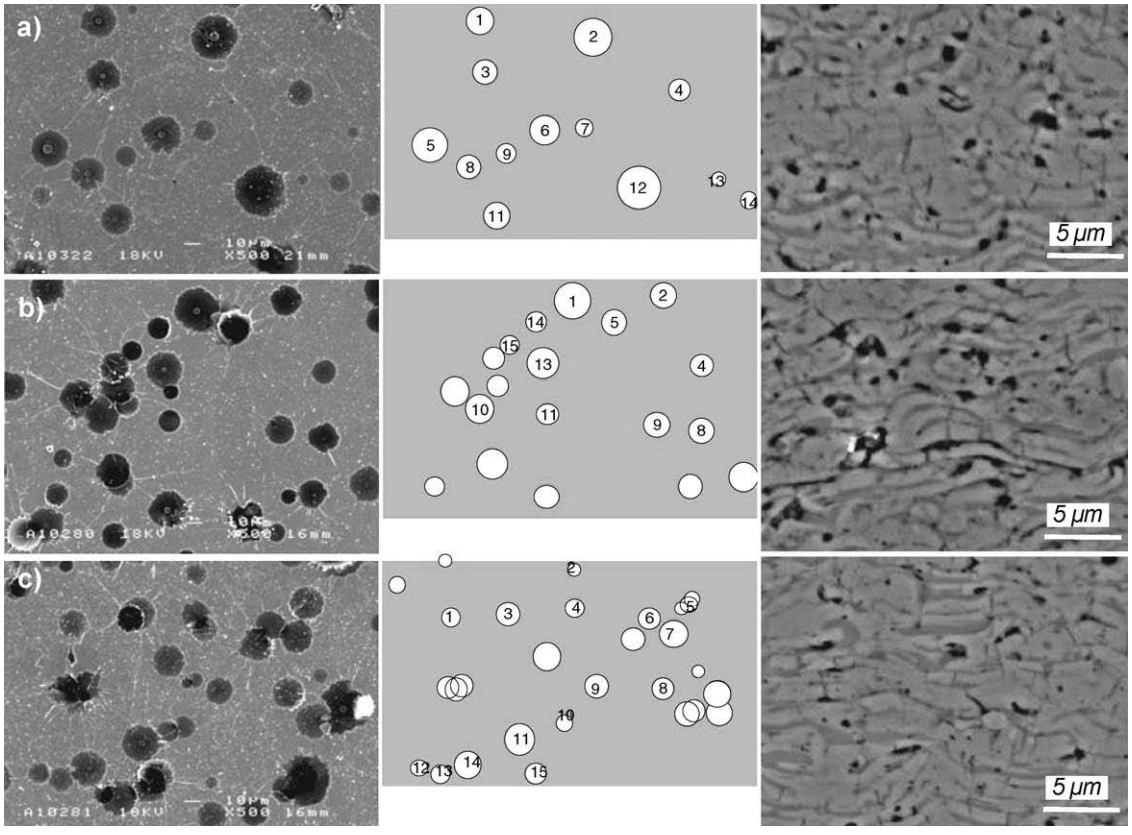

Fig. 3. The SEM images of the collected splat populations, and splat outlining by image analysis for size measurements, as well as the structure of corresponding coating cross-section for each spray condition: a) condition A, b) condition B, c) condition D.

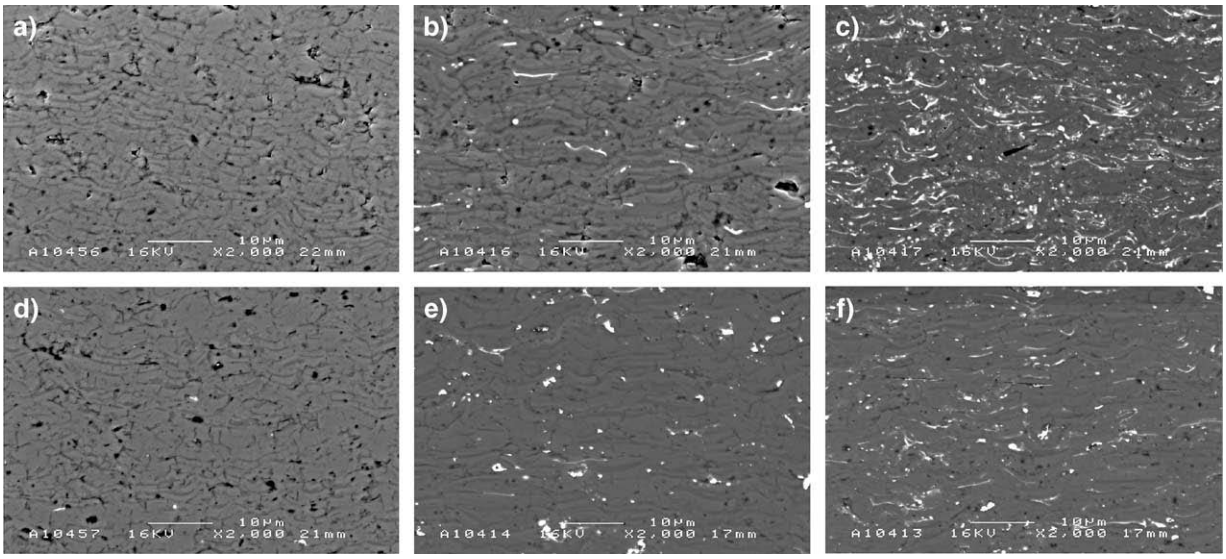

Fig. 5. SEM–BEI micrograph of the polished cross-sections for the coatings sprayed with different spray parameters: a) n-Al_2O_3 (A), b) n-Al_2O_3–2%Ni (A), c) n-Al_2O_3–5%Ni (A), d) n-Al_2O_3 (D), e) n-Al_2O_3–2%Ni (D), f) n-Al_2O_3–5%Ni (D).

measured by EDS from the cross section of the coating showed that the content of the nickel varied depending on the spray parameters. Loss of nickel was the highest in spray condition D, being 34% for the starting powder containing 5% nickel. For condition A the loss was 10%, and for condition B it was 19%. A detailed spot analysis from the alumina matrix, where nickel was not observed visually from the BEI image showed that spray conditions also influenced the content of nickel within the lamellae. The content of the intralamellar nickel was 2.8% for coating I, 3.1% for coating II and 2.3% for coating III, respectively.

Decrease of nickel content was also observed in X-ray diffraction of the coating produced in condition D. The XRD diffraction curve for the coatings sprayed from the powder alloyed with 2% of nickel is presented in Fig. 6. The loss of nickel when using spray condition D can clearly be observed.

3.5. Coating properties

Mechanical properties of the coatings were determined by abrasive wear resistance tests, hardness measurements, and by measuring cracks formed around a Vickers indentation after hardness measurements. A summary of the mechanical properties of the coatings is given in Fig. 7(a) to (c). In Fig. 7(a) Vickers hardness numbers of the coatings are presented. Hardness is highest for the n-coatings sprayed with condition D that was the condition

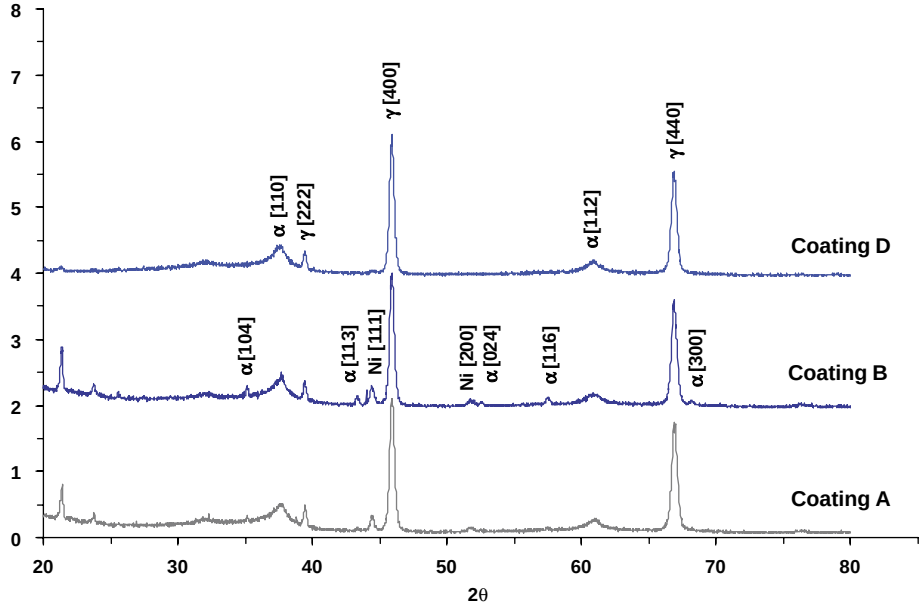

Fig. 6. X-ray diffraction curve for the coatings manufactured from the n-Al_2O_3–2%Ni powder with different spray conditions.

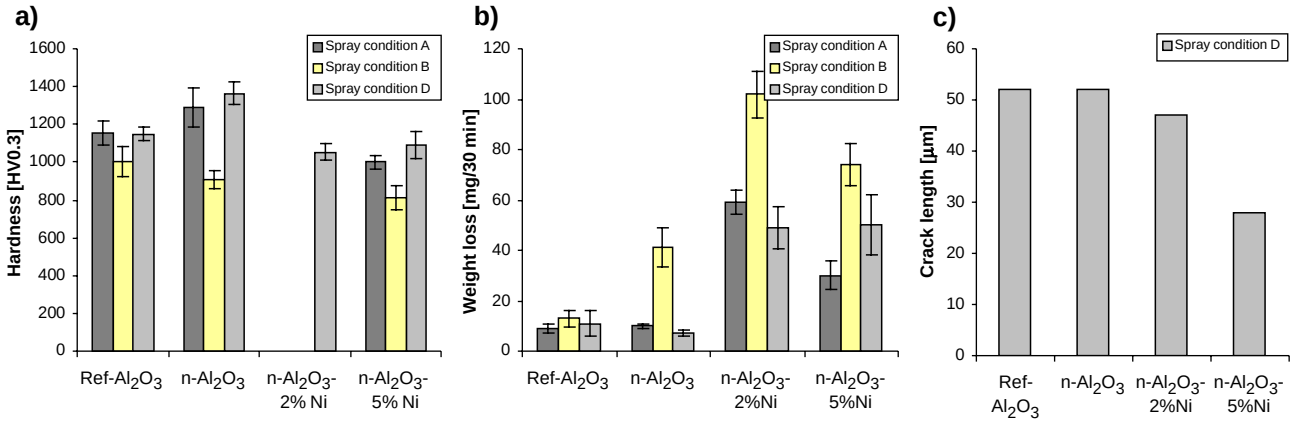

Fig. 7. a) Vickers hardness (HV0.3), b) weight loss in rubber wheel abrasion test, and c) cumulative length of horizontal cracks around a Vickers indentation.

producing thinnest flats. For reference material hardness is equal for spray conditions A and D. Comparison between pure nanoalumina coating (n-Al_2O_3) and the reference coating shows that the hardness is higher for n-Al_2O_3 coatings. This is believed to arise from the use of nanocrystalline feedstock, which results in the refinement of the coating microstructure. However, introduction of nickel into the coating again decreases the hardness.

In order to qualitatively estimate the toughness of the coatings the cumulative length of horizontal cracks around a Vickers indentation (HV0.3) at coating cross sections was measured. The length of cracks is found to decrease with increasing Ni-content as shown in Fig. 7(c).

4. Discussion

In on-line spray diagnostic measurements maximum particle temperatures were detected when the hydrogen/oxygen ratio was either 2.48 or 2.85. This correlates well with the previously reported measurements [3] carried out with same spray set up. Increase of spray distance from 150 mm to 200 mm by keeping other spray conditions constant decreases the surface temperature of the particle. The increase of total gas flow rate has the same effect. Also a decrease in H_2/O_2-gas ratio towards the theoretical stoichiometric value of 2.0 decreases the surface temperature of the particle.

The measured particle velocities around 1000 m/s are quite high as compared to those reported before [3] where maximum velocities were around 800 m/s. This discrepancy results from the used diagnostic equipment. Presently used equipment, Spraywatch, is capable to measure only those particles that are bright enough. In the case of ceramics this means that mainly small particles having higher velocities are measured. The diagnostic system, DVP-2000, which is used in Ref. [3] is capable to measure all particles thus giving lower medium particle velocities. However, the results give the trend between different spray conditions. Highest velocities were measured for the hydrogen/oxygen ratio of 2.48 and 2.85. The velocity decreased when spraying distance was increased or H_2/O_2-gas ratio was decreased. Also, lower total gas flow rate decreased particle velocity.

Splat studies show that flattening rate correlates well with the diagnostic studies. E.g., low particle temperature and velocity is observed for the condition B because of longer spray distance. On the other hand, despite the higher particle temperature in the condition E, the melting stage is lower than in condition B due to the higher particle velocity and shorter dwell time of the particle in the flame. XRD analyses support the results obtained from the diagnostic and splat studies. The amount of alpha phase is smaller when condition D is used. Splat studies and XRD studies show also that melting of the agglomerated nanofraction powder is higher compared to the reference powder, which is fused and crushed. Already, spray condition A produces a denser coating with a lower amount of alpha phase when the nanostructured powder is used instead of the reference powder. According to the splat studies this is a result of improved melting of the agglomerated nanostructured powder at spray flame as compared to that of the fused and crushed reference powder.

The alpha alumina content of the resulting coating is relatively low in all spray conditions. As known from a previous study on alumina coatings [21], alpha alumina content is always low in thermally sprayed coatings due to the fast cooling of the particles. This may have an influence on the mechanical properties of the coating. However, when aiming at good environmental protection properties it is more important to ensure good lamellar bonding and dense structure for the coating. Also, while attempting to increase coating fracture toughness by modifying coating microstructure inside one lamella, the bonding between lamellae must be good enough in order to obtain the improved properties over the complete coating structure. Otherwise, the lamella interface will dominate the overall behavior for the coating despite the microstructure. Therefore, in selection of spray parameters those resulting in good interlamellar bonding should be prioritized over those resulting in high alpha/gamma ratio.

Coatings sprayed in conditions A and D had dense structures. Correlation between flattening rate and coating microstructure for the coating hardness values is obvious. Wear resistance of the coatings (Fig. 7(b)) seems to have a similar dependency on the type of the coating as the coating hardness. While the wear resistance of ceramic coatings is sometimes related to its fracture toughness [22] it seems that in these current materials wear resistance depends rather on the coating hardness and therefore decreases with increasing nickel content.

By using spray condition D, a dense coating structure is obtained with high hardness and good wear resistance. This is believed to correlate with good interlamellar adhesion. Especially in the case of n-Al_2O_3 powder, coating III produced using spray parameter D seems to be superior. Despite the fact that conditions A are "hottest", the dwell time in the flame is shorter and no complete melting has occurred. This can be observed from the α/γ ratio as well as from the coating microstructure. Due to the lower particle velocity in condition B, the coating II has a porous structure and obviously lower interlamellar adhesion resulting in poor wear behaviour. More similarity in coating properties despite the used spray conditions was observed for reference powder. The spray process for the reference material seems to be more robust, which might be caused by denser structure of the fused and crushed powder.

The introduction of nickel into the coating resulted in more variations in the coating structure at different spray conditions. The condition D seems to result in a more radical redistribution of nickel of the original powder into the coating because of the higher melting stage of the particles in this spray condition. Amount of nickel is lower in these coatings both inside the alumina matrix as well as at the lamella boundaries. This has an effect on the mechanical properties of the coating. Especially in the case of n-Al_2O_3–5%Ni the weight loss in abrasive wear test of the coating is increased if the coating is sprayed by using parameter D.

In summary, by introducing nickel into the coating, the fracture toughness seems to improve but simultaneously the hardness and abrasive wear resistance are decreased.

5. Conclusions

In this paper the development of Al_2O_3 and Al_2O_3–Ni HVOF sprayed nanocomposite spray powders and coatings has been described. It was found that by optimizing spray parameters high quality coatings can be obtained.

Introduction of nanopowders to the coating process improves the hardness and wear resistance of the pure Al_2O_3-coating. Introduction of nickel alloying decreases hardness and wear resistance of the coatings, but increases toughness of the coatings.

By adding a small amount of nickel into alumina a coating with high hardness and good fracture toughness is produced. This type of coating is considered to be a potential candidate for a protective coating in the harsh environments where good fracture toughness combined with excellent chemical and corrosion resistance of ceramics is needed.

Acknowledgement

This work was sponsored by TEKES, The National Technology Agency of Finland, VTT Industrial Systems and Finnish industries (Kemira Pigments Oy, Fortum Oil Oy, Rautaruukki Oyj, OMG Kokkola Chemicals Oy, Outokumpu Research Oy, ABR Innova Oy, Pikoteknik Oy, Ionhawk Oy, and Stratum Oy).

References

[1] A.J. Sturgeon, et al., British Ceramic Proceedings, vol. 54, 1997, p. 57.
[2] A. Kulkarni, J. Gutleber, S. Sampath, A. Goland, W.B. Lindquist, H. Herman, A.J. Allen, B. Dowd, Mater. Sci. Eng., A Struct. Mater.: Prop. Microstruct. Process. 369 (2004) 124.
[3] E. Turunen, T. Varis, S.-P. Hannula, A. Kulkarni, J. Gutleber, A. Vaidya, S. Sampath, H. Herman, Mater. Sci. Eng. (submitted for publication).
[4] Y.K. Jeong, K. Niihara, Nanostruct. Mater. 9 (1997) 193.
[5] Masahiro Nawa, Noriko Bamba, Tohru Sekino, Koichi Niihara, J. Eur. Ceram. Soc. 18 (3) (1998) 209.
[6] Sung-Tag Oh, Mutsuo Sando, Koichi Niihara, Scr. Mater. 39 (1998) 1413.
[7] S.-P. Hannula, J. Koskinen, E. Haimi, R. Nowak, in: H.S. Nalwa (Ed.), Encyclopedia of Nanoscience and Nanotechnology, vol. 5, American Scientific Publishers, USA, 2004, p. 131.
[8] M.J. Mayo, Nanostruct. Mater. 9 (1997) 717.
[9] A. Mohammed, Y. Li, Mater. Sci. Eng. 298A (2001) 1.
[10] R. Goswami, H. Herman, S. Sampath, X. Jiang, Y. Tian, G. Halada, Surf. Coat. Technol. 141 (2001) 220.
[11] S.D. Parukuttyamma, J. Margolis, H. Liu, J.B. Parise, C.P. Grey, S. Sampath, P. Gouma, H. Herman, Materials Research Society, Solid-State Chemistry of Inorganic Materials, vol. III, 2001, p. GG6.29.1, USA.
[12] M. Gell, E.H. Jordan, Y.H. Sohn, D. Goberman, L. Shaw, D. Xiao, Surf. Coat. Technol. 146–147 (2001) 48.
[13] E.H. Jordan, M. Gell, Y.H. Sohn, D. Goberman, L. Shaw, S. Jiang, M. Wang, T.D. Xiao, Y. Wang, P. Strutt, Mater. Sci. Eng. 301 (2001) 80.
[14] D. Goberman, Y.H. Sohn, L. Shaw, E. Jordan, M. Gell, Acta Mater. 50 (2002) 1141.
[15] L.L. Shaw, D. Goberman, R. Ren, M. Gell, S. Jiang, Y. Wang, T.D. Xiao, P.R. Strutt, Surf. Coat. Technol. 130 (2000) 1.
[16] R.S. Lima, B.R. Marple, Surf. Coat. Technol. (in press) (available online February 1, 2005).
[17] S. Sampath, X. Jiang, A. Kulkarni, J. Matejicek, D.L. Gilmore, R.A. Neiser, Mater. Sci. Eng., A Struct. Mater.: Prop. Microstruct. Process. 348 (2003) 54.
[18] J. Vattulainen, E. Hämäläinen, R. Hernberg, P. Vuoristo, T. Mäntylä, J. Therm. Spray Technol. 10 (1) (2001) 94.
[19] J.S. Field, M.V. Swain, J. Mater. Res. 8 (1993) 297.
[20] J.S. Field, M.V. Swain, J. Mater. Res. 10 (1995) 101.
[21] D.A.J. Ramm, T.W. Clyne, A.J. Sturgeon, S. Dunkerton, Correlations between Spray Conditions and Microstructure for Alumina Coatings Produced by HVOF and VPS, National Thermal Spray Conference, 20–24 June, Boston, USA, 1994, p. 239.
[22] Y. Liu, T.E. Fischer, A. Dent, Surf. Coat. Technol. 167 (2003) 68.

PUBLICATION VI

Process optimization and performance of nanoreinforced HVOF-sprayed ceramic coatings

In: Proceedings of 16th International Plansee Seminar. May 30–June 3, 2005. Reutte, Austria 2005. 12 p.

Process optimization and performance of nanoreinforced HVOF-sprayed ceramic coatings

E. Turunen[1], T. Varis[1], T.E.Gustafsson[1], J. Keskinen[2], P.Lintunen[2], T. Fält[3], S-P. Hannula[1,3]

[1]VTT Industrial Systems, Espoo, Finland
[2] VTT Processes, Tampere, Finland
[3] Helsinki University of Technology, Materials Science, Espoo Finland

Summary

Improved mechanical properties have widely been demonstrated for bulk nanocrystalline materials. Especially with ceramic materials decreasing of grain size has been found to be favourable. Nanocrystalline materials offer better thermal shock resistance, lower thermal conductivity and better wear resistance than their conventional counterparts. For nanostrucutured bulk composites with nanosized metal precipitations in the nanocrystalline ceramic matrix improved fracture toughness properties have also been reported. An increasing effort has been made to transfer such improvements also into thermal sprayed ceramic coatings. Mainly work has been carried out with plasma spray systems, but recently it has been shown that HVOF (High Velocity Oxy-Fuel) process can produce much denser coatings and hence better environmental protection capacity. In this paper we describe the development of HVOF sprayed nanocrystalline Al_2O_3-composite coatings, where the grain size of Al_2O_3 has been decreased and a few percents of alloying elements has been added in order to toughen the coating.

---

* S-P. Hannula is a joint professor of Helsinki University of Technology and VTT Industrial Systems

Keywords

Thermal spraying, HVOF, process optimization, alumina, nanostructure

1. Introduction

Thermal spraying is an effective and low cost method to produce thick coatings and change surface properties of the component. Because the coating is built-up from the melted or semi-molten droplets via fast cooling, thermal spraying offers an ideal means to produce coatings from a wide range of the materials. Thermal sprayed coatings are often used as environmental (wear, corrosion and/or thermal) or electrical barriers.

Ceramic coatings offer an interesting alternative to produce a protective layer over a steel structure due their excellent chemical, corrosion and thermal resistance. Plasma spraying is the mainly used method to produce a thick ceramic coating. Recently it has been shown that HVOF process can produce much denser coatings and hence better environmental protection properties than plasma sprayed coatings [1,2,3].

Even though HVOF coatings are much denser as compared to ordinary plasma sprayed coatings, the coating properties are inferior as compared to bulk ceramics because of pores and microcracks, which influence adversely the coating properties, i.e. toughness, hardness and wear resistance. The denser the coating is, the more limitations are observed due to the residual stresses and mismatches in CTE compared to the steel structure.

One strategy to improve the properties of the coatings is to decrease the grain size of the ceramic phase and to add toughening elements to the microstructure. Nanocrystalline material have been found to offer better thermal shock resistance, lower thermal conductivity and better wear resistance than their conventional counterparts. There are several recent reviews on mechanical properties of nanocrystalline materials [4,5,6]. For bulk materials also better fracture toughness is reported for nanostructure composites having nanosized metal precipitations in the nanostructured alumina matrix [7,8].

Thermal spraying is a complex process including a number of variables. Particle melting stage and possible phase transformations during its flight in the flame must be controlled as well as coating buildup mechanism including splat interface and stress

development. In order to produce a coating with desired properties, e.g. with high fracture strength, it is not sufficient to control material structure only inside one lamella. Also interactions between lamella, stress stages of the final coating, its adhesion to the substrate and cracking must be controlled. These different phenomena influencing on the final quality of the coating are depicted schematically in Figure 1.

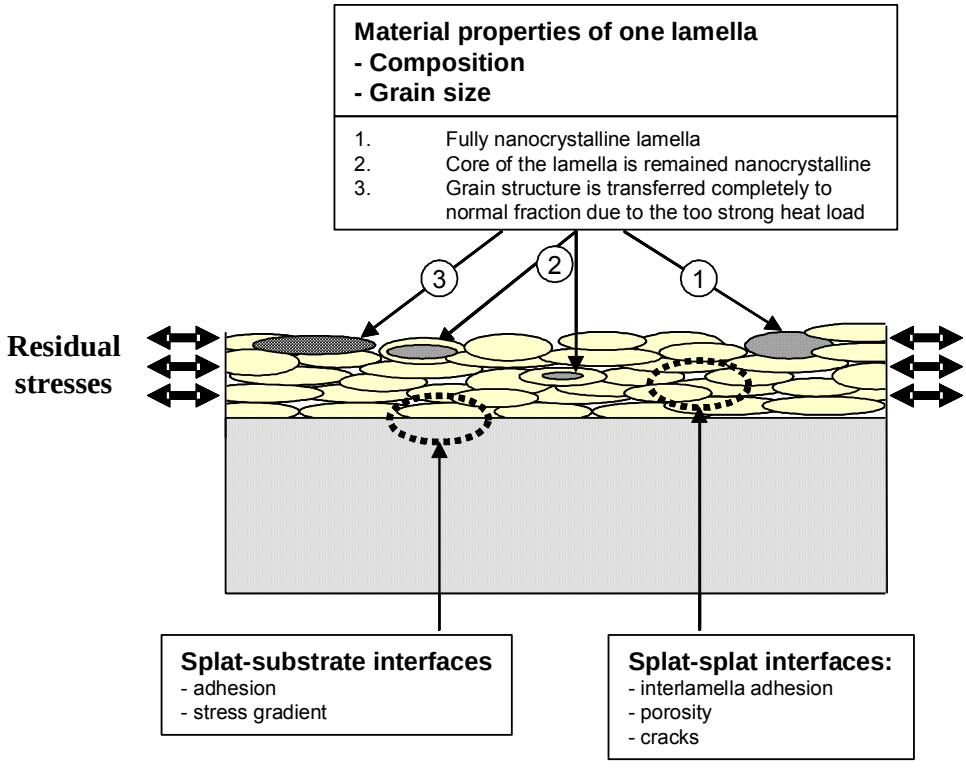

Fig. 1. Factors influencing the properties of thermally sprayed coating.

In this paper we describe the development of HVOF sprayed nanocrystalline Al_2O_3-coatings, where the grain size of Al_2O_3 has been decreased and a few percents of alloying material has been added in order to toughen the coating. Raw material development, process optimisation for HVOF process and coating properties for different composite coatings including 5-vol% alloying of nickel, nickel oxide, zirconium oxide, and silicon carbide is discussed.

2. Experimental Details

2.1. Spray Powder Development

Different alloying elements were selected to obtain different melting temperatures. The used alloying elements were Ni, NiO, SiC and ZrO_2 having melting temperatures of 1455 °C, 1957 °C, 2500 °C and 2800°C, respectively. Melting temperature for alumina is 2054 °C.

There is a number of ways to produce ceramic nanocomposite powders. In the present work the synthesis of Al_2O_3 powder with and without Ni-nanoparticles was carried out using boehmite (AlO(OH)) as a starting media. The process is initiated by diluting $Ni(NO_3)_2$ to ethanol and then adding AlO(OH). After drying the resulting powder is calcinated at 500 °C to obtain NiO - γ−Al_2O_3. Both oxides in the powder (nickeloxide and alumina) are in the form of nanosized particles.

After calcination the nanopowder mixture was agglomerated into larger particle agglomerates by spray drying. After agglomeration the powder was heat-treated to reduce NiO to metallic nickel and to transform γ−alumina to α−alumina and to sinter particles loosely together. In the case of n-Al_2O_3 -5% NiO material the powder was manufactured in the way described above, but it was further heat treated in air at 700 ^oC to transform nickel into nickel oxide.

The n-Al_2O_3 -5% SiC powder was processed by first making dispersions of SiC powder and boehmite. These were mixed in a propeller agitator, spray dried and sintered. Mixture of n-Al_2O_3-5% ZrO_2 was made from nanosized yttria stabilized zirconia that was ball milled in water together with boehmite. Also this mixture was spray dried and sintered to obtain the desired powder for thermal spraying.

Pure nanostructured alumina powders were manufactured from boehmite. Boehmite was agglomerated by spray drying, heat treated to alumina and finally sintered. Praxair Al-1110HP Al_2O_3 powder was used as reference material having grain size in the micron range.

2.2. Thermal Spray Test Setup

Coating deposition and spray diagnostics were accomplished with a Praxair HV-2000 spray gun, fitted with 22mm combustion chamber allowing for varying process

parameters. Nitrogen was selected for a carrier gas, along with hydrogen as fuel gas. A two-axis traverse unit was used to manipulate the gun during coating deposition. Thermico CPF-2HP powder feeder was used to ensure sufficient powder feed rate also for experimental powders having a non-optimal size distribution and flow capability. *On-line diagnostics* by using the Spraywatch 3i equipment were carried out at different spray conditions to measure the particle velocity and temperature. The measurement is based on the two-colour pyrometry and a fast CCD camera [9]. *Coatings* were sprayed onto the steel plates having a size of 25×50×2 mm for microstructural and property characterization. The microstructural development was controlled by controlling the traverse rate of the gun and the powder feed rate resulting to a certain thickness per pass.

2.3. Characterization

Powder agglomerate size was determined by using Lecotrac – LT100 particle size analyzer. The crystal structures of the powders and the coatings were characterized by X-ray diffraction (XRD) using Cu-Kα and Mo-Kα radiation. Electron microscopy using JEOL JSM-6400 (SEM) combined with PGT PRISM 2000 X-ray analyzer, LEO982 Gemini (FEG-SEM), and Philips CM 200 (FEG-STEM) combined with Noran Voyager X-ray analyzer were used to study the coating microstructures.

Hardness of the coatings was determined by Vickers micro hardness method using a weight of 300 grams. Instrumented nanoindentation with a Nanotest 550 instrument equipped with a 0.79 mm ball indenter was used to characterize the elasto-plastic properties of the coating. Calculation of elastic modulus was made by using the method developed by Field and Swain [10,11]. Wear resistance of the coatings was evaluated by rubber wheel abrasion test according to standard ASTM G 65-91.

3. Results and Discussion

3.1 Powder Microstructure

Powders were analyzed before HVOF spray tests to confirm the phase structure of the particles. Powders consisted of α-alumina and appearance of each alloying element was approved for each powder type. Size distribution of the powder fraction was measured to be between 2 and 29 µm. Detailed information of the produced powders and the reference powder are presented in Table 1. Typical morphology for the powders is presented in Fig. 2.

Table 1. Spray powders for HVOF experiments.

Powder	**Material code**	**Manufacturer and method**	**Agglomerate size**	**Crystal size for alumina**
Al-1110	ref-Al_2O_3	Praxair, fused and crushed	5-22 µm	Conventional
Boehmite	n-Al_2O_3	VTT, agglomerated and sintered	2-25 µm	nano
Boehmite	n-Al_2O_3 -5% Ni	VTT, agglomerated and sintered	2-26 µm	nano
Boehmite	n-Al_2O_3 -5% NiO	VTT, agglomerated and sintered	2-21 µm	nano
Boehmite	n-Al_2O_3 -5% ZrO_2	VTT, agglomerated and sintered	2-29 µm	nano
Boehmite	n-Al_2O_3 -5% SiC	VTT, agglomerated and sintered	2-29 µm	nano

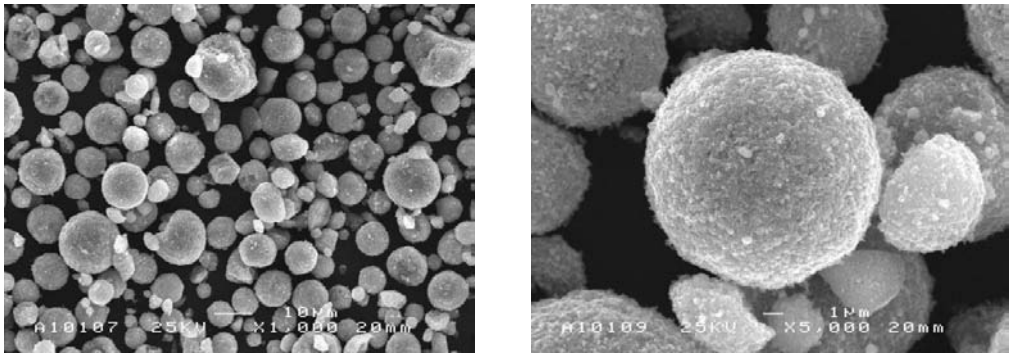

Fig. 2. SEM micrographs of the spray dried Al_2O_3 – 5%Ni particles at the magnification of 600× and 3000×.

3.2 Spray Process Optimisation

Spray parameters were optimised in order to produce coating with a dense structure combined with a desired phase structure. Large amount of different spray conditions were studied varying the gas ration of hydrogen and oxygen to produce different melting stages for the particles. Particle velocities and temperatures were measured with the on-line diagnostic. Selection and optimization of spraying parameters is described in detail elsewhere [12].

Two spraying conditions were selected for more detailed studies: condition 1 with gas parameters of H_2:775 l/min; O_2 270 l/min; N_2: 20 l/min, and condition 2 with gas parameters of H_2:700 l/min; O_2 350 l/min; N_2: 20 l/min. Spray distance in both cases was 150 mm. Both the conditions produced high particle velocities with slightly different particle temperatures.

3.3 Coating Microstructure

In this paper the results for the coatings produced by spray condition 1 are presented. The microstructure of the coatings was studied from the polished cross sections as well as from the fracture surfaces of the coatings. Polished cross sections were analyzed by SEM in BEI mode, which ensures good contrast for studying flattening rate of the particles and adhesion of the lamellae. All coatings had a dense structure with good lamellar bonding as shown in Fig. 3.

The distribution of nickel in the cross section of the sample produced using n-Al_2O_3-5%Ni powder is shown in Figure 3c. The light areas indicate the presence of nickel in the lamella boundaries of the coating. In the coating produced from the powder n-Al_2O_3-5%NiO also some light areas in the cross section can be observed (Fig 3d). These were analyzed by XRD and EDS to be also metallic nickel. Both micrographs indicate that some amount of nickel is deposited into the splat boundaries, i.e. interlamellarily. Amount of nickel in the lamella boundaries of the coating produced from the powder n-Al_2O_3-5%NiO is however much lower compared to the coating n-Al_2O_3-5%Ni using metallic nickel as alloying material in the spray powder.

More detailed analysis for the n-Al_2O_3-5%Ni coating showed that some amount of nickel still exists inside the matrix as nano sized particles, while some of the nickel is transferred to the lamella boundaries, and some nickel is apparently lost during the HVOF spray process [13,14].

Coatings made of a mixture of Al_2O_3 and ZrO_2 (Fig. 3 e) or Al_2O_3 and SiC (Fig. 3f) particles are homogenous, and no clear two phase structure is observed. This suggests that ZrO_2 and SiC may be located inside lamellas as small precipitations. However some limitations to separate these two phases in BEI mode exist and further TEM analysis to confirm this is under way.

Different melting temperatures of the alloying elements produced different coating microstructures. Despite the fact that particles in the HVOF process are in the molten stage only for a few milliseconds, the time is long enough for nickel partly to transfer into the lamella boundaries. Original nanosized nickel structure has remained only partly in the alumina matrix. While introducing alloying elements with higher melting temperature, the lower amount of alloying element is transferred to the lamella boundaries. In the case of powder n-Al_2O_3-5%NiO, nickel oxide seems to be reduced to the metallic nickel during HVOF spray process. Despite this reaction the amount of nickel observed in the lamella boundaries is not as high as it is in the case of coating produced from the powder n-Al_2O_3-5%Ni.

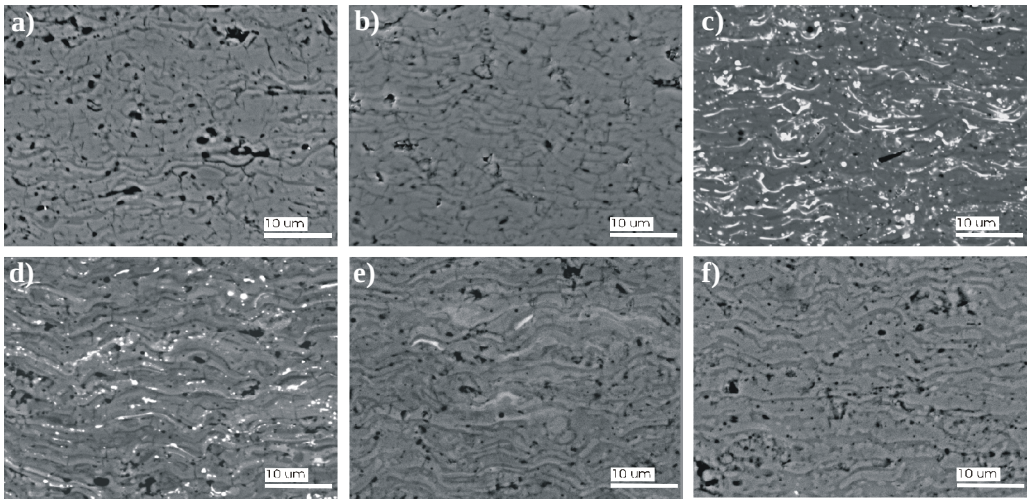

Fig 3. SEM-BEI micrograph of the polished cross sections fort he coatings a) ref-Al_2O_3, b) n-Al_2O_3, c) n-Al_2O_3 -5% Ni, d) n-Al_2O_3 -5% NiO, e) n-Al_2O_3 -5% ZrO_2, and f) n-Al_2O_3 -5% SiC.

3.3 Coating Properties

Micro hardness and abrasive wear loss were determined for all coatings. Results are presented in Fig. 4. As compared to the reference coating, which is sprayed by using a commercially available powder, the hardness is clearly improved, when the nanocrystalline coating structure is introduced. Introducing alloying elements such as NiO, ZrO_2 and SiC slightly reduces the hardness, but it still remains higher than for the reference coating. Introduction of the metallic nickel to the structure decreases the hardness below the reference sample. A large amount of metal located in the lamella boundaries is assumed to cause such a decrease.

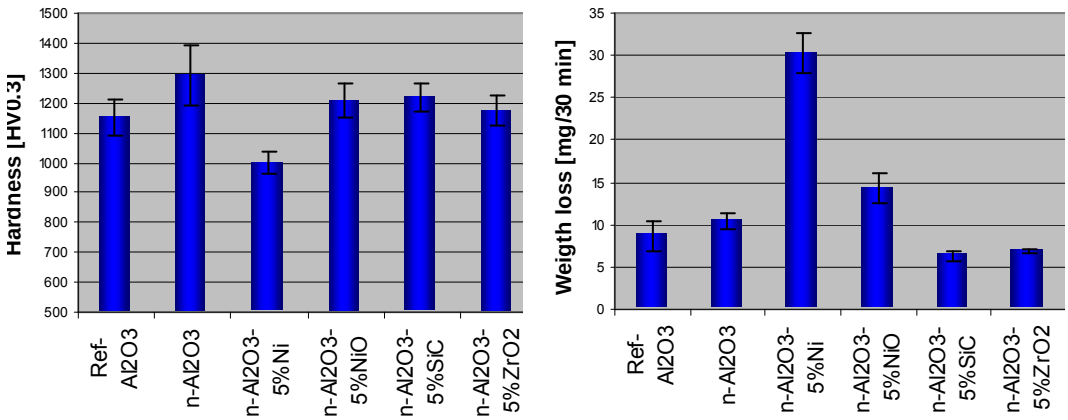

Fig 4. a) Vickers hardness (HV0.3) number and b) the weight loss in rubber wheel abrasion test.

Wear resistance of the coatings seems to correlate with the coating hardness as presented in Fig. 5b. The nickel alloyed coating having the lowest hardness has the highest wear rate obviously due to the appearance of metallic nickel in the lamellar boundaries. In the same way the coating produced from NiO-alloyed powder, having also some metallic nickel in the lamellae boundaries has higher wear rate as compared to the other coatings. Introduction of nanocomposite structure seems to decrease the wear rate of the coatings. The lowest wear rates were observed for the coatings n-Al_2O_3 -5% ZrO_2 and n-Al_2O_3 -5% SiC, as shown in Fig 5b. It can be concluded that introduction of alloying that remains through the HVOF spray process improves the coating wear resistance. This may be partly explained by the higher fracture toughness, which is still under investigation by the authors. Good fracture toughness for the Al_2O_3-Ni-type of coatings has been demonstrated earlier [13].

The elastic modulus was determined for the coatings ref-Al_2O_3, n-Al_2O_3 and n-Al_2O_3 -5%Ni. Measured values were 95 MPa for ref-Al_2O_3, 114 MPa for n-Al_2O_3 and 118 MPa for n-Al_2O_3 -5%Ni, respectively. According to the instrumented indentation measurements, the elastic modulus remains in nanostructured coatings approximately at the same level independent of nickel content. The values obtained, however, are clearly higher than those of the reference coating and those published for plasma sprayed alumina coatings [1].

4. Conclusions

In this paper raw material development and HVOF process to produce nanocomposite alumina coatings have been described). It was found out that by introducing nanocomposite structure in to the dense ceramic coating the wear resistance and hardness of the coating can be improved. By varying alloying material, the microstructure and properties of the produced coating can be varied. Depending on the application each of produced coatings can offer potential protective capacity.

Produced types of coatings are considered to be a potential candidate for a protective coating in the harsh environments, where excellent chemical and corrosion resistance is needed.

Acknowledgement

This work was sponsored by TEKES (The National Technology Agency of Finland), VTT (Technical Research Centre of Finland), and Finnish industries (Kemira Pigments Oy, Fortum Oil Oy, Rautaruukki Oyj, OMG Kokkola Chemicals Oy, Outokumpu Research Oy, ABR Innova Oy, Pikoteknik Oy, Ionhawk Oy, and Stratum Oy).

References

[1] A. Kulkarni, J. Gutleber, S. Sampath, A. Goland, W.B. Lindquist, H. Herman, A.J. Allen, B. Dowd, Materials Science and Engineering A369 (2004) 124–137.

[2] Sturgeon A.J. et.al., British Ceramic Proceedings, Vol 54 (1997) pp.57-64.

[3] E. Turunen, T. Varis, S-P. Hannula, A. Kulkarni, J. Gutleber, A. Vaidya, S. Sampath, H. Herman, Materials Science and Engineering, submitted (2005).

[4] S.-P. Hannula, J. Koskinen, E. Haimi, and R. Nowak: Encyclopedia of Nanoscience and Nanotechnology, vol. 5, H.S. Nalwa, Ed, American Scientific Publishers, USA, 2004, p. 131.

[5] M. J. Mayo, High and low temperature superplasticity in nanocrystalline materials. Nanostruct. Mater. Vol. 9 (1997) pp. 717-726.

[6] F. A. Mohammed, Y. Li, Mater. Sci. Eng., Volume 298A (2001), pp. 1-15.

[7] Y. K. Jeong and K. Niihara, Nanostructured Materials, Volume 9 (1997), pp. 193-196.

[8] Sung-Tag Oh, Mutsuo Sando and Koichi Niihara, Scripta Materialia, Vol. 39 (1998), pp. 1413–1418.

[9] J. Vattulainen, E. Hämäläinen, R. Hernberg, P. Vuoristo, T. Mäntylä, Journal of Thermal Spray Technology Vol. 10(1) (2001) p. 94.

[10] J.S. Field and M.V. Swain, J. Mater. Res., 8 (1993) p. 297.

[11] J.S. Field and M.V. Swain, J. Mater. Res., 10 (1995) p. 101.

[12] E. Turunen, T. Varis, Tom. E. Gustafsson, Jari Keskinen, Teppo Fält and S-P. Hannula, Surface and Coatings Technology, submitted (2005).

[13] E. Turunen, T. Varis, S-P. Hannula, J.Keskinen, P.Lintunen, T. Fält, International Thermal Spray Conference, ITSC 2005, 2-4 May 2005, Basel, Switzerland, (2005), 6 p.

[14] S-P. Hannula, E. Turunen, J. Keskinen, T. Varis, T. Fält, T. E. Gustafsson and R. Nowak, Ceramic Society of Japan for the CSJ Series Vol 13, submitted (2004)

Published by

Series title, number and report code of publication

VTT Publications 583
VTT–PUBS–583

Author(s)
Turunen, Erja

Title

Diagnostic tools for HVOF process optimization

Abstract

In the thermal spray process the coating is built up from lamellas formed by rapid solidification of the melted or semi-melted droplets attached to the substrate. A typical structure for the coating is a pancake-like lamellar structure, where the flattening stage and adhesion between the lamellas, together with the coating material itself, define the main properties of the coating. Thermal spray coatings are often applied for better corrosion and wear resistance. Therefore, low porosity and good adhesion are desired properties for the coating. High velocity processes – especially HVOF (High velocity oxy-fuel) spraying – are the most potential methods for producing a good adherent coating with low porosity.

From a scientific point of view, particle velocity and particle temperature, together with substrate temperature, are the main parameters affecting the deposit formation. They determine the deposit build-up process and deposit properties. Particle velocity and temperature affect the deposit efficiency as well as the microstructure.

The aim of this work was to show the workability of diagnostic tools in the HVOF process. The focus was on first order process mapping, including on-line diagnostics and single splat studies. Nanocrystalline alumina composites and quasicrystals were selected, two materials that are complex to spray. With both materials the melting state of the particles must be well optimized in order to produce dense, well-adhered coating without unwanted changes in coating phase structure.

The main focus was on the HVOF spraying of alumina. The target was to obtain a systematic understanding of the influence of the process conditions on the microstructure development in HVOF alumina coatings. Conventional limits of gas ratios and flows were exceeded to obtain a wide velocity-temperature range. The study aimed to produce information for a first order process map, and was carried out at a much deeper level than previously reported. Propylene and hydrogen as fuel gases were compared, and other variables, such as total gas flow rate, fuel gas/oxygen ratio, and standoff distance were also varied. The obtained data was applied for nanostructured alumina composite coatings, and the effect of the process conditions was compared on the obtained coating microstructure and properties.

On-line diagnostic measurements, in which particle temperatures and velocities in the flame can be measured, were performed. The main work was carried out for alumina by using a DPV-2000 system. Two clear regions of different temperature and velocity arise from the use of different fuel gases. Single splat studies correlated well with the obtained coating properties, and a first order process map for alumina was created showing the window for the spray parameters producing best coating quality plotted against coating hardness and abrasive wear resistance.

It was shown that diagnostic results can be correlated with the coating microstructure and coating properties in HVOF spraying. It was also demonstrated that the coating properties and coating quality can be improved by optimizing and carefully selecting the spray parameters.

Keywords

thermal spraying, HVOF, high velocity oxi-fuels, process optimizatic diagnostics, single splat studies, surface coatings, alumina, quasicrystals, nanofractions

Activity unit

VTT Industrial Systems, Metallimiehenkuja 8, P.O.Box 1703, FI–02044 VTT, Finland

ISBN			Project number
951–38–6677–7 (soft back ed.) 951–38–6678–5 (URL:http://www.inf.vtt.fi/pdf/)			
Date November 2005	Language English	Pages 66 p. + app. 92 p.	Price
Name of project		Commissioned by	
Series title and ISSN VTT Publications 1235–0621 (soft back ed.) 1455–0849 (URL: http://www.vtt.fi/inf/pdf/)		Sold by VTT Information Service P.O.Box 2000, FI–02044 VTT, Finland Phone internat. +358 20 722 4404 Fax +358 20 722 4374	

In the thermal spray process the coating is built up from lamellas formed by rapid solidification of the melted or semimelted droplets attached to the substrate. A typical structure for the coating is a pancake-like lamellar structure, where the flattening stage and adhesion between the lamellas, together with the coating material itself, define the main properties of the coating. High velocity processes especially HVOF (High velocity oxy-fuel) spraying are the most potential methods for producing a good adherent coating with low porosity.

From a scientific point of view, particle velocity and particle temperature, together with substrate temperature, are the main parameters affecting the deposit formation. They determine the deposit build-up process and deposit properties.

The aim of this work was to show the workability of diagnostic tools in the HVOF process. The focus was on first order process mapping, including on-line diagnostics and single splat studies. The main focus was on the HVOF spraying of alumina. The target was to obtain a systematic understanding of the influence of the process conditions on the microstructure development in HVOF alumina coatings. The study aimed to produce information for a first order process map, and was carried out at a much deeper level than previously reported. The obtained data was applied for nanostructured alumina composite coatings, and the effect of the process conditions was compared on the obtained coating microstructure and properties. Also quasicrystalline materials were studied by using same methods.

It was shown that diagnostic results can be correlated with the coating microstructure and coating properties in HVOF spraying. It was also demonstrated that the coating properties and coating quality can be improved by optimizing and carefully selecting the spray parameters.

Tätä julkaisua myy

VTT TIETOPALVELU
PL 2000
02044 VTT
Puh. 020 722 4404
Faksi 020 722 4374

Denna publikation säljs av

VTT INFORMATIONSTJÄNST
PB 2000
02044 VTT
Tel. 020 722 4404
Fax 020 722 4374

This publication is available from

VTT INFORMATION SERVICE
P.O.Box 2000
FI–02044 VTT, Finland
Phone internat. +358 20 722 4404
Fax +358 20 722 4374

ISBN 951-38-6677-7 (soft back ed.)
ISSN 1235-0621 (soft back ed.)

ISBN 951-38-6678-5 (URL: http://www.vtt.fi/inf/pdf/)
ISSN 1455-0849 (URL: http://www.vtt.fi/inf/pdf/)

Erja Turunen